STUDY OF DISCHARGE COEFFICIENT AND TRENDS IN FILM COOLING EFFECTIVENESS OF CONICAL HOLES WITH INCREASING DIFFUSION ANGLES

by

HUMBERTO A. ZÚNIGA
B.S.A.E. University of Central Florida, 2000

A thesis submitted in partial fulfillment of the requirements
for the degree of Master of Science
in the Department of Mechanical, Materials and Aerospace Engineering
in the College of Engineering and Computer Science
at the University of Central Florida
Orlando, Florida

Fall Term
2006

ABSTRACT

Previous studies indicate that increasing the diffusion angle in conical film-cooling holes leads to an improvement in their film cooling effectiveness. Discharge coefficient and film cooling effectiveness measurements are conducted to characterize this behavior. Part of the focus of this investigation is to find out how this trend develops and attempt to ascertain the optimum cone angle, if possible. Six test plates, each with one row of eight conical-shaped cooling holes of equal diffusion angles of 0, 1, 2, 3, 6, or 8º, with respect to the hole axis are used in this study. The ratios of the hole exit areas to the inlet areas range from 1 to 2.85. Coolant injection angle for all holes is at 35 degrees to the horizontal, in the direction of the main flow. Coefficients of discharge of all holes are reported under flow conditions. Temperature sensitive paint, TSP, is the technique used to find the temperature distribution downstream of the cooling holes and determine the laterally averaged film-cooling effectiveness. Data are obtained for blowing ratios ranging from 0.5 to 1.5, at a constant density ratio of 1.26. Results and trends are compared with established literature, which also recommends that a cylindrical entry length for diffused holes should be at least 4 diameters long. The effect that an added entry length has on the 3-degree conical plate's cooling effectiveness is also explored. Data are compared to baseline cylindrical holes, as well as to fan-shaped film holes found in open literature. Results indicate that the conical holes with larger diffusion angles provide strikingly even film protection and outperform fan shaped and cylindrical holes under certain conditions over extended downstream distances. Also, the addition of a cylindrical entry length to a conical hole, by providing a manageable metering diameter, should ease their usage while providing the full benefits of the conical geometry which may one day lead to numerous industrial applications.

To my family and loved ones, for all their support and devotion in helping me reach my goals.

To the memory of my brother William, whose intellectual prowess always inspired me.

ACKNOWLEDGMENTS

I am forever grateful to my mentor, Dr. Jayanta S. Kapat, for giving me a chance to work under him and always challenging me to excel, be it academics, our funded research projects, or my own research. I remember a time in which I had no direction and I gave him call. He received me warmly. This thesis is one of the many results from that Wednesday morning meeting.

Thanks to my thesis committee: Dr. E. Petersen, Dr. R. Chen and Dr. C. Ling for their invaluable input and taking the time to review my work.

Many thanks to my friends, who are more like a family, in Building 44, for helping me in all aspects of testing, revising, presenting, and just being there all the time, literally! Thanks for the comradery and support in all activities, academic and extracurricular. I wish them the most successful lives and careers.

Thanks to my friends and loved ones, who have given me their affection and support. Their presence in my life has been a great source of motivation.

TABLE OF CONTENTS

LIST OF FIGURES

LIST OF TABLES

LIST OF ABBREVIATIONS

C_D Discharge Coefficient

D Metering diameter of hole inlet

DA Diffusion Angle – DA6 refers to coupon with diffusion angle of 6º w/r/t hole axis

DR Density ratio

I Momentum flux ratio,

IR Intensity Ratio

L Length of hole

M Blowing ratio, $M=\frac{\rho_c U_c}{\rho_m U_m}$

N Number of holes

P Pressure

PI Pitch

R Fluid's gas constant

S Equivalent slot length

T Temperature

U Velocity

X Distance downstream of center of the hole

a Half length of major axis of ellipse

b Half length of minor axis of ellipse

m Mass flow rate through the hole

Greek

α	Angle of hole-axis inclination
η	Film cooling effectiveness
κ	Ratio of specific heats
ρ	Density

Subscripts

0	Stagnation value
aw	Adiabatic wall
c	Coolant
cl	Centerline
i	Inlet
e	Exit
la	Laterally averaged
m	Main flow
r	Recovery

CHAPTER 1

INTRODUCTION

1.1 Film Cooling

Film cooling is a technique used in many systems to protect component surfaces exposed to high-temperature gas streams. Applications have been widespread, particularly in gas turbines, where combustor liners, turbine shrouds, blades and other hot parts of the engine have used air, bled off from the compressor outlet, as the coolant film. Such techniques reduce the thermal stresses that tend to occur with an increase of inlet temperature to the first-stage turbine of high-performance gas turbine systems. Turbine engines with effective cooling schemes permit higher turbine inlet temperatures, which in turn help in increasing the overall efficiency of the system. Industry has taken advantage of such techniques over the recent decades, pushing the limits of materials and achieving unprecedented levels of performance using film cooling and other techniques, as well as the use of sophisticated ceramic coatings. Figure 1-2 shows a generalized progression of turbine cooling technology over time, from early un-cooled turbines to simple cooling schemes, to advanced impingement and film cooled parts. Unfortunately, cool film protection from heat flux comes at a price. The source of the coolant is bleed-off air from the last stage of the compressor section. This high pressure air bypasses the combustor, and is maintained at much lower temperatures than the core turbine flow. The bleed-off air thus is removed from the core mass flow and subtracts from the engine's efficiency. Of course, the

engine designer's aim is to minimize the amount of bleed-off required to cool the blades, vanes and shrouds. Figure 1-1 shows a design of a gas turbine for power generation.

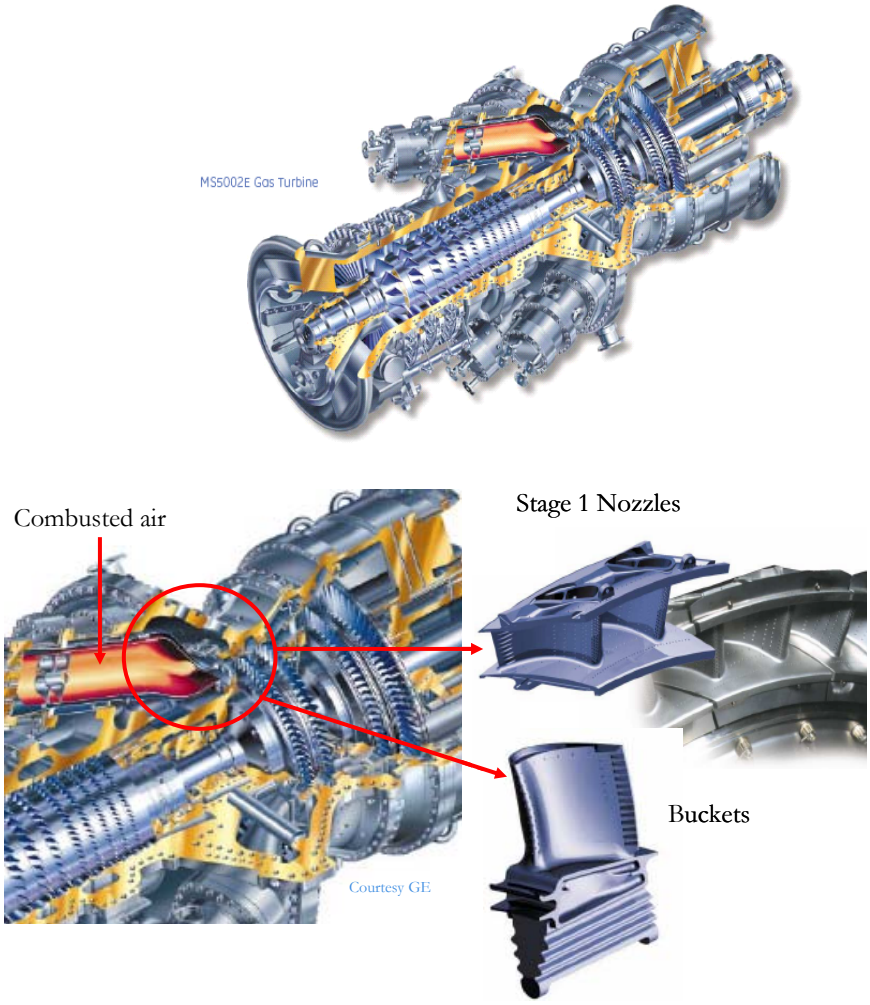

Figure 1-1 – MS5002E gas turbine and first stage detail (Courtesy GE)

To illustrate typical engine conditions for the first stage, where film cooling is most critical, combusted air enters the turbine at temperatures between 1500 and 2100 K, well above the melting point of the blade alloys. The centrifugal force acting on each blade as a result of rotation (12000 – 14000 rpm) is also on the order of several tons (Moustapha et al, 2003). The air's pressure, at this point has been compressed by a factor between 10 and 28. So, it is easy to

imagine an environment in which the first stage blades encounter highly unsteady, corrosive, thermally and structurally taxing conditions in which they must operate over extended periods of time. Moustapha et al. (2003) assert that the amount of energy in the form of heat that needs to be removed from the blades in order to keep them sufficiently cooled is enough to power 14 average homes per blade. Therefore, improvements in cooling technology are necessary in order to achieve higher turbine inlet temperatures and higher engine power output while at the same time maintaining or extending the service life of engine components.

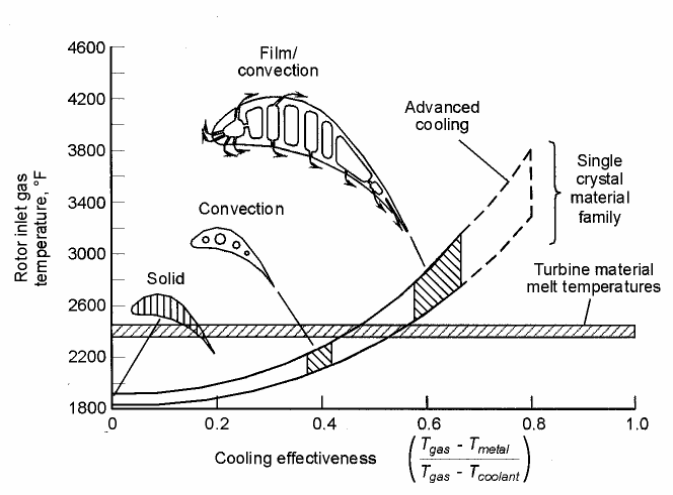

Figure 1-2 – Trends in turbine film cooling (Moustapha et al., 2003)

Due mostly to structural issues, discrete-hole film cooling is preferred over the historical slot injection film cooling for external cooling. The discrete-hole geometry leads to three-dimensional flow and temperature fields downstream of injection. Figure 1-3 illustrates a common employment of film cooling in turbine vanes and blades, as well as the endwalls or shrouds.

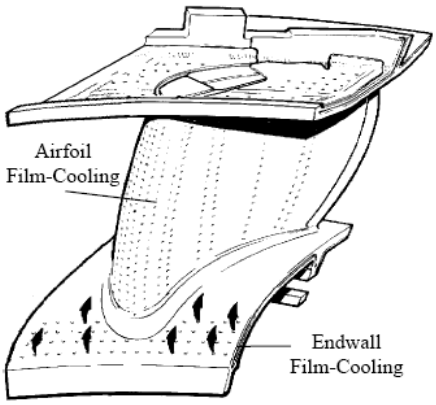

Figure 1-3 – Endwall and airfoil film cooling schematic

1.2 Film Cooling Effectiveness

Jet lift-off, high turbulence intensity in the shear layer and double counter rotating vortices are important features of film cooling cited by many researchers. The performance of film cooling is usually characterized by the non-dimensional adiabatic wall temperature (effectiveness) and heat transfer coefficient.

Heat transfer in engines is driven by the temperature difference $T_{aw} - T_w$. However, it is more convenient to examine a dimensionless form of this temperature difference. This dimensionless parameter is defined as the adiabatic film cooling effectiveness, η:

$$\eta = \frac{T_r - T_{aw}}{T_r - Tc} \qquad (1\text{-}1)$$

This parameter was discussed at length by Goldstein, 1971. He states that this adiabatic wall temperature is a function of the temperatures of the coolant and the mainstream, and that the assumptions that go into formulating equation (1-1) are that the film has low speed and constant

properties. Effectiveness is also dependent on the primary and secondary flows, as well as the position on the surface. The value of η varies from 1, at the point of injection, to 0, at large downstream distances. At the point of injection, T_{aw} approaches T_c, and far downstream, T_{aw} approaches T_m.

Goldstein also goes on to mention that the boundary layer of the mainstream is affected considerably by the injection of the coolant, as shown in analysis of various studies from the previous decades, as well as presenting numerous correlations developed in an attempt to predict numerically the behavior of η from the point of injection, through distances downstream, while interacting with the mainstream.

1.3 Motivation and Objectives

Film cooling is not only a product of engineers tackling the problems of keeping the metal surfaces protected from the hostile environment inside engines, it is also a concerted effort from other disciplines such as manufacturing and materials. Film cooling holes are manufactured using a wide array of techniques suited to specific locations on the vanes, blades, and shroud. One of these techniques involves EDM, electrical discharge machining. EDM works by eroding material in the path of electrical discharges that form an arc between an electrode tool and a work piece. In die sinking, the EDM machine uses a machined graphite or copper electrode to erode the desired shape into the part or assembly; this is true for shaped holes. To create a potential difference between the work piece and the tool, sometimes the part is submerged in a dielectric fluid which is circulated to flush away debris. Another technique that has gained wide use is LASER drilling, shown in figure 1-4. High power industrial lasers

such as Nd:YAG (neodymium yttrium-aluminum-garnet) drill holes very quickly and cost effectively. A combustor, for example, is made of several sheet-metal-formed parts with many thousands of holes with changing patterns, at multiple angles, and of different diameter (typically 0.4–0.8 mm). Percussion drilling, in which the laser beam pecks at the material, is one of the ways to work with such setup. Another technique used for drilling holes is abrasive waterjet. An abrasive material of controlled grading is embedded into the waterjet and is blasted through a nozzle to drill a hole. This technology is capable of producing shaped holes in hard to penetrate materials, including high strength alloys, ceramics or heat-sensitive laminates, yielding holes that are as small as 0.38 mm in diameter.

Figure 1-4 – A LASER drilling holes into a blade surface

As diverse as they are, all manufacturing techniques have shortcomings in the form of deviations from the desired hole shape, more specifically, in maintaining the uniformity of the cylindrical shape they are designed to produce. For example, all the previously mentioned techniques generate residues during the manufacturing process that must be flushed out of the holes. In waterjets, it's easy to imagine that the jet would lose some of its strength when drilling deep holes, requiring some adjustments as it goes deeper. Also, continuous use causes EDM

electrodes to wear out, requiring constant inspection. If there were a threshold of wear that the EDM electrode had to meet before being replaced, would that mean that the last hole the electrode makes will the same shape as the very first one? This line of thinking sparked the origin of this study. What shape does a cylindrical hole become if the tool that is used to drill it or carve it out is not uniform? What shape does the hole end up having if the entrance of the hole is continuously bombarded by debris being flushed out while production is undergoing? For a hole that is significantly deep compared to its diameter, this may mean a significant deviation in diameter from the point of insertion of the electrode to the exit of the hole, i.e. the exit area of the hole would be different form the inlet.

At the University of Central Florida, Dr. S. Bharani asked that question, and suggested a study of conical holes. In industry, these holes are not used because of reported difficulties in keeping the metering diameter uniform. However, industry does not run on perfectly cylindrical, smooth cooling holes. Thus, it was proposed that a study be made on the cooling effectiveness of conical holes of varying angles, and that the performance of these be compared to that of cylindrical holes. It was later suggested that to address the question of metering diameter, a set of conical holes with a cylindrical entry length also be made, so that the cylindrical part can act as a metering diameter.

The next chapter of this thesis presents a review of the literature on the subject of film cooling, cataloging concepts that will aid in understanding the collected data. Unfortunately, not much literature on the subject of conical cooling holes could be found. Three studies, mainly Cho et al. (1999), Yu et al. (2002), and Taslim and Ugarte (2004) were found having to do specifically with conical holes.

The present study is unique in that it concentrates on the conical hole geometry alone, and focuses on varying the diffusion angle over a modest range. The effect of such variation is shown in the light of discharge coefficients and laterally averaged effectiveness. The study also provides a hint into the effects of modifying the conical geometry, with promising results. The ultimate goal of this study is to provide useful information and new tools that will aid in the design process of film cooling holes for turbines, and any unforeseen future technology.

The objectives of this thesis are:

- to measure and explore the behavior of the discharge coefficient of conical holes of varying angles of diffusion over a range of pressure ratios
- to measure and study trends in span-averaged conical hole film cooling effectiveness and determine, if possible, the angle which provides the best protection
- to study conical holes with a prescribed entry length and its effect on the discharge coefficient and film cooling effectiveness versus pure conical configurations
- to attempt to provide a modest reference for conical diffuse holes in a sparse field of the open literature

CHAPTER 2

LITERATURE REVIEW

Over the past few decades, investigations have been performed by various researchers in order to understand the fundamental physics of film cooling, and to improve the technology in economical ways. The following studies have had an impact on the understanding of the physics of film cooling and provide insight into the interaction of the coolant and main-flow, as well as the importance of specific geometric features. Even though the literature on conical film cooling is sparse, these well established ideas still apply when studying conical holes. The majority of the studies discussed in this chapter have a direct bearing on the interpretation and discussion of results obtained in this thesis.

In the late sixties, Goldstein, Eckert and Ramsey (1968), published a study on film cooling effectiveness with discrete cooling holes. At the time, discrete film cooling was a novelty, at least in the open literature, and the complex interaction of the discrete jets with the mainstream and between them was not well understood, yet they were able to make far reaching conclusions from their data which apply even today. They showed some of the effects of Reynolds number on film cooling effectiveness, as well as the effect of inclination angle of the cooling holes. One of their major conclusions was that at low blowing ratios, the spreading of the jets is almost the same, and that an increase in the mass flow rate through the holes leads to an increase in the centerline effectiveness downstream of the holes.

In 1977, Pedersen et al. studied the effects of the density ratio on the film cooling effectiveness of cylindrical holes at an inclination angle of 35 degrees, with a pitch-to-diameter

(PI/D) ratio of 3, and holes of length-to-diameter ratio (L/D) of 40. The richness of data produced in this study would become a staple in the literature and a standard source for comparisons.

Following their example, Sinha et al. in 1991, expanded on the Pedersen paper and studied the effect of varying the coolant-to-mainstream density ratio (DR) over a range from 1.2 to 2.0. They used holes with 1.27 cm diameter, PI/D of 3, and L/D of 1.75. The large amount of data in their study allowed them to make some generalizations on the behavior of the jet interaction with the mainstream, mainly quantifying the momentum flux ratio, I, at which jet detachment occurs, as well as generalizations about the conditions for jet reattachment or complete detachment. They were also able to provide laterally averaged effectiveness values for their different blowing ratios. They concluded that increasing the mass flow rate causes the effectiveness values to fall off at a slower rate for attached jets. They also showed that detachment occurs at values of I greater than 0.3, but that the jets reattach quickly. However, as I is increased, the location of reattachment occurs further downstream, and that values of I greater than 0.7 lead to complete detachment. Figure 2-1 illustrates the concept of detachment. For cylindrical plates, the values of I also correspond to ranges of the blowing ratio, M.

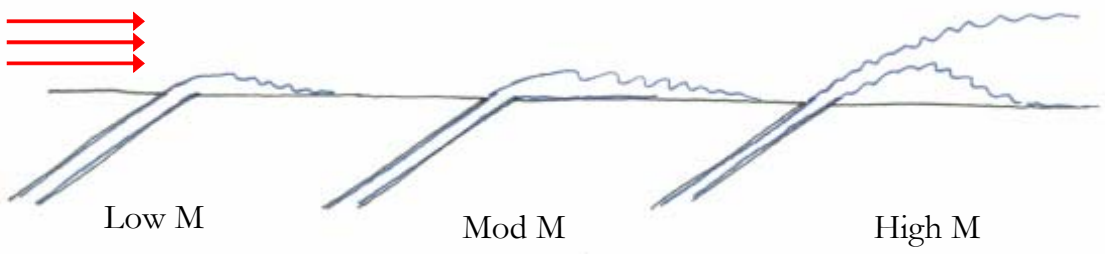

Figure 2-1 – Jet/film behavior at different blowing ratios

Sinha et al. also concluded that laterally averaged effectiveness is strongly dependent on the lateral spreading of the jets, a fact that would explain the quick rise in the use of fan-shaped cooling holes in the 1990's.

Lutum and Johnson, in 1999 noticed that although data were reported at similar blowing ratios or momentum flux ratios, there were always discrepancies and disagreements between studies when reporting values of film cooling effectiveness (η), especially laterally averaged η. They pointed out that early, high impact studies like Goldstein et al., (1968), Pedersen et al., (1977), and Sinha et al., (1991), show a wide range of length-to-diameter ratios (L/D), from 1.75 to 40. They theorized that L/D plays a significant role in the value of η, since L/D directly impacts the internal flow of the coolant holes. Up to this point, film cooling studies had concentrated on coolant flow ratios and gas path characteristics. So, they ran a study on 4-mm holes with L/D values of 1.75, 3.5, 5, 7, and 18. Unfortunately, their PI/D was 2.86, and not 3 like all the previous studies (this would cause their laterally averaged η to be slightly higher due to increased lateral coverage). Their blowing ratios went from 0.5 to 1.56. Their findings suggest that after an L/D of 5 and up, L/D does not greatly impact the value of η. The biggest changes in the value of laterally averaged effectiveness (η_{la}) were noticed between L/D of 1.75, 3.5 and 5, in which η_{la} increases 20 to 25% from L/D of 1.75 to 3.5, and even further from L/D of 3.5 to 5 for low blowing ratios. At the mid and high blowing ratios, holes with L/D of 1.75 and 3.5 behave similarly, but less effectively when compared to holes with L/D of 5 and higher. Although their study was ambitiously designed to tie in very important previous findings, their data did not compare well versus that of Sinha et al. This is an important fact that will be discussed in the results and conclusion chapters.

A major advancement in film cooling technology has been the change from round film holes to shaped film holes. Most commonly, all shaped holes applied in practice have fan-shaped diffuser exits with divergence angles between 10° and 15° on each side as well as on the side into the surface, with the great majority of studies utilizing axial holes with centerline angles (α) of 30° to 35°. Most shaped holes studied can be classified into one of four hole geometries, shown in figure 2-2, (i) classical shaped film hole that includes both lateral expansion, also known as fan-shaped, and expansion into the surface, also known as laidback, (ii) only lateral exit expansion, (iii) only laidback expansion, and (iv) a conical film hole that expands from inlet to exit equally in each direction around its centerline. In actual application geometry (i) is very common because of performance and ease in manufacturing, while (ii) and (iii) are not widely used as it is difficult to produce the pure single angle expansion direction in these cases.

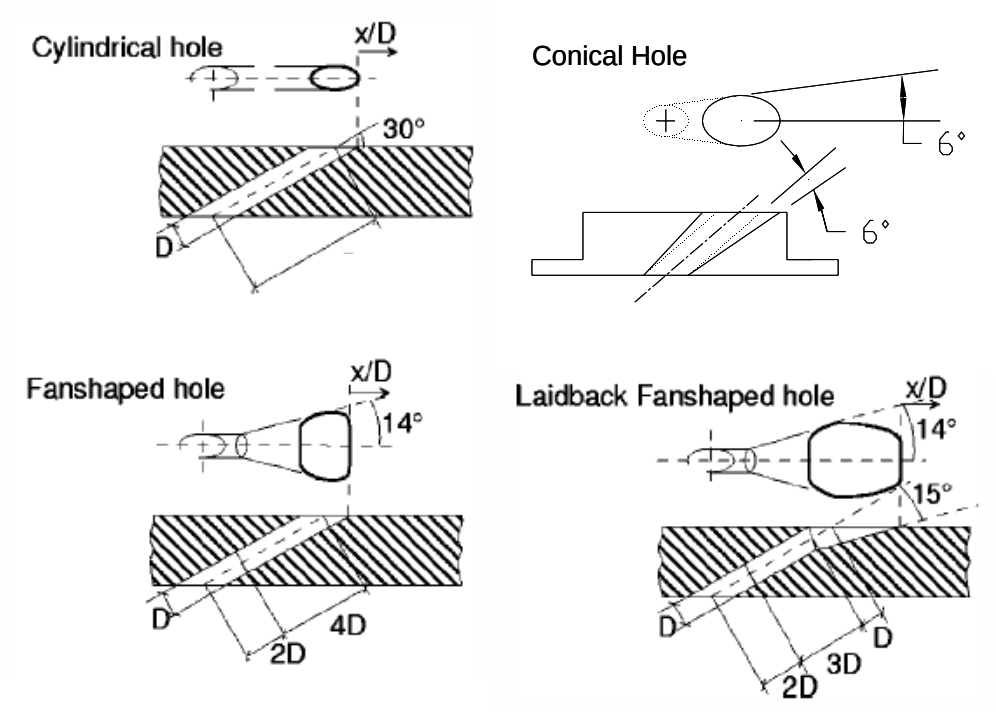

Figure 2-2 – Film cooling-hole configurations (hatched diagrams from Saumweber et al. 2003)

Investigations reported in a lower compressible flow range by Thole et al. in 1998 on a single hole test set-up indicated that by expanding the exit of the cooling holes, both penetration of the cooling jet and the intense shear regions are significantly reduced relative to a round hole. They observed that the peak turbulence for the fan-shaped holes was located at the exit of the cooling hole resulting from the expansion angle being too large, while for the round hole it was located downstream of the hole exit where velocity gradients were very large. Gritsch et al. also in 1998, using the same set-up, presented the adiabatic effectiveness distribution at Mach numbers of 0.3, 0.6 and 1.2 and the coolant passage Mach numbers of 0 and 0.6. They also observed higher effectiveness values for holes with expanded exits. Moreover, the effectiveness values were higher with a free-stream Mach number of 1.2 than when the free-stream was subsonic.

More recently, in 2003, Dittmar et al. assessed the performance of various cooling hole shapes, including compound angle fan shape. They reported that at low blowing ratios all the hole configurations showed similar film-cooling effectiveness, while at higher blowing ratios the fan-shaped holes out-performed the others. By the end of the 1990's, the impact of slowing down the momentum of the coolant was well understood and the use of shaped holes to achieve this was well established in industry. It is not surprising that a major study by Goldstein et al. back in 1974 had shown that with flared holes, the lateral spreading of jets over blade surfaces was enhanced, and concluded that slowing down the jets through diffusion in the flares, allows higher injection rates before jet liftoff occurs. Even so, in the 1990's the subject of conical holes as a means of diffusing jet momentum was not popular because of concerns about metering diameter and unpredictability about quality in manufacturing such geometry.

However, some conical hole studies did become available back then, such as a limited study by Camci and Arts (1990), as well as a study by Hay and Lampard (1995) investigating the discharge coefficient of two flared hole configurations with a cylindrical starting length. The importance of the latter study is that, at the time, there was not much literature focusing solely on conical geometry. Hay and Lampard arrived at a number of conclusions including that the C_D of flared holes is higher than that for cylindrical holes. This would offer the advantage of a smaller pressure drop requirement for a given flow rate, at the same time helping to reduce the momentum of the jet at the exit, which in turn would improve film cooling performance. This improvement in C_D is most visible at lower pressure ratios. The study also concluded that the cylindrical entry length "should be at least 2 diameters long and preferably 4 diameters. This allows flow to reattach to the walls of the hole before entering the flare, thereby improving the diffusing effect of the flare." The conclusions reached in their study were of particular pertinence to the design of the test geometry for the present study, since it provides guidelines for entry length geometry, as well as expectations for the values of C_D.

Another case of conical diffusion research is the flow visualization study presented by Haven et al. in 1997 on fan-shaped and conical holes for a blowing ratio of 1.0. It was observed that the so-called anti-kidney flow structure with vortices was developing in the opposite sense for diffusing holes to those associated with cylindrical holes. It was also observed that kidney vortices tend to separate the cooling fluid layer, potentially leading to lower film effectiveness downstream.

In 2001, Cho et al. studied two geometric configurations involving conical holes with entry lengths, following guidelines set by Hay and Lampard in 1995. The study involved a purely conical hole with diffusion angle of 4 and L/D of 8.1, half of which was the cylindrical

entry. Although their findings are not specifically of use to the present study, since they concentrated on near-hole local effectiveness and heat transfer coefficient, they did conclude that the "penetration of the jet is reduced and higher cooling performance is obtained even at relatively high blowing rates because the increased hole exit area reduces hole exit velocity."

In 2002, a study by Yu et al. attempted to reduce the momentum of the injected flow while still trying to cool far downstream. Their idea involved a cylindrical hole at a 30 degree inclination, with L/D of 10 compared to two other similar geometries: downstream flared (laidback) and laidback with lateral flare. The flares occurred very close to the hole exit (L/D = 0.8). Their results suggest that the lateral expansion is a more effective mechanism to increase η. That same year also produced a very ambitious study by Baldauf et al. In their paper, they provide a correlation for film cooling η based on an extensive systematic study into the effects of blowing ratio, density ratio, mainstream turbulence intensity, inclination angle of the coolant holes, pitch to diameter ratio, and L/D on the value of η, conducted with infrared thermography, in conjunction with CFD analysis. While their study does not provide conical hole data, many of the parameters they isolated and investigated are important to the present study. Their discussion of the effect of the blowing rate on η is very insightful. In addition, the extensive amount of data generated in their publication provides many opportunities to compare results with the present study.

Saumweber el al. in 2003 studied the effects of turbulence on film cooling with shaped holes and found that cylindrical and shaped holes show different behavior under turbulent conditions. Moreover, they found that increased turbulence is detrimental to the performance of shaped holes. They also mentioned cases in which turbulence in the areas between the holes, downstream of the exits, increases effectiveness between 50% and 100% solely because of the

accelerated spanwise diffusion. Their findings showed that low levels of turbulence allowed shaped hole jets to remain attached, even at higher blowing ratios; and that for shaped holes that are close together, increased levels of turbulence actually reduce the effectiveness, since at the exit, the jets begin to interact immediately, and that high turbulence only does not help, at the very least.

One of the most recent studies involving conical holes was performed by Taslim and Ugarte in 2004. They studied C_D for a 7 degree diffusing conical hole at various inclination angles for a very large range of pressure ratios, from 1 to 5. They showed that at higher pressure ratios, conical holes have higher C_D than cylindrical holes and that lower inclination angles lead to decreases in C_D.

In 2005, Gritsch et al. conducted a study on shaped holes in order to determine the effect of isolated geometric parameters such as AR, coverage/pitch (C/PI), PI/D, L/D, and compound angle. The wealth of data provided by their paper provides a great source of parameters for comparison in the present study. Their findings however, suggested that varying the above mentioned parameters did not yield significant changes in film cooling effectiveness. For example, they changed AR from 3.5 to 4.2 to 4.7, without noticing any significant changes; they cautioned, though, that maybe within that range, the variation has no effect.

The review of current literature reveals that very sparse investigations have been done on film cooling effectiveness for uniformly diffusing conical holes. To extend the limited understanding of effectiveness with conical holes, the present study was carried out with a single row of holes and five different configurations, DA1, DA2, DA3, DA6 and DA8, having uniform diffusion angles of 1, 2, 3, 6, and 8 degrees, respectively. Results are compared with a row of 8 nominal cylindrical holes (DA0), as well as a modified configuration of a three degree conical

hole with a four diameter entry length. Investigations were performed in a range of blowing ratios, with the density ratio held constant at 1.26. The choices for the investigated geometric parameters, blowing ratios, and other details are based on previous studies of cylindrical holes, and are explained in the next chapter.

CHAPTER 3

EXPERIMENTAL SETUP

3.1 Test Conditions

Tests were conducted in the Basic Film Cooling (BFC) rig in the Engineering Field Lab facilities located on the main campus of the University of Central Florida. The rig operates at a temperature of 68 ± 1°C and a Mach number of 0.14 at the test section. The operating temperature is mainly dictated by the blower, which does work on the air mass, thus heating it up. Freestream turbulence intensity is less than 1% at the test section. Having a tunnel that is closed loop led to the choice of nitrogen as a coolant, which keeps the density ratio at 1.26. One major advantage of using this particular wind tunnel is that its test section walls are made of Plexiglas, a clear material adequate for optical data acquisition, the principal method used in this study.

3.2 The Basic Film Cooling Rig

All measurements were performed in the Basic Film Cooling rig, shown in Figure 3-1. The rig is a closed loop system capable of operating around the clock.

Figure 3-1 – Photograph of BFC rig (foreground)

The BFC rig can be divided into five sections: 1) the blower, 2) flow conditioning, 3) test section, 4) the grommet, and 5) the diffuser and the re-circulating apparatus. Figure 3-2 shows a schematic of the main components of the BFC rig.

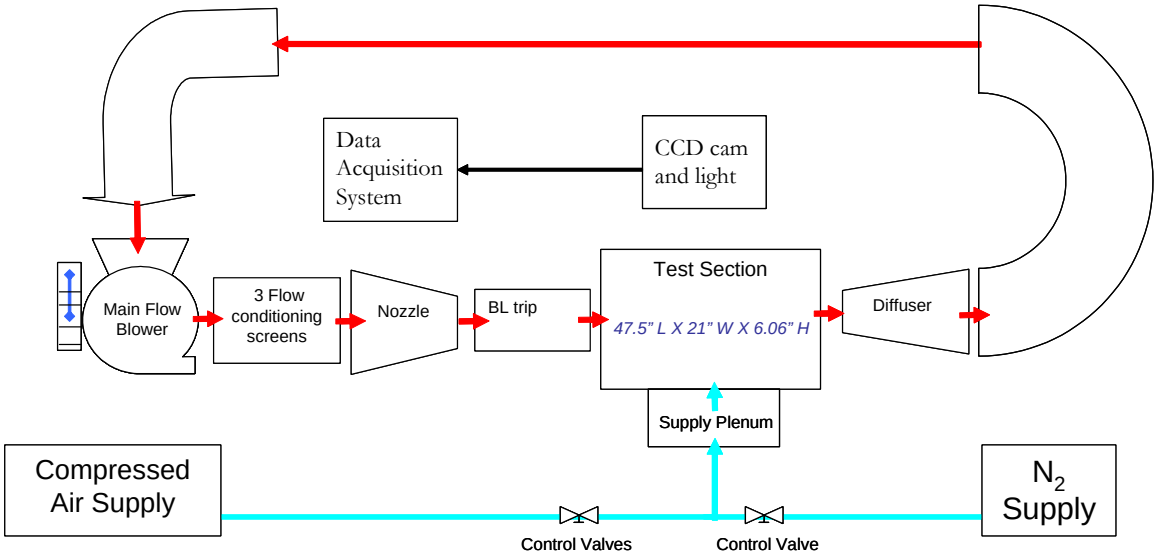

Figure 3-2 – BFC rig schematic

3.2.1 The Blower

The freestream air inside the rig begins at room temperature. It is recirculated and slowly heated by a 15-kW blower. This blower is capable of supplying air at a rate of 4.72 m^3/s, yielding a velocity of 52 m/s at the test-section inlet. It normally takes about 3.5 hours for the freestream air to heat up to 68 °C. However, to ensure that the tunnel wall temperature is close to the freestream air temperature, the tunnel is allowed to warm up an extra half hour. The difference in temperature between the wall and the freestream is monitored with a thermocouple encrusted in the floor of the test section, but close to the surface exposed to the mainstream. After the period of 4 hours, this difference in temperature is less than 1.5 °C and does not change more than 0.1°C in 10 minutes; the tunnel is considered to have reached steady state. Figure 3-3 shows the casing for the blower.

Figure 3-3 – Blower casing with motor

3.2.2 Flow Conditioning and Nozzle

Immediately downstream of the blower is the flow conditioning section, which consists of a honeycomb and three screens. Figure 3-4 shows the setup of the screens and the nozzle. The tunnel, at this point, has a cross-section 44.5 cm high by 53 cm wide. The honeycomb screen is 12.7 mm thick and is followed by the three remaining fine wire screens, spaced at 8.9-cm intervals. Following the screens is the start of the 2-dimensional Plexiglas nozzle. This nozzle contracts from a cross-section height of 44.5 cm to 16.5 cm, over a length of 73.7 cm, while keeping the cross-sectional width constant.

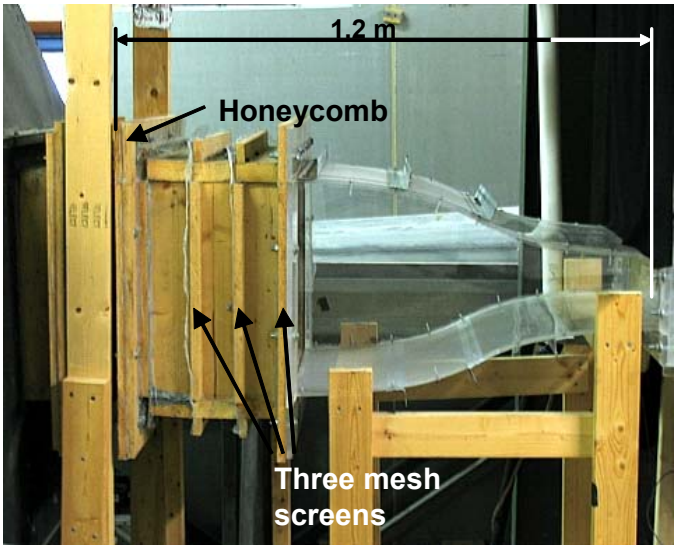

Figure 3-4 – Flow conditioning screens and nozzle

3.2.3 The Test Section

The exit of the nozzle leads to the test section, which is made up of 12.7-mm thick transparent Plexiglas panes. It has a length of 1.2 m, 53-cm width, and 15.4-cm height. The top Plexiglas pane is removable for easy access and cleanup during preparation of the test subjects,

and is sealed with weather-stripping and is clamped during tests. At the bottom surface of the test section, in the center, there is a 2.54-cm by 8.9-cm slot for the test coupons. Figure 3-5 shows in detail the internal components of the test section, as well as the outside insulation.

In order to provide stability and rigidity to the test section, a second pane of Plexiglas was installed underneath the original bottom pane. It has the same dimensions as the original pane (now called upper pane), and provides a layer of sealing in order to prevent leakage into the test section while this runs at sub-atmospheric pressure. The major difference between the lower and upper floor panes is that the lower pane has a 40.6-cm disk cutout in the center. This disk cutout has been replaced with a stainless steel disk. The stainless disk has a built in support system of tabs in order to hold the test plates rigidly and prevent warping during tests. The main purpose of the disk, besides holding the coupons in place, is to provide rigidity to the upper acrylic plane. In order to accomplish this, a pattern of holes was drilled into the upper pane and through the metal disk to press both tightly. The stainless steel in the disk has also been kept separated from the upper Plexiglas pane by an air gap and weather-stripping, which assures that there are no large conduction effects influencing the upper pane of the test section bottom. Additional measures were taken in order to prevent thermal leakage, such as installation of two layers of 25-mm thick insulation along the bottom of the test section and around the plenum.

Before running a test, the test coupons are inserted from under the test section into the slot, and are supported by the grommet. The layer of temperature sensitive paint, TSP, discussed in section 3.4.2, lies downstream of the coupon slot.

Figure 3-5 – Detail of test section as seen from above

3.2.4 The Grommet

Under the test-section, directly in the center are located the plenum and grommet. These two components are integral parts of the support and sealing of the test subjects. The plenum is discussed in 3.3.2. The grommet is an aluminum sleeve whose primary function is to press the coupon tightly against the bottom of the stainless steel disk, through the slot in the test section floor. The grommet's shape can be best described as a hollow prism 10.16-cm long, 3.8-cm wide, and 2.54-cm high, with walls 6.35-mm thick. It is hollow along the long and wide dimensions, with a tab at the bottom extending 2.54-cm outward along the perimeter. This tab had six holes drilled for the purpose of screwing the grommet to the metal plate while holding up the test coupon, i.e. the coupon is sandwiched between the grommet and the metal plate and has only its top surface inside the actual test section. For a more descriptive representation, please

refer to figure 3-6. In order to avoid contact between the grommet and the test coupon, a layer of weather-stripping 1.5-mm thick is applied to the lip of the grommet and also over the tabs. This weather-stripping also assures that there is no leakage of coolant between the grommet and the test coupon. The inner surfaces of the grommet are also lined with 12.7-mm thick Rohacell, a rigid, rough porous material that provides insulation for the coolant as it flows through the inner part of the grommet, and prevents it from picking up heat as it approaches the coolant holes.

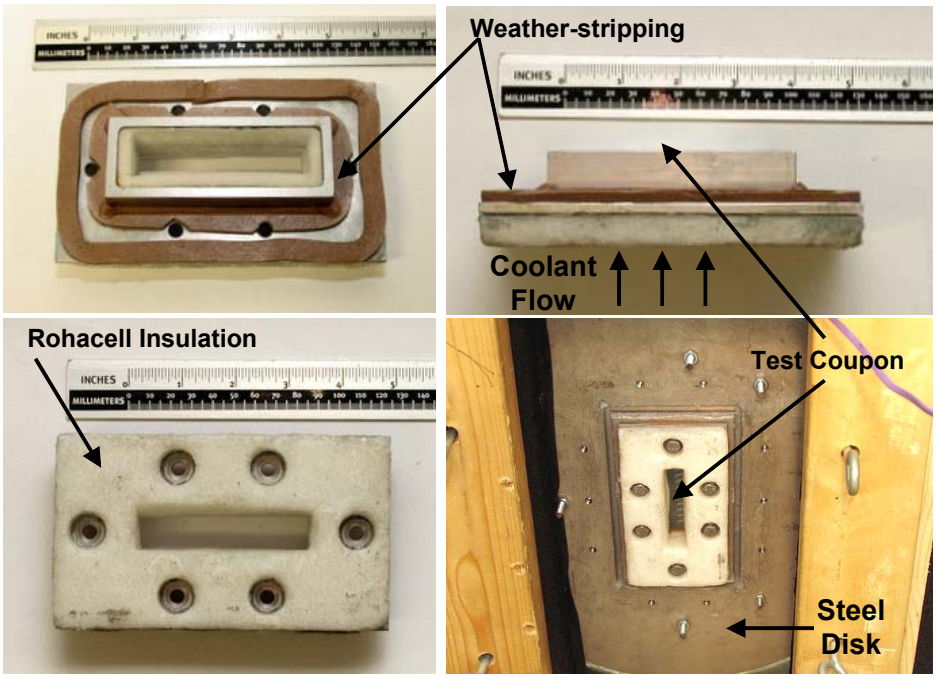

Figure 3-6 – Grommet placement, support and function

The immediate volume under the test coupon is considered a smaller supply plenum. This smaller plenum is 17-mm long (in the direction of the main flow), 67.5-mm wide and 31-mm tall. The bottom surface of the grommet is also insulated with 2.54-mm thick Rohacell, ($k = 0.02$ W/m·K) since allowing the coolant to come into direct contact with this area, which does warm up during testing, would contribute to heat leakage from the test section.

3.2.5 The Diffuser and Flow Recirculation

Once the flow has made it through the test section, it goes through a diffuser. The diffuser is a wooden 2-dimensional-flow structure which allows the flow to recover pressure. This diffuser is 2.22-m long and with an area ratio of 3.5. The exit of the diffuser leads to an elbow in the tunnel, which begins the recirculation process. After this bend, the flow continues through a duct with a 0.4-m^2 square cross-section and a length of 4.6 m. At the end of the square duct lies another bend. This is a 90° bend redirects the flow back into the blower. Figure 3-7 shows the diffuser and the structures used to turn the flow.

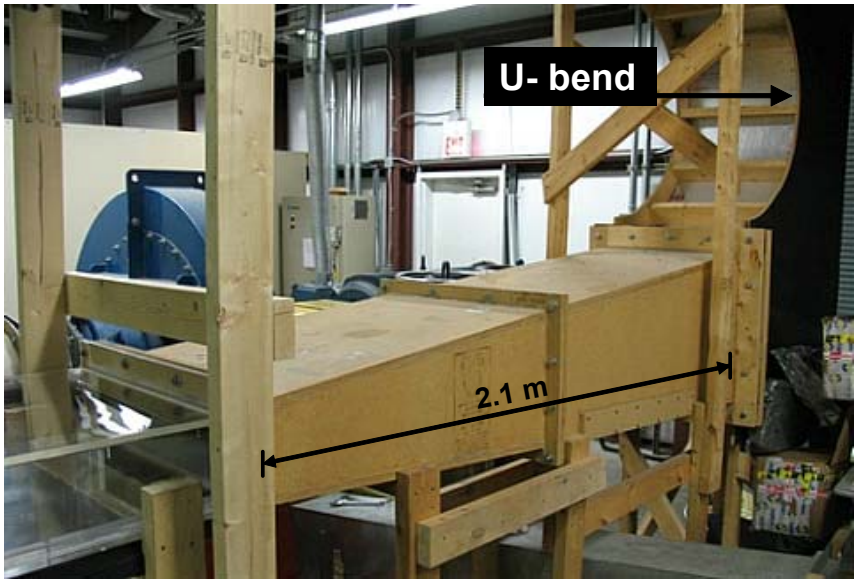

Figure 3-7 – Diffuser and flow recirculation detail

Before reaching the blower, there is a slot on the side of the tunnel that allows for the insertion of filters or other obstructions for the purpose of "tuning" the speed of the flow. For the present study, there are six small wooden pieces that keep the speed of the flow at about 52 m/s.

3.3 Test Coupons and Cooling System

3.3.1 Test Coupon Design

The test subjects in this investigation are acrylic coupons with different hole geometry configurations. All coupons were machined to have the same size and shape and fit snugly in the test section slot.

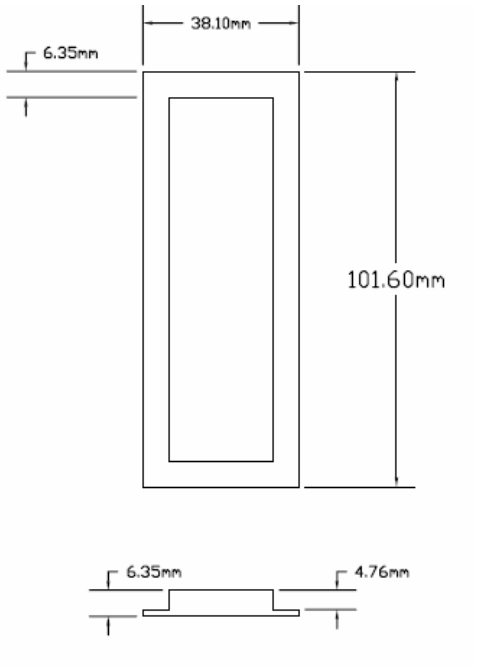

Figure 3-8 – Basic test coupon design (top- and side-views)

The test section was designed for specific objectives in mind by other researchers and its structure was not meant to be easily changed. This meant that basic dimensions such as the coupon's length and thickness had restrictions which could not be changed without major changes to the rig. Figure 3-8 shows the basic coupon dimensions that are meant to be used in the slot at the bottom of the test section.

In this study the focus is on two configurations: Coupons with pure conical holes of increasing diffusion angle, and coupons with conical holes with a cylindrical entry length. Many parameters had to be considered in designing the acrylic coupons, but there was also the need to compare the results to published data. To this effect, considered when designing the holes were: test section setup geometric restrictions, hole inclination angle, diameter (D), length-to-diameter ratio (L/D), pitch-to-diameter ratio (PI/D), and coolant system capacity.

It was found that the most important parameter when starting the design of the coupons is the inclination of the holes with respect to the direction of the flow. Common angles used in the literature are 30, 35 and 45 degrees. Careful analysis of literature testing conditions, and blowing ratios led to the choice of the 35° geometry. The next things to consider were the geometric constraints of the rig itself. For example, holes of 1.27 cm diameter and an L/D of 1.75 were used in Sinha et al.'s paper, and while the coupons can accommodate the L/D of this test, they cannot have holes of that diameter, they are simply too big. We decided to keep the L/D of 3.5 as in the study by Lutum and Johnson in 1999. From then on, the thinking process for deciding the rest of the parameters is as follows: the test coupons have a thickness of 6.35 mm, which implies that at an angle of 35°, the length of the holes would be 11.11 mm, this means the diameter of said holes would have to be 3.175 mm to keep an L/D of 3.5. These dimensions were deemed appropriate. Next for consideration was the pitch-to-diameter ratio (PI/D). Pitch is the distance between the centerlines of the holes, which is commonly measured in terms of multiples of the diameter. Figure 3-9 illustrates the concept of PI/D for cylindrical holes, in which the exit diameter is the same that for the inlet. A common value for PI/D is 3, that is, the pitch is 3 diameters long. Thus, picking an angle of 35° helped in deciding most of the dimensions of the coupon holes. The number of holes per coupon was chosen so as to have the

most holes in a row, without compromising the structural integrity of the coupon itself, which yielded a number of 8 holes per coupon. Having 8 holes also meant having a larger amount of area from which to collect information.

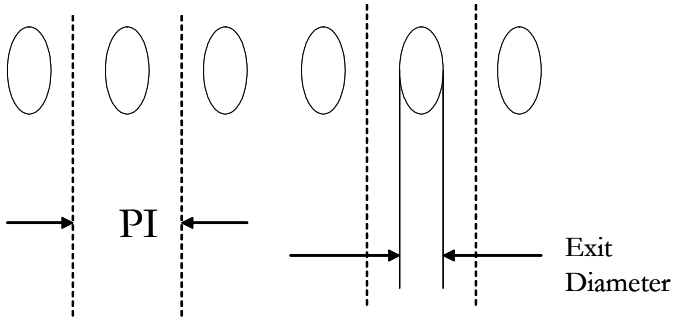

Figure 3-9 – Pitch-to-Diameter ratio, PI/D

The next step was deciding the conical angles of the holes. The concept of the conical holes and studying trends as the angles changed had been suggested long before this work by a colleague. Discussions with the author's advisor led, at first, to choosing angles of 1°, 2°, and 3°, and also a reference angle from the literature. In this case, the most convenient would be a coupon with perfectly cylindrical holes, i.e. a coupon with 0° diffusion. Having decided, these plates were manufactured and studied. A decision was later made to continue the observed trends and to build plates with 4°, 6° and 8° conical holes. Since the original configuration was purely conical, meaning it has a diffusing shape from the beginning of the hole to the exit, it was also decided to test a configuration in which the conical hole begins after a certain cylindrical "entry length." The study by Hay, and Lampard (1995) suggested that the shortest entry length used should be no less than 4 diameters long in order to make sure the flow is attached to the walls of the cooling hole. Following their suggestion, the new holes were designed to have a cylindrical entry length of 4 diameters, followed by a conical diffuser of 3.5 diameters. The diameter value would have to be changed in order to keep the plate dimensions the same. The

overall L/D of these holes was now 7.5, so keeping the same plate thickness would lead to a hole diameter of 1.476 mm. Due to difficulties mentioned by machinists for manufacturing the 1.476-mm holes, it was decided that the diameter would be kept at 2 mm. Adjustments were made and the thickness of the test coupon was changed to 8.6 mm, without compromising the seal of the test section. The smaller hole configuration led to a smaller pitch, but same PI/D. With the smaller pitch, the number of holes was changed to 12. It was then decided that only a specific geometry should be studied to see if the entry length would have a big effect on the results. The 3° (DA3) configuration was chosen, a choice in the middle of the range of the conical set. This coupon's holes were to have a 2-mm diameter, a cylindrical section of 4 diameters length, followed by a conical diffusing section, 3.5 diameters long, at a diffusion angle of 3°. Also, in order to have some reference with which to compare these results, a coupon with purely cylindrical holes of 2-mm diameter was designed. These two coupons were also manufactured and studied for the present work. The only exception being the 4-degree configuration, which was manufactured unsatisfactorily, and thus not included in this study.

The following figures and tables summarize the dimensions of the test coupon configurations and show their manufactured counterparts.

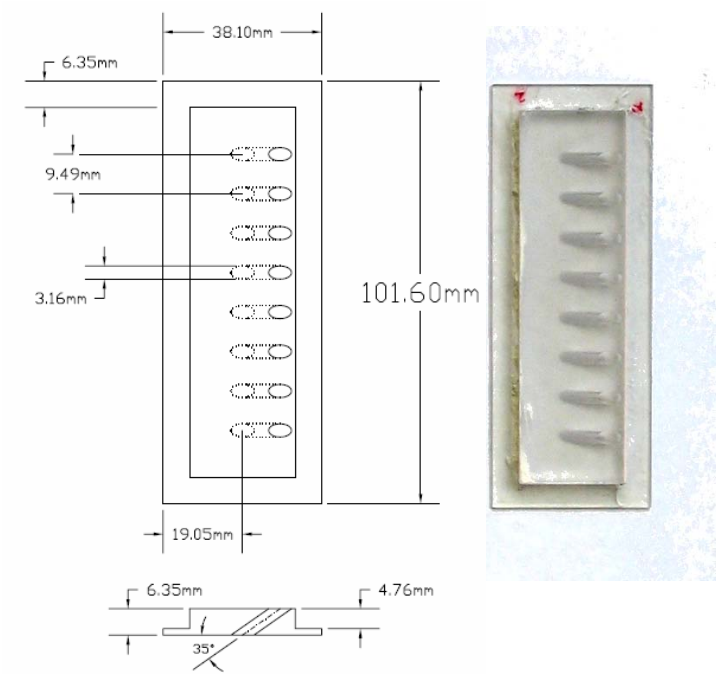

Figure 3-10 – Nominal cylindrical hole coupon (DA0) design vs. manufactured piece

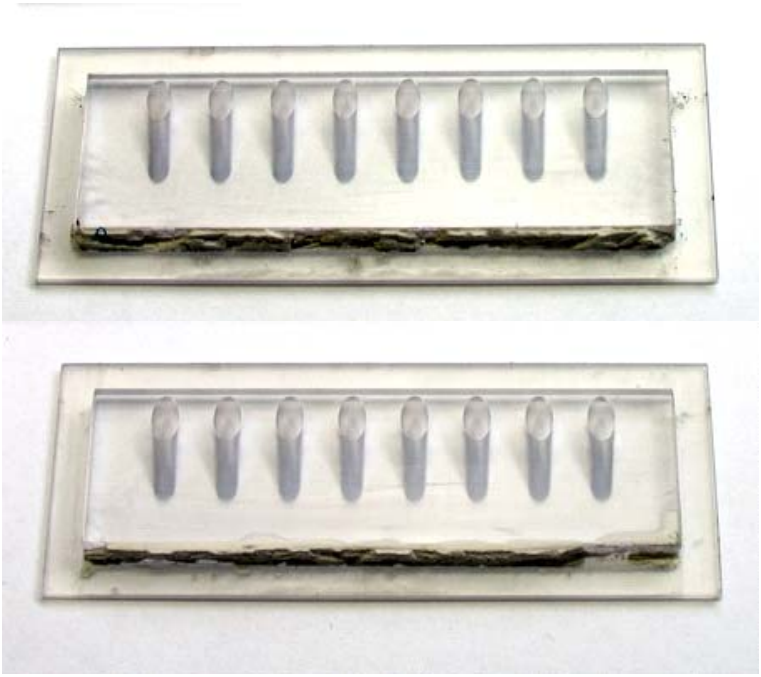

Figure 3-11 – Comparison of DA1 (top) and DA2 manufactured coupons

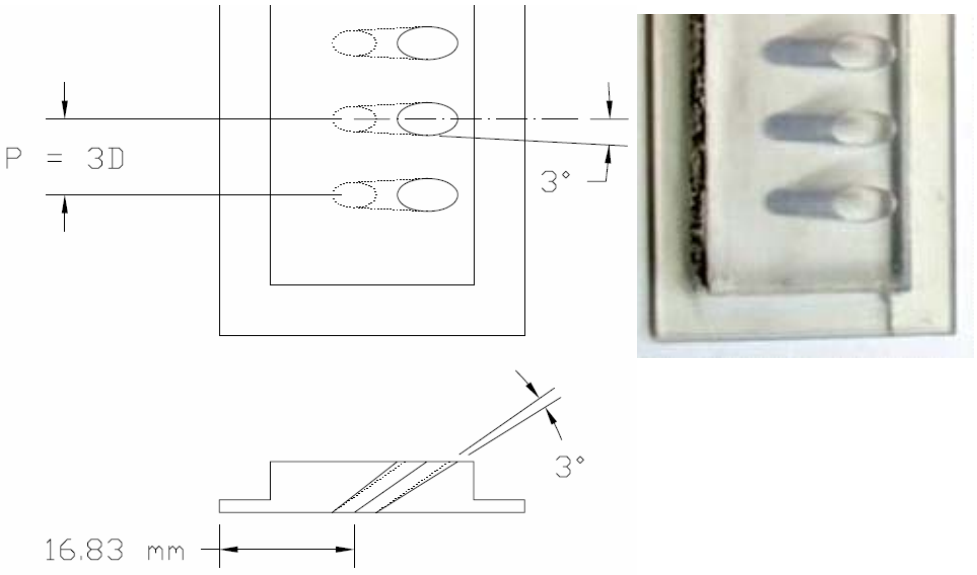

Figure 3-12 – Detail of DA3 schematic vs. manufactured piece

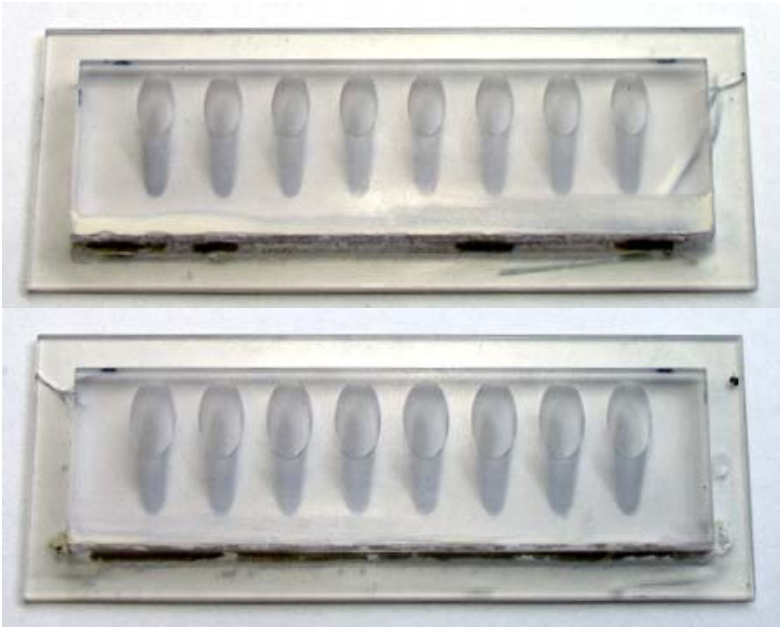

Figure 3-13 – Comparison of DA6 (top) and DA8 coupons

3.3.2 The Plenum

A plenum is an enclosure in which a fluid is kept at a pressure different from the ambient. In the context of fluids experiments, a plenum should also homogenize the flow's properties, such as pressure, velocity and temperature, in order to avoid impingement on the test coupon, or bringing in other sources of error. For our current test, the plenum's functions are multiple: it guides and stabilizes the coolant before it goes into the coupons and ultimately into the test section, and homogenizes the flow, all while providing housing to the instruments used during testing. The plenum, shown in figure 3-14, is shaped as an open box, with walls 12.7-mm thick. It is made of Plexiglas, which is also an insulator, and works to keep the coolant from picking up heat as it makes its way out of the cooling circuit. The dimensions of the plenum box are: 17.75-cm wide, by 10.16-cm long, by 16.5-cm high. At the main opening, the plenum has short tabs 6.4-mm thick which match the grooves in the stainless disk. These grooves are filled with silicon for extra sealing when the plenum is put into place for testing. For support of the plenum, there are four acrylic tabs extending outward at the top. These tabs, much like the grommet's tabs, have screws which hold the plenum up firmly against the stainless plate.

Inside the plenum, at half the depth, there is an acrylic plate across the entire cross-section, held in place with epoxy. This acrylic plate is 12.7-mm thick and divides the plenum in two. The acrylic plate has an array of 5-mm diameter "pinholes" which act to straighten the coolant flow. Coolant is supplied though a 12.7-mm opening at the bottom wall of the plenum box. But, before going through the pinhole plate, the flow must go through a small acrylic box which has pinholes only through the side walls, located at the bottom of the plenum. This pinhole box forces the coolant to go only sideways. Allowing the coolant to shoot straight up

through the plenum undisrupted, would make the flow impinge on the test coupon, giving uneven flow from the cooling holes. Once the flow comes out of the pinhole box, it must flow vertically through the pinhole acrylic plate, straighten up and finally pass into the smaller plenum between the walls of the grommet, and out the cooling holes. The instrumentation housed by the plenum is critical for the current work and is discussed in section 3.4.

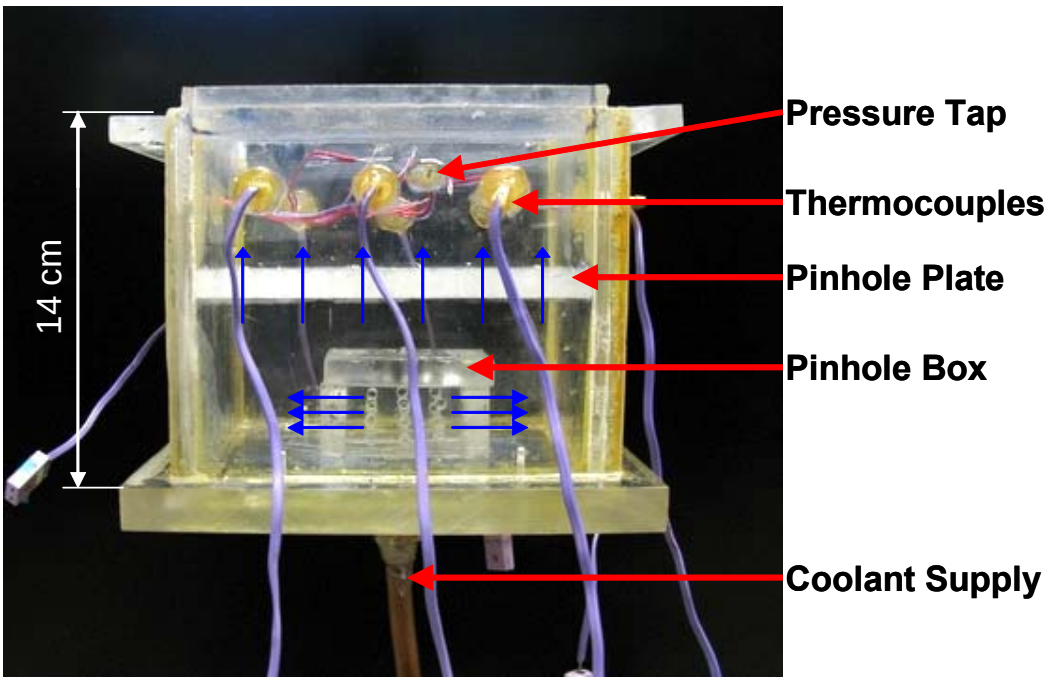

Figure 3-14 – Supply plenum (blue arrows indicate coolant flow)

The plenum is supplied with either air or nitrogen during testing. Both gases are supplied from different sources, but share some of the same circuitry leading them to the plenum. Figure 3-15 shows a schematic of the supply for both gases, as well as the parts they share in common.

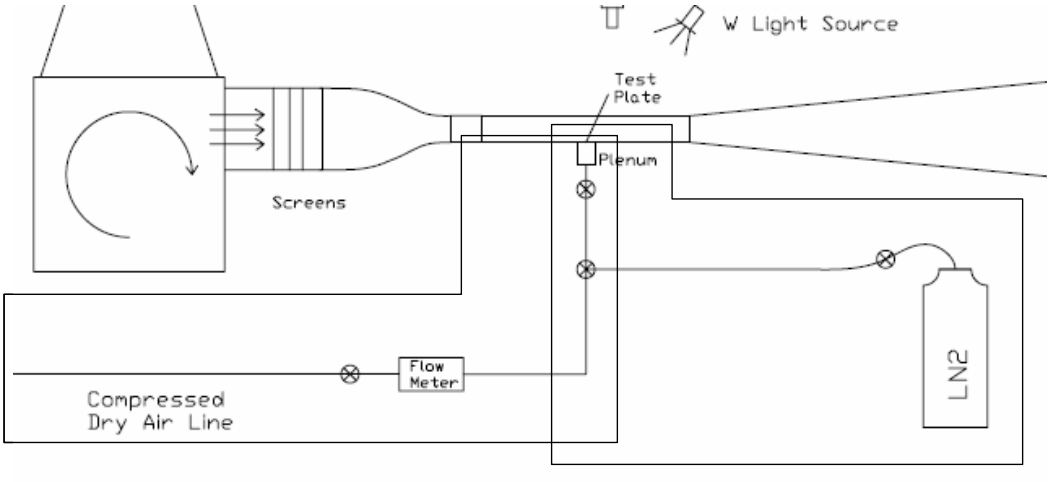

Figure 3-15 – Air supply and nitrogen supply circuits

3.3.3 Air Supply

For the discharge coefficient tests, the coolant used is air. Air is supplied to an 8.5-m^3 tank by a compressor, equipped with a dryer and filter. The air is also circulated through a ZEKS condenser, which further eliminates humidity from the tank. The air is then circulated through 21 meters of 8.5-cm pipe in order to bring it to the BFC rig. Once the 8.5-cm pipe reaches the rig, it is reduced to a 1.27-cm copper pipe, which is connected to a flowmeter and then the plenum. There are a total of five valves in the air's path before reaching the plenum. The air supply system is shown on the left in figure 3-15.

3.3.4 The Nitrogen Supply

For the film cooling effectiveness tests, the coolant used was nitrogen gas. Nitrogen gas is obtained from the boil off of liquid nitrogen contained in dewars (large storage, vacuum-insulated tanks) commonly at 1.62 MPa. Using a system of valves, and liquid nitrogen's natural thermal instability, gas flow is obtained at controllable rates. The temperature at which the gas exits the vessel depends on the mass flow rate of the gas; the larger the amount being released, the colder the gas temperature. If a large enough amount of gas is released continuously, the resulting outflow will be liquid. Therefore, while running a test, in order to achieve nitrogen gas flow at a desired temperature, the mass flow rate must be monitored.

Nitrogen gas exits the tank through a main-flow control valve and into an insulated 1.27 cm diameter copper pipe. The copper pipe runs an approximate length of 7 meters before reaching a t-junction. The t-junction allows the diversion of excess nitrogen into the ambient. For example, if the plenum is to be kept at 1.723 kPa-gage, but the nitrogen gas is flowing out of the tank at a rate that would keep the plenum at 3.45 kPa-gage, then the excess gas must be diverted, or the flow from the tank should be reduced. Reducing the amount of flow from the tank, would warm the flow of the nitrogen gas, therefore this is not an acceptable option. Thus, at the t-junction there is a valve to allow for the release of excess gas, while keeping the plenum at the desired conditions of pressure and temperature. Two meters after the t-junction, the nitrogen flows through the plenum valve and into the plenum. For a detailed view, please refer to figure 3-15.

3.4 Instrumentation

In order to capture the conditions in the BFC rig as well as those of the coolant in the plenum and the temperature distribution downstream of the film cooling holes, the following instruments were used:

3.4.1 Thermocouples

Type E thermocouples were placed in multiple locations of the BFC rig and the plenum in order to capture the temperature of the mainstream and the coolant while the rig warmed up, and while TSP images were being captured. Figure 3-16 shows the location of the thermocouples.

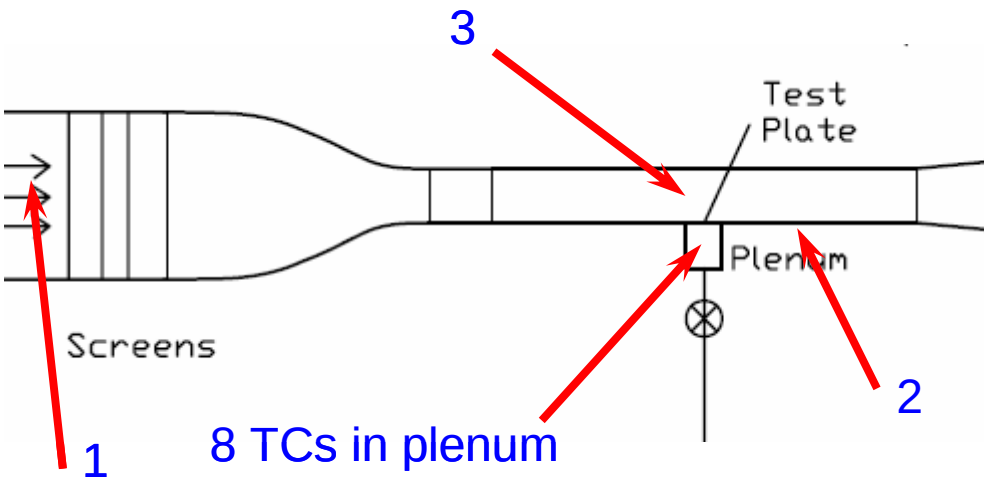

Figure 3-16 – Location of thermocouples in BFC rig

The thermocouple in location 1 was used primarily to measure the mainstream temperature. This temperature started at about 25 ºC and could reach up to 69 ºC in 2.5 hours. The thermocouple in location 3 was also used to monitor the temperature of the mainstream, but

it always registered the same temperature of location 1, so it was seldom used. The thermocouple in location 2 was used to monitor the recovery temperature of the test section floor. While the mainstream could warm up in as little as two hours to 62ºC, location 2 took longer to catch up to the mainstream temperature, and this was by design. A hole was drilled through the metal disk and the acrylic in the test section floor, and the thermocouple was inserted. Care was taken to place the thermocouple just inside the surface of the acrylic. The material in which it is embedded is putty. The temperature reading takes approximately three and a half hours to stabilize since the rig heats up very slowly. When steady state is reached in the rig, the difference between the temperature registered on the floor of the test section and that of the mainstream becomes about 1.5 ºC and remains quite steady throughout the test. The uncertainty in measurements with these thermocouples is 1.0ºC.

3.4.2 Temperature Sensitive Paint

Uni-coat Temperature Sensitive Paint, TSP, formulated by ISSI, is used in this study. The effective temperature range is 0-100 ºC, beyond which the temperature sensitivity of TSP becomes weaker. It is packaged in aerosol cans and can be applied easily with a spray. After it is heat treated above 100 ºC for 30 minutes the temperature sensitivity of the paint is about 0.93ºC, (Liu, 2006). The TSP painted surface is smooth. The emission spectrum of TSP is shown in figure 3-17. An optical 590-nm long pass filter is also used on the camera to separate the excitation light and emission light from the paint.

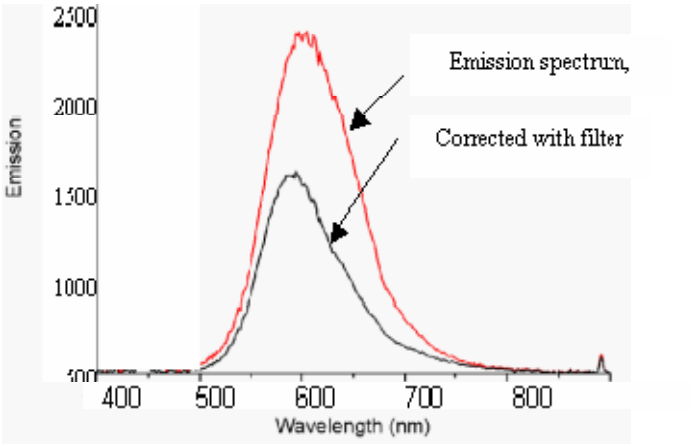

Figure 3-17 – Emission spectrum of TSP (Liu, 2006)

TSP incorporates luminescent molecules in paint together with a transparent polymer binder. Light of the proper wavelength is directed at the painted model to excite the luminescent molecules. The sensor molecules become excited electronically to an elevated energy state. The molecules undergo transition back to the ground state by several mechanisms, predominantly radiative decay (luminescence). Sensor molecules emit luminescent light of a longer wavelength than that of the excitation light. The appropriate filters can separate excitation light and luminescent emission light, and the intensity of the luminescent light can be determined using a photodetector. The excited energy state can also be deactivated by quenching processes. Through two important photo-physical processes known as thermal- and oxygen-quenching, the luminescent intensity of the paint emission is inversely proportional to local temperature.

In principle, a full spatial distribution of the surface temperature can be obtained by using the TSP technique. Figure 3-18 shows a typical TSP set up.

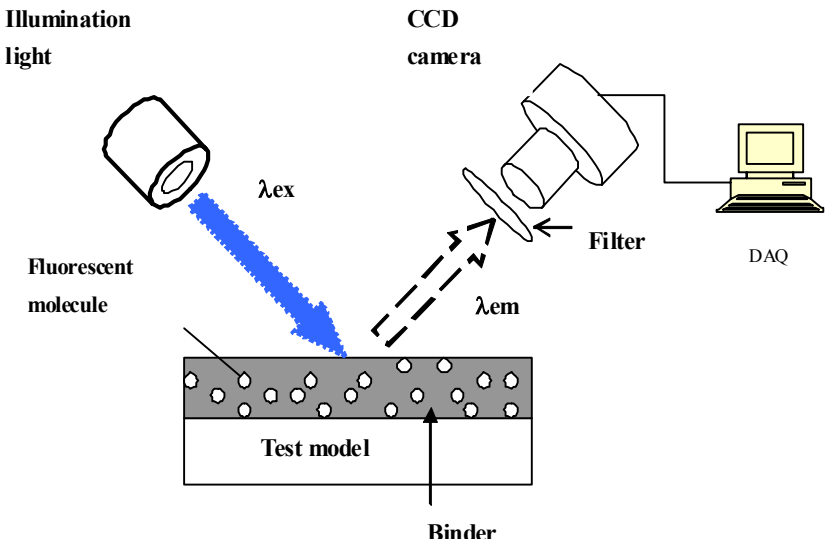

Figure 3-18 – Typical TSP setup and instrumentation (Liu, 2006)

For a more thorough description and theoretical explanation of the properties of TSP, please refer to the study by Liu et al., (2003) as well as Liu, 2006.

3.4.3 CCD Camera

A high resolution 14-bit CCD (Charged Couple Device) camera was utilized for this study. It is a PCO-1600 CCD camera, shown in figure 3-19, provided by the Cooke Corporation with spatial resolution of 1200 by 1600 pixels. The image data is transferred via an IEEE 1394 ("firewire") cable and firewire PCI card to a data collection PC. "CamWare" software provided by Cooke Corp. is used in the Windows operating system to control initialization, exposure time and image acquisition. The acquired image data are processed using MATLAB. The camera is thermo-electrically cooled and has a high quantum efficiency at the paint emission wavelengths. The choice and quality of the scientific-grade camera dictate the measurement accuracy.

Figure 3-19 – CCD camera and light source

3.4.4 Light Source

LED-based illumination source (peak wavelength at 464 nm) was selected as the excitation light for the TSP. The stability of the light source provided by ISSI is within 1% after 10 minute warm up. The excitation spectrum of LED is shown in figure 3-20.

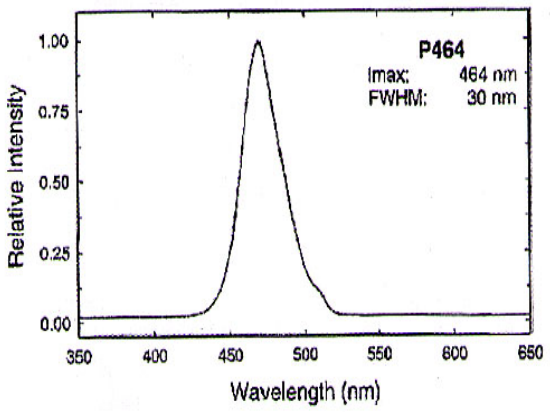

Figure 3-20 – Spectrum of LED source (Liu, 2006)

3.4.5 Pressure Measurements

Pressure measurements were made with pressure taps connected to a Scanivalve pressure transducer. The range of the transducer is from -34.5 kPa to 34.5 kPa, and has a sensitivity of 6.9 Pa (0.001 psi). It is connected to the plenum through a pressure tap located on the side of the plenum, and was used to monitor coolant static pressure. Other measurements involved the static pressure of the test section, performed regularly to assure tunnel stability. Figure 3-21 shows the NIST-certified calibration of the Scanivalve.

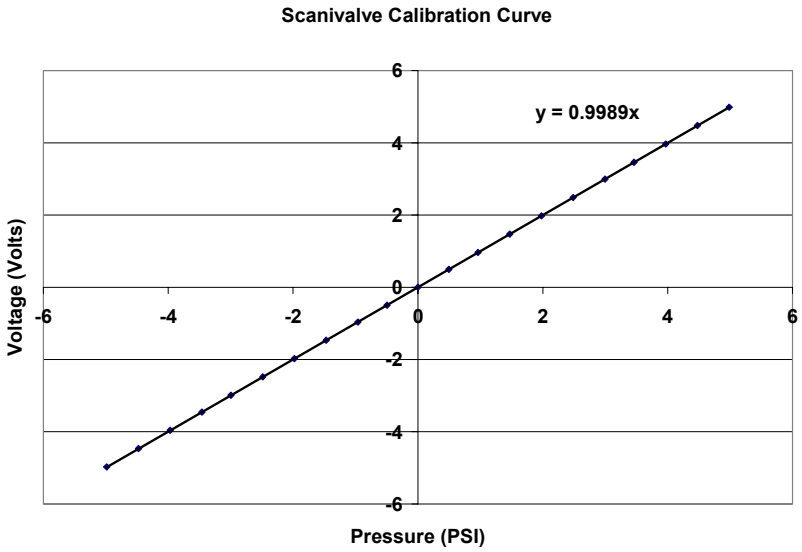

Figure 3-21 – Scanivalve calibration curve

3.4.6 Mass Flow Measurements

Flow measurements were made with two different thermal mass flow meters, high range and low range to cover the entire range of testing, and keep the accuracy as high as possible. The high range meter was a SIERRA 730 Series Accu-Mass thermal flow meter with a

range of 0-1100 L/min, a response time of 200 ms, and an accuracy of 1% of full scale. The low range flow meter used was a McMillan 50K-14C, with a range of 0-500 SCFH, also with an accuracy of 1% of full scale. Figure 3-22 shows both flow meters.

During testing, it was ensured that the company-recommended tubing schemes were followed. Tests were performed first with the low flow rate, for the lower pressure ratios, and then with the high flow meter to cover the high pressure ratios.

Figure 3-22 – Flow meters

3.5 Test Matrix

Testing was performed in a two-step process. First the rig was set up for CD, which required air as a coolant, and very controlled plenum situations, especially when monitoring leakage. When the tests were finished and the data was processed, the resulting C_D curves were used to find the plenum pressures corresponding to the desired blowing ratios, but this time adjusted for N_2 as the coolant. Table 3-1 shows what flow meters were used to find the C_D for each plate, as well as at what blowing ratios the effectiveness tests were performed.

Table 3-1 – Matrix of tests for each coupon

Coupon	CD TESTS		EFFECTIVENESS TESTS
	Flow Meters used		Blowing Ratios Tested
DA0	low	high	0.3, 0.5, 0.75, 1.0, 1.5
DA1	low	high	0.5, 0.75, 1.0
DA2	low	high	0.5, 0.75, 1.0
DA3	low	high	0.5, 0.75, 1.0
DA6		high	0.5, 0.75, 1.0, 1.5
DA8		high	0.5, 0.75, 1.0, 1.5
DA0(2mm)	low	high	0.5, 0.75, 1.0, 1.5
DA3(2mm)	low	high	0.5, 0.75, 1.0, 1.5

3.6 Testing Procedure

As mentioned in section 3.5, two types of tests conducted in this study: flow tests (C_D) and film cooling tests. The procedures for both types of tests are explained as follows:

3.6.1 Flow Tests

The discharge coefficient is calculated from the results of the flow tests. The main objective of this test is to measure the amount of mass flow through a given coupon at increasing pressure ratios. The first step is to insert the coupon into the slot at the bottom of the test section and press it in to place with the grommet, making sure that the grommet has all the necessary weather-stripping layers. Once the grommet is in place, the grooves in the steel plate on the outside of the test section are filled with silicone. The plenum is inspected for cleanliness to make sure that no debris is present inside. Thermocouples are aligned to make sure they will not be touching any walls or each other. Once the plenum is ready, a layer of silicone is applied to

the uppermost edges that will be inserted into the steel disk grooves. The layer of silicone ensures that the plenum will be sealed.

Going back to the test section, any gaps between the coupon and the floor of the test section must be sealed with a putty or wood filler, which must then be allowed to dry before sanding for smoothness. The exit holes of the coupon are then covered with metal adhesive tape. The plenum is then connected to the pipe that provides compressed air. All valves are sealed. A pressure tap connects the plenum to the Scanivalve pressure transducer. The flow meter is turned on and allowed to stabilize. The valves are opened and the plenum is slowly allowed to pressurize up to 20 kPa. Once the plenum is at a constant pressure, the mass flow rate is observed, and if it changes by less than 3 SCFH, then the plenum is considered to be sealed and the test can proceed. All the tape is removed, the test section is sealed and the tunnel is started.

Once the tunnel has warmed up to 65ºC, the pressure in the plenum is increased at very small intervals and the mass flow rate is taken for each pressure. The temperature of the coolant air must be allowed to stabilize, since the plenum warms up while the tunnel warms up. So, a certain amount of air must be allowed to flow to bring the plenum to the same temperature as the coolant. Once the coolant temperature is constant, the test can proceed. Coolant temperature, static pressure and mainstream temperature are the main data taken for this test. Once the highest pressure has been recorded, the tunnel can be stopped. Pressure and mass flow rate biases are averaged between the beginning of the test and the end. The reduction procedure for this data is explained in the analysis section, Chapter 4.

3.6.2 Film Cooling Tests

The procedure for the film cooling tests starts the same as that for the flow tests. The coupon is inserted and the plenum is sealed as in 3.5.2. However, in this case, the desired data is not a flow rate, but the temperature distribution downstream of the cooling holes. As explained in 3.4.3, the main means of obtaining a temperature distribution downstream of the cooling holes is through utilization of TSP and a CCD camera. The CCD camera obtains pictures containing intensity distributions, I(x,y), which must then converted to temperature. A layer of TSP is applied to a rectangular section of the test-section, downstream of the cooling holes. Once it is dry, it is cured to a temperature above the range needed for the experiments. The LED light source is suspended at a location above the test section, which will allow it to irradiate the TSP layer without obstruction. The CCD camera is also suspended perpendicular to the TSP layer, aligned with the test coupon. The experiment in now ready to begin.

At the start of the test, conditions in the room must be known, especially the TSP temperature. A set of pictures of the TSP radiated with the light source is taken. A set is normally four images. These are called the reference pictures. The tunnel is started and the plenum valves are closed so no air or leakage of any sort flows through the coolant holes into the test section. Once the four hour warm up period passes, a set of pictures is taken of the TSP layer. These images are analyzed in situ to avoid the introduction of erroneous temperature distributions, and make sure that the temperature distribution on the TSP is uniform. If that is the case, then this set of images is called the BR0 set. BR0 stands for blowing ratio of zero, and once processed these images yield the recovery temperature distribution on the TSP, T_r. Once this set of images is obtained, cooling can begin. Cold nitrogen gas is allowed to flow through

the plenum, at the desired temperatures and pressure ratios. Once a pressure ratio has been held for a period of approximately 10 minutes, then a set of pictures can be taken. This is called a "run." After all the runs are finished, the tunnel and cooling are stopped, and the test has ended. All images are saved and the equipment is turned off. The next step is to process the data to obtain the results.

CHAPTER 4

ANALYSIS

4.1 Discharge Coefficient

Viscous effects, paired with the effects of geometry, give rise to deviations from ideal conditions on the flow entering a cooling hole. These deviations can be identified and quantified, since there are equations that predict ideal behavior. A prime example of such deviation is the vena contracta, a contraction in the flow area which forms as fluids turn sharp corners into orifices. Thus, as a fluid enters an orifice, its very presence in the orifice entrance reduces the actual area through which it can flow. And while theory for compressible flow may predict a certain amount of fluid passing through the cooling hole, in reality only a fraction does flow through. The discharge coefficient, C_D, is a ratio that compares the observed amount of flow going through a hole, or number of holes, to the predicted flow, based on the compressible flow equation for a specific physical area.

For this study, the equation used for the discharge coefficient is:

$$C_D := \frac{\frac{m_a}{N}}{\frac{\pi}{4}\cdot D^2 \cdot P_c \cdot \left(\frac{P_{stat}}{P_c}\right)^{\frac{\kappa+1}{2\cdot\kappa}} \cdot \sqrt{\frac{2\cdot\kappa}{\kappa-1}\cdot\frac{1}{R\cdot T_c}\cdot\left[\left(\frac{P_c}{P_{stat}}\right)^{\frac{\kappa-1}{\kappa}} - 1\right]}} \qquad (4\text{-}1)$$

The numerator terms in equation 4-1 are the measurand, while the denominator terms are the predicted ideal amount of flow. Thus, if flow behaved ideally, and there were no friction effects

of any kind, both numerator and denominator would be equal, yielding a discharge coefficient of unity.

C_D tests were performed with air as the coolant as explained in 3.5.1. During these tests, the measured variables were: the volumetric flow rate, which was then multiplied by the density to yield the mass flow rate, m_a; T_c, the temperature of the coolant inside the plenum; P_c, the static pressure of the coolant inside the plenum; and P_{stat}, the main flow static pressure, at the test section. The remaining terms, N, κ, R, and D were know constants, or obtained from tables. The data were reduced with the aid of a Mathcad table in which the test data was entered in the form of vectors. Please refer to the Appendix B for the Mathcad code.

4.2 Analysis of Cooling Hole Geometry and Related Parameters

Of all the terms in the C_D equation, the one that presented difficulties in quantifying was the diameter term, D. Per the figures 4-1 to 4-8, the diameter term used in this study is the minor axis of the ellipse formed by the intersection of the cylindrical hole and the inlet plane of any cooling hole. For cylindrical holes, the minor axis of the ellipse at the inlet is the diameter of the cylindrical hole. Following this same logic, the previous definition was also applied to the inlet of the conical holes. However, under close inspection, the cooling holes had deviations from their design, mainly in their diameter. Since the diameter is such a crucial parameter in this investigation, a thorough study of the geometries of the holes was performed in order to quantify deviations from the design, as well as to measure other important parameters influential in the computation of the blowing ratios, coverage area, and uncertainty.

4.2.1 Diameter

The test coupons were taken to CREOL and had their inlets photographed, hole by hole, under a microscope. A 1/100th-inch (0.254-mm) scale was used to measure their minor axis. The images were later analyzed and their diameter calculated. The images are presented as follows:

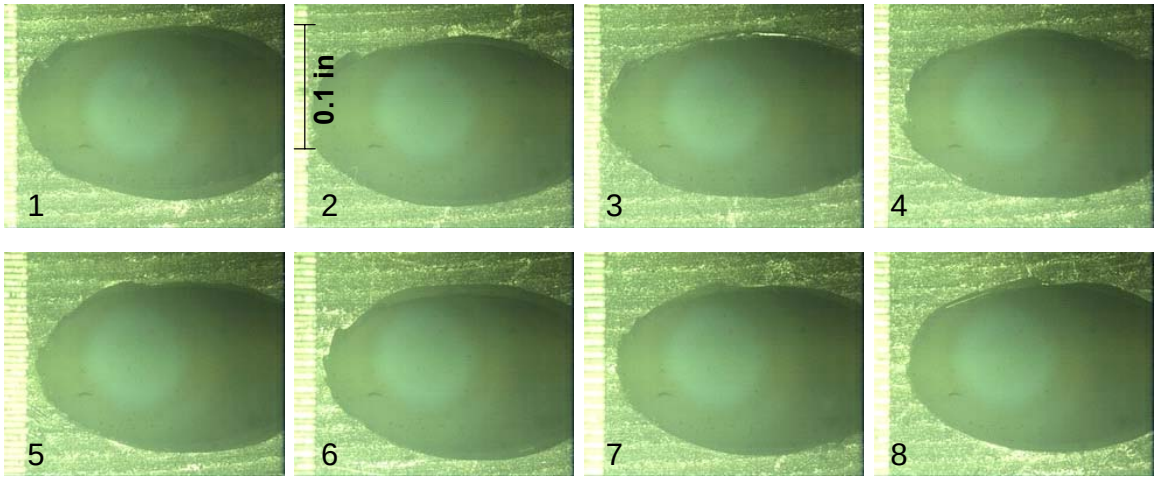

Figure 4-1 – DA0 coupon hole inlets

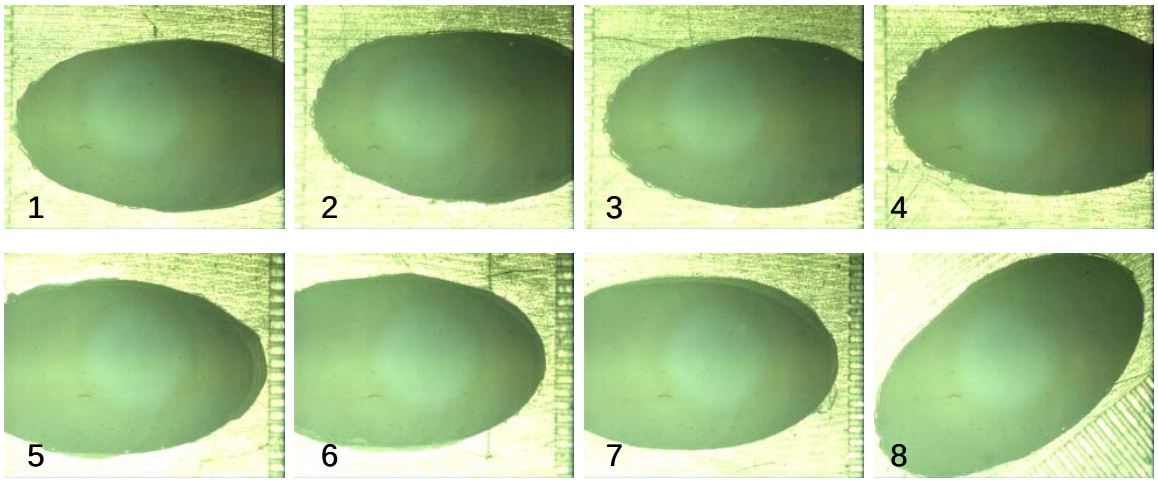

Figure 4-2 – DA1 coupon hole inlets

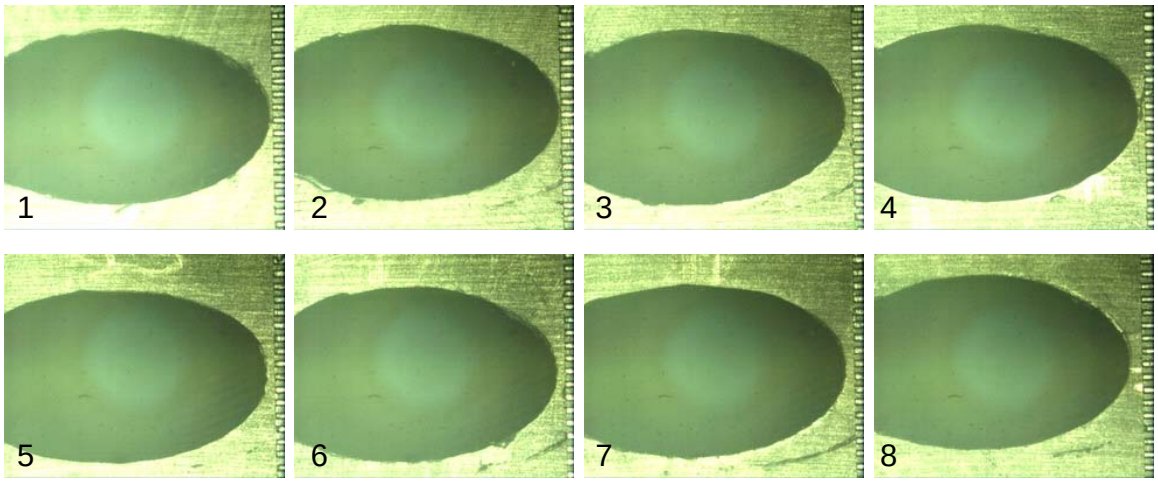

Figure 4-3 – DA2 coupon hole inlets

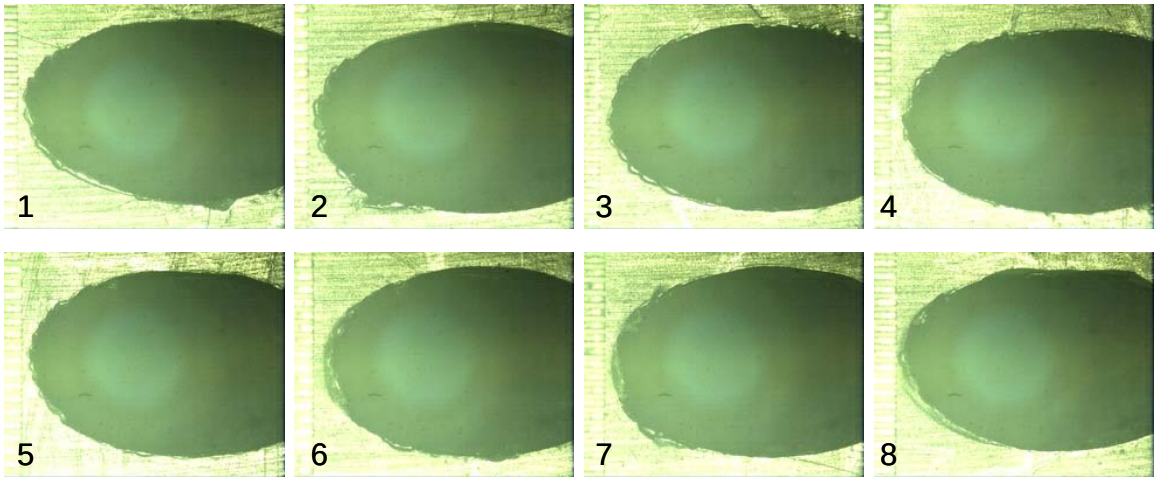

Figure 4-4 – DA3 coupon hole inlets

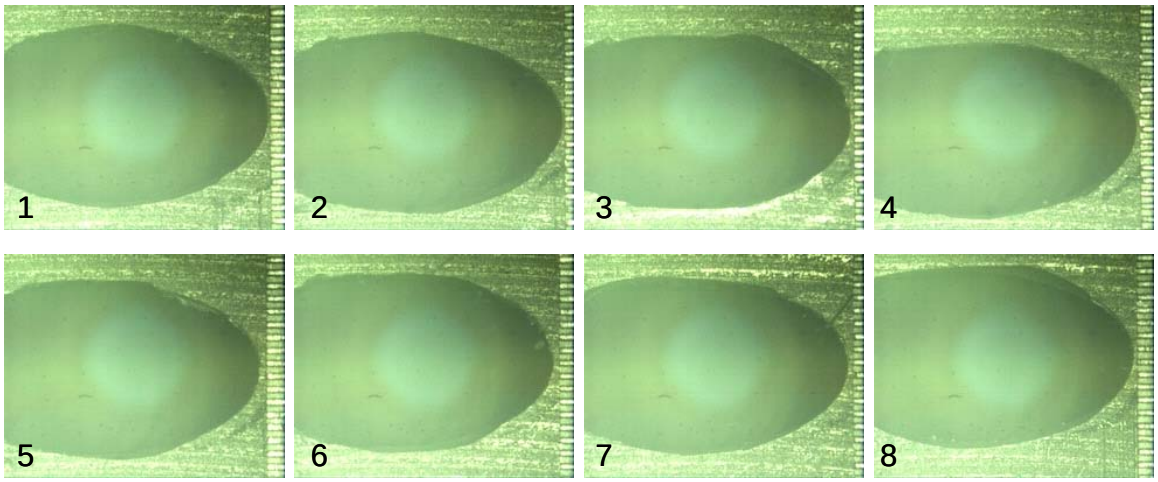

Figure 4-5 – DA6 coupon hole inlets

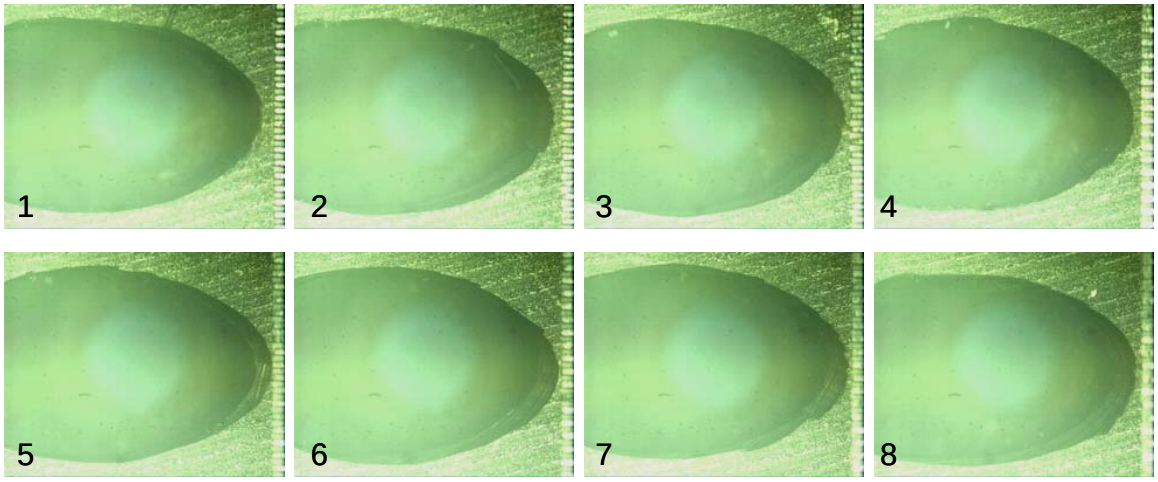

Figure 4-6 – DA8 coupon hole inlets

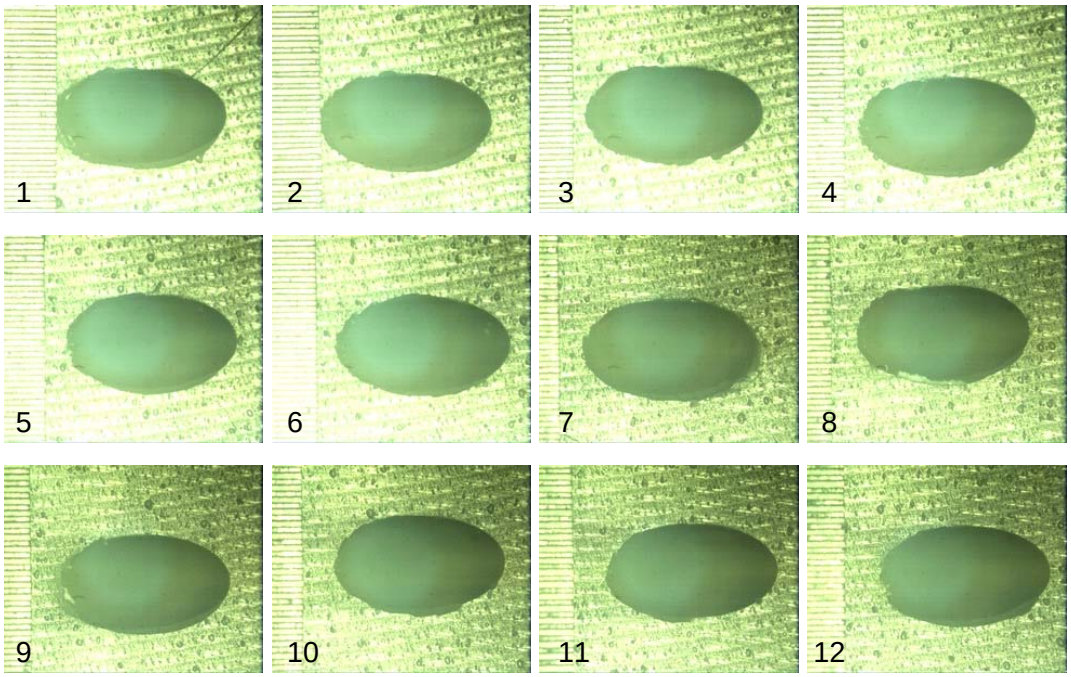

Figure 4-7 – DA0(2mm) coupon hole inlets

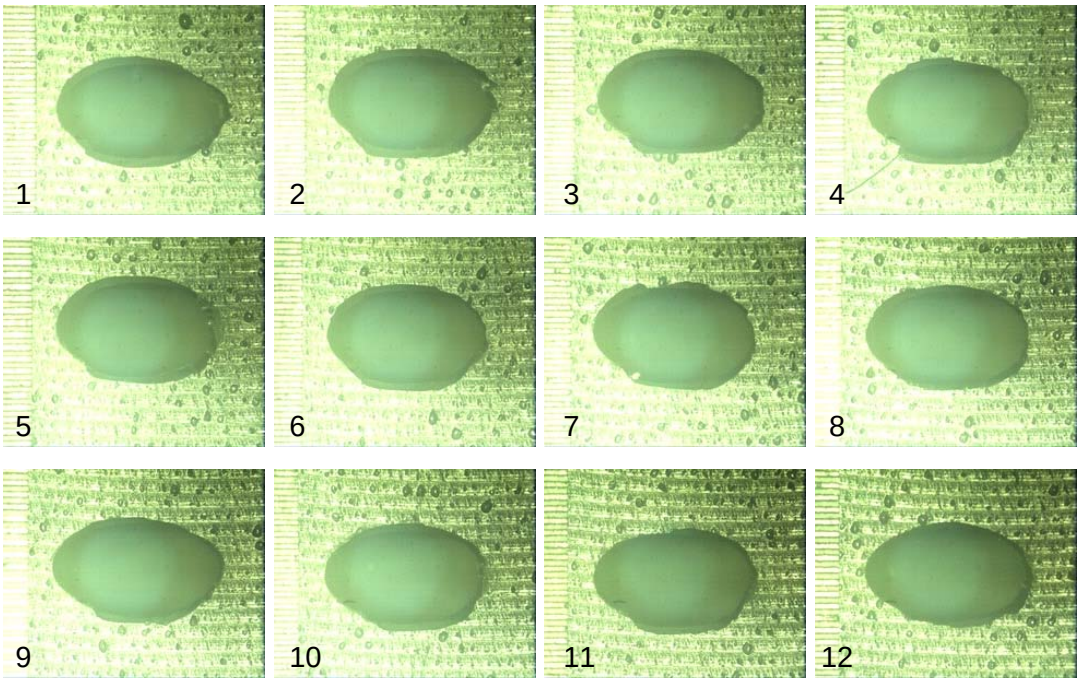

Figure 4-8 – DA3(2mm) coupon hole inlets

The diameter dimension turned out to be even more complicated than first perceived, since many of the holes exhibited what appeared to be inner and outer edges, or a combination. The reader may refer to figure 4-6 and observe the lighter colored "band" at the entrance (lower right hand corner) of the holes, also present in other configurations. The duality in diameters led to the decision to only count the innermost edges as the real edges of the hole. When there was only one edge present, then that edge became the de facto inner edge. Table 4-1 shows the mean diameters for each coupon, in millimeters, as well as the measured inner and outer diameters. If a particular hole did not have an inner diameter, it was not averaged in the inner diameter. The average diameter comes from the shortest distance across the edges of the hole entrance, be it between inner and outer diameters, or a combination.

Table 4-1 – Cooling hole inlet diameter data (all diameters in mm)

Coupon	Inner Diameter	Outer Diameter	Mean Diameter	Deviation from Design %
DA0	3.107	3.363	3.152	-0.72
DA1	3.285	3.410	3.312	4.31
DA2	3.332	3.427	3.411	7.43
DA3	3.502	3.678	3.624	14.14
DA6	3.445	3.521	3.445	8.50
DA8	3.774	3.818	3.774	18.87
DA0(2mm)	1.947	2.117	1.947	-1.67
DA3(2mm)	1.95	2.1	1.95	-1.57

It can be observed that most of the holes do not conform to the design specifications. This is a common occurrence when working with small acrylic parts. The deviations from design were taken into account when calculating the rest of the important geometric parameters discussed next. Table 4-2 lists the rest of the parameters.

Table 4-2 – Parameters derived from geometry of coupons

Plate	Diam. (mm)	Exit Area (sq.mm)	Area Ratio	Coverage (%)	L/D	Exit Slot Length Se (mm)	Inlet Slot Length Si (mm)
DA0	3.152	7.80	1.014	33	3.5-cone	0.825	0.825
DA1	3.312	9.89	1.148	37.4	3.5-cone	0.995	0.867
DA2	3.411	12.17	1.332	45	3.5-cone	1.190	0.893
DA3	3.624	14.68	1.423	49.6	3.5-cone	1.350	0.949
DA6	3.445	23.68	2.541	58.7	3.5-cone	2.292	0.902
DA8	3.774	30.91	2.763	65	3.5-cone	2.730	0.988
DA0(2mm)	1.947	2.98	1.030	33	4-cyl+3.5-cone	0.510	0.510
DA3(2mm)	1.95	5.87	1.964	40.2	4-cyl+3.5-cone	1.003	0.511

4.2.2 Area Ratio

The area ratio (AR) arises from the conical nature of the cooling holes. Simply put, AR is a ratio of the exit area to the inlet area of a cooling hole. The areas considered are normal to the axis of the hole. For conical holes, as well these areas are circles. The area of the inlet circle is dictated by the length of the minor axis of the inlet, D_i. The area of the exit circle is dictated by the diameter of the circle at the exit, D_e, measured where the axis of the hole passes through the exit plane of the plate. Simplifying, AR then becomes:

$$AR = (D_e/D_i) \tag{4-2}$$

Looking at Table 4-2, it is easy to see that, as expected, coupon DA8 has the largest area ratio. AR is also influential in the diffusing process of the coolant as it travels through the coupon. Diffusion lowers the velocity of the flow and allows it to adhere more easily to the walls and provide more effective film cooling while increasing the amounts of coolant. From a stand point of momentum flux ratio I, Sinha et al. (1991) found that values larger than 0.3 lead to coolant detachment. All things being equal, cylindrical holes are at a disadvantage because they

do not actively diffuse the flow, while cone shaped holes act as natural diffusers, thus giving lower values of I at the hole exit, for the same amount of coolant.

4.2.3 Coverage and Equivalent Slot Length

When measuring the span-averaged effectiveness of a row of holes, it is necessary to know what kind of coverage cooling holes provide to the area immediately downstream of the hole exits. A simple definition of the coverage is the percentage of the pitch that the actual hole exit diameter occupies. In other words, between the centerlines of two holes, there is a portion of that space from which coolant flows out; to find out the coverage one asks: what percentage of the total distance between the hole centers is actually the cooling hole. Coverage also indicates what the maximum cooling effectiveness of a row of holes will be when reporting span-averaged effectiveness. If coolant exits a hole, and attaches perfectly to the surface immediately downstream, the effectiveness is 1 or 100% at the centerline. In the region between two cooling holes, there is no coolant, so the effectiveness is 0 or 0%. Table 2 shows the coverage values for the holes in the present study. One can see that the coverage ranges from 33% for the cylindrical holes, to 65% for DA8. Again, coupon DA8 was expected to provide the largest coverage since it expands the most. This also means that when looking at laterally averaged effectiveness data for DA8, one has to keep in mind that the largest value the coupon can provide is 0.65.

If instead of discrete cooling holes, a slot were used, the maximum span-averaged effectiveness would be 100%. The effective slot length value is commonly used in literature for comparison purposes as a means to non-dimensionalize the distance X from the exit of the cooling holes. To calculate the slot length, one has to know the area of the cooling hole inlet, the

circular area, not the elliptical one. Then, that area must be distributed over a rectangular area with a length of 3 diameters by a width of s. For the inlet of the holes, the classical definition for a row of holes with PI/D = 3, is given by

$$s = \frac{\pi D}{12} \tag{4-3}$$

However, the classical definition does not deal with conical holes, since S was meant to compare the emerging cylindrical hole cooling method against the established slot cooling method. Thus, the modified definition applied to the conical holes to find the equivalent slot length becomes:

$$s = \frac{\pi}{12} \cdot \frac{D_e^{\,2}}{D_i}, \tag{4-4}$$

The diameter values for D_e and D_i do not cancel out because they are not equal.

4.3 Determination of Blowing Ratio and Momentum Flux Ratio

The blowing ratio, also called the mass flux ratio, is a dimensionless number used in film cooling to quantify the ratio of the mass flow rate per unit area of the coolant to that of the mainstream. When all simplifications are done, what is left is the density ratio multiplied by the velocity ratio of the coolant to the mainstream.

$$M = \frac{\left(\frac{\dot{m}}{A}\right)_c}{\left(\frac{\dot{m}}{A}\right)_m} = \frac{\frac{(\rho \cdot U \cdot A)_c}{A_c}}{\frac{(\rho \cdot U \cdot A)_m}{A_m}} = \frac{\rho_c \cdot U_c}{\rho_m \cdot U_m} \tag{4-5}$$

For the current test set up, M is calculated using the following simplification:

$$M = \frac{\frac{m_a}{N_h}}{\frac{(A_c)}{(\rho \cdot V)_m}} \tag{4-6}$$

The blowing ratio is also very convenient to use because in the current setup, it is a function of the pressure ratio. However, some issues come up when calculating the mass flow rate of the coolant in the effectiveness tests. For the C_D tests, the coolant used is air at about ambient conditions, while in the effectiveness measurements, the coolant used is nitrogen gas, at about -15°C. The subzero temperatures of the nitrogen prevent the measurement of its flow rate with the current flow meters. However, it is possible to back-calculate the flow rate using the C_D curve, adjusting ρ and κ of the nitrogen for the cooler temperatures.

Keeping in mind that PR, the coolant-to-mainstream static pressure ratio is controllable, one must back-calculate the blowing ratio prior to running the effectiveness tests. The procedure used to determine the blowing ratio using nitrogen is as follows: 1) decide a coolant pressure, P_c, since $P_{stat,m}$ is known, find PR; 2) rearrange the C_D equation, solving for m_a; 3) from the C_D curve for that particular hole, find C_D for the current PR and insert into the new m_a equation, this yields the value of m_a; 4) with m_a of coolant, use equation (4-6) and obtain M. It is important to note that this is an iterative process that must be done to find the pressure ratios for the desired blowing ratios at which to keep plenum conditions when measuring effectiveness.

The momentum flux ratio, I, is defined similarly to the blowing ratio. While the blowing ratio is based on the velocity of the coolant, the momentum flux ratio is more closely related to the energy of the coolant. It compares the momentum of the coolant versus that of the mainstream. The momentum flux ratio is classically defined as:

$$I = \frac{\rho_c \cdot \left(U^2\right)_c}{\rho_m \cdot \left(U^2\right)_m} \tag{4-7}$$

Since the density ratio, DR, is kept nearly constant at 1.26, the momentum flux ratio can be obtained by squaring the blowing ratio, and dividing by DR,

$$I = \frac{M^2}{DR}, \tag{4-8}$$

where DR is given by:

$$DR = \frac{\rho_c}{\rho_m} \tag{4-9}$$

4.4 Cooling Effectiveness Calculation

Film cooling effectiveness (η) measurement is one of the primary goals in this study. However, obtaining the final plots of η requires a significant amount of data reduction. As mentioned before, η has been commonly defined as follows:

$$\eta = \frac{T_m - T_{aw}}{T_m - Tc} \tag{4-10}$$

Notice that this definition involves the mainstream temperature, which is sensitive to the injection of coolant. Said definition applies only if there are no conduction effects on the test section as a result of cooling, heat leakage, or other sources of thermal noise that would cause a temperature difference between the mainstream and the TSP surface, or render the conditions downstream of the cooling holes non-adiabatic. An additional consideration is the fact that the test section is exposed to a significantly high velocity flow (>52 m/s), which means there will

also be a recovery temperature due to viscous dissipation. Since the actual data collection occurs at the floor of the test section, under steady, un-cooled conditions, this floor's temperature is the recovery temperature, T_r. To reflect this fact the following adjustment has been made to the definition of η:

$$\eta = \frac{T_r - T_{aw}}{T_r - Tc} \tag{4-11}$$

The recovery temperature is measured once the tunnel has reached steady state conditions without any cooling. Steady state is defined as having the temperature of the mainstream not change by 0.1°C in 10 minutes. This condition leads to the temperature difference between thermocouples A and B to be no more than 1.5 °C. During experiments, it has been shown on the BFC rig that after the experiments have started, the T_r changes little, even under cooling conditions. It takes the bottom of the section less than ten minutes after cooling has stopped to go back to its original recovery temperature, under steady flow conditions..

4.4.1 Reduction of Temperature Data

To calculate film cooling effectiveness, three temperatures must be known: T_c – the coolant temperature, T_{aw} – the adiabatic wall temperature distribution downstream of the cooling holes, and T_r – the recovery temperature of the test section. To analyze the TSP pictures, matrix handling software such as MATLAB is used. The images are read into a matrix containing the intensity information over every pixel of the TSP.

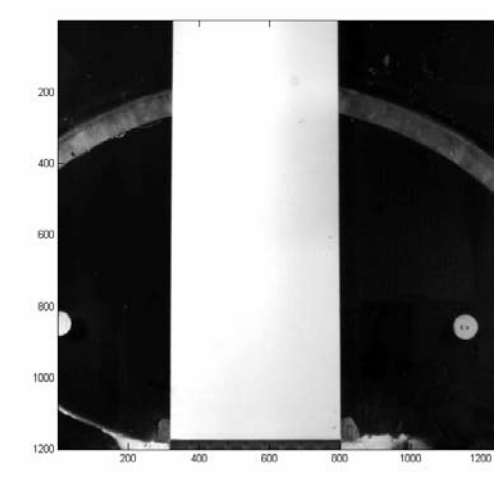

Figure 4-9 – Normal image of TSP layer

Figure 4-9 shows an image of the TSP downstream of the coolant holes (bottom). This image was taken under non-test conditions, without any LED lighting, and is used mainly for locating the holes with respect to the edges of the paint layer. The coolant holes are very difficult to see under testing conditions because they reflect back very little light.

Figure 4-10 shows the same image, but this time under LED lighting. If the TSP is at room conditions, and testing is ready to begin, then this image becomes the reference image, and the intensity from any pixel becomes $I(T_R)$. The LED light is kept on throughout the duration of the test. Neither the camera nor the LED light may be moved, or the usage of the reference image will not be valid due to changes in lighting conditions. Precautions must be taken to ensure that the data will not be polluted due to outside lighting condition changes. For all tests and blowing ratios, images are taken in sets of four, which are then averaged to filter out any fluctuations. For the reference image, the temperature must be uniform, and known. Typical reference temperatures are around 25 ºC, or room temperature.

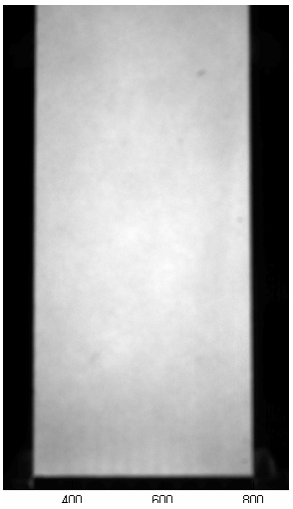

Figure 4-10 – Reference Image

As mentioned in the film cooling test procedure, section 3.6.2, the tunnel is allowed to warm up for over four hours. At that point another set of pictures is picture is taken. The images look just like the reference image, but the intensity is lower due to the higher temperature. TSP intensity is inversely proportional to temperature. These images, called T_r, are be processed in the same way all flow images are processed, and whose procedure is explained next.

To obtain a flow image, first the plenum must be kept at a constant pressure and temperature for approximately 8-10 minutes to achieve the desired blowing ratio, and thus film cooling conditions over the paint. Once these conditions are met, the set of images can be taken. Figure 4-11 shows TSP under cooling conditions. The darker sections of the paint indicate higher temperatures, the lighter sections, cooler paint. Hence, the cooling jets can be observed as light colored. One must keep in mind that the "lighter and darker" sections are relative to the reference images, not compared to other sections of the TSP. Following this concept, the T_r image would look uniformly darker than the reference.

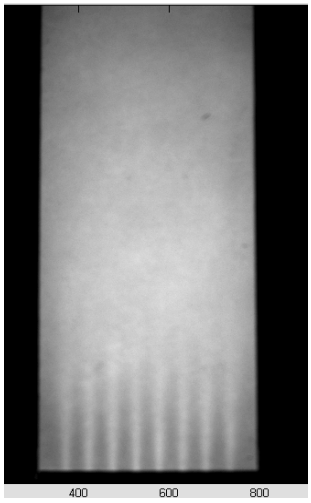

Figure 4-11 – Image of TSP showing coolant flow

The process of taking images continues until all the blowing ratios are taken. Once this has occurred, the testing ends and the images can be processed.

During testing, the camera might shift slightly, on the order of a couple of pixels, so the images must be cropped to only study the area of interest. This is usually the TSP area only. The new cropped images contain only the TSP, from left edge to right edge, from upper edge to the holes. This cropping must be done carefully, making sure that any feature on the paint has the same pixel position value in all cropped images. In other words, when looking at the cropped image of run 1, it must be identical in size and position as the reference images and all the other runs. Supposing there is a dot on the TSP, on all cropped images, that dot should be at exactly the same position. This is important in the processing of all images because temperature is obtained as follows: the ratio of emission intensity I(T) at any temperature T to the emission intensity $I(T_R)$ at an unspecified reference temperature T_R is

$$IR = \frac{I(T)}{I(T_R)} = f_n(T, T_R) \tag{4-12}$$

In terms of images, this means, we divide each pixel intensity value for figure 4-11 by that of figure 4-10 to obtain figure 4-12. The intensity ratio IR is also called the relative intensity. Figure 4-12 illustrates the ratio of intensity of 4-10 and 4-11.

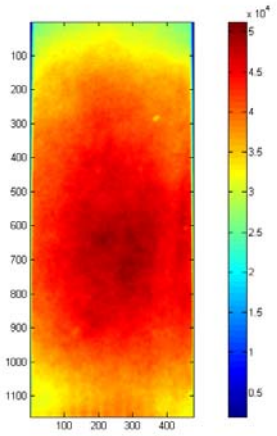

Figure 4-12 – Relative intensity ratio, IR

The effects of lighting and paint thickness are, in principle, eliminated by taking the ratio IR (Liu, 2006). The next step is to convert these local ratios into temperature values. This is accomplished with the use of the calibration curve of the paint. Figure 4-13 shows a typical calibration curve for TSP.

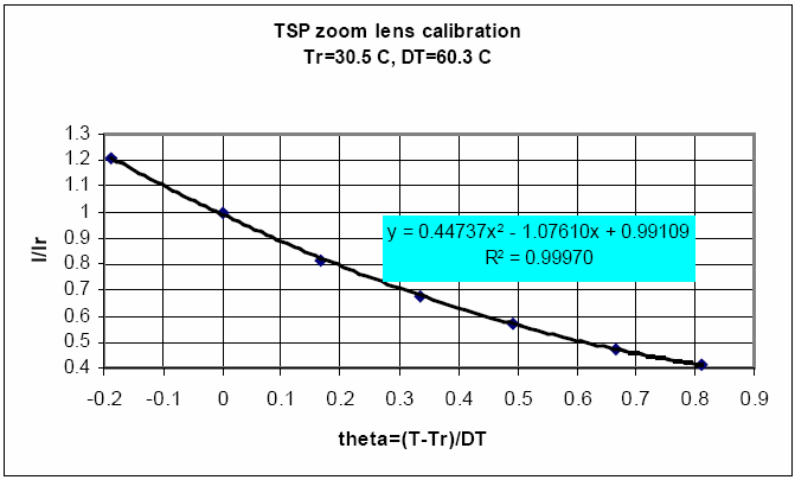

Figure 4-13 – TSP calibration curve

The function theta can be determined by fitting non-dimensionalized calibration data with a polynomial. The polynomial is then used to back-calculate the temperature from the intensity ratios. From the value of theta, T can be solved since Tr and DT are known quantities established during calibration. The manipulation is done with software on a per-pixel level. Once the processing is done, the intensity information yields temperatures. This is how the recovery temperature and the adiabatic wall temperature distributions are obtained. Please refer to Appendix B for the MATLAB codes used to process the intensity images.

Figure 4-14 shows the final result from processing. In that figure, the jets are clearly discernible. Section 4.4.2 explains further the process of data reduction from this point.

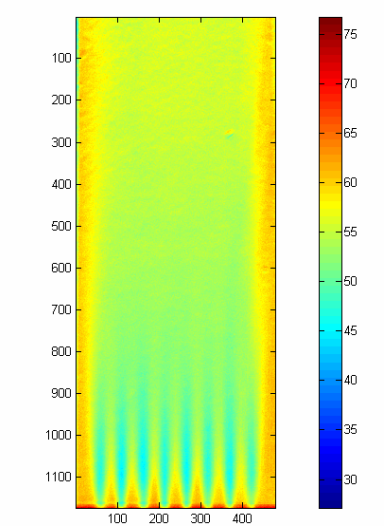

Figure 4-14 – Raw temperature image from TSP

4.4.2 Conversion of Temperature Data to Film Cooling Effectiveness

To calculate the span-wise-averaged cooling effectiveness, several physical factors are considered such as edge effects, the number of cooling holes and the diameter of the holes. To

discount edge effects from influencing the temperature data, only holes close to the middle of the coupon center are included in the averaging step. Since the conical-hole coupons have only eight cooling holes, the holes used are the middle four. This means that temperature averaging occurs from the line exactly between the second and third hole, to the line between the sixth and seventh holes, for the all the coupons with L/D of 3.5. For the compound coupons, since there are twelve holes in this arrangement, the holes considered are the middle six holes. This assures that flow passing through the part of the test section that is not cooled, and which may interact with the cooling process by entrainment, will not affect the temperature data in the averaging process.

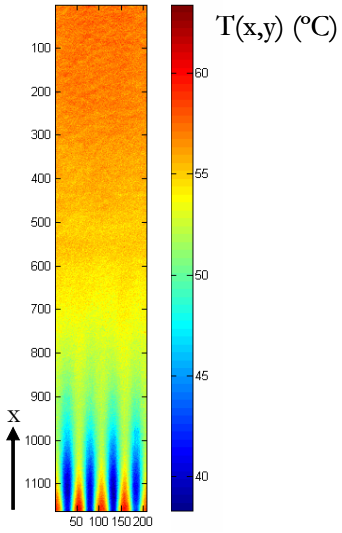

Figure 4-15 – Temperature plot cropped for processing

Figure 4-15 shows the temperatures downstream of the cooling holes considered for the calculation of the effectiveness. In that figure, another important parameter shown is X. X is the distance downstream of the holes. In figure 4-15, X is reported from the downstream edge of the paint in pixels. This is corrected during processing using the pixel-per-millimeter resolution and dividing the resulting millimeter values by the diameter of the holes, to reflect the distance

downstream from the exit of the holes. This yields X/D, a dimensionless distance commonly used for cooling effectiveness measurements in the literature.

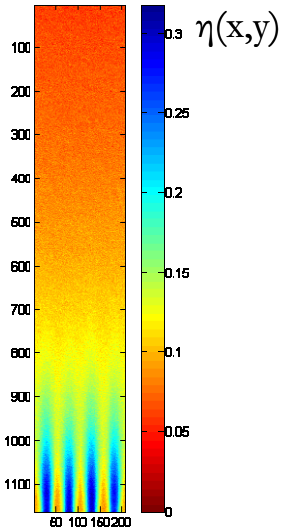

Figure 4-16 – Film cooling effectiveness distribution

Once the intensity data has been reduced to pixel temperature data, the second part of the processing focuses on finding the film cooling effectiveness over the TSP surface. This step can be done with MATLAB in two ways: 1) equation (4-11) can be applied to the temperature distribution in figure 4-15 by subtracting it from the T_r obtained after the tunnel warmed up, with no cooling. This difference is divided, pixel-by-pixel, by the difference between Tr and T_c, which is known from testing. This yields an effectiveness distribution, like the one shown in figure 4-16. It must be stated, that the resolution of η obtained with this method is too low to show local or centerline effectiveness. In other words, it is not recommendable to use centerline values from these images because the local values are themselves fuzzy "averages" due to the low resolution. Once the effectiveness distribution is obtained, it is averaged spanwise and collapsed into a two column matrix. The first column contains the value of X/D, the second

contains the value of η_{la}. The result of this process is shown in figure 4-17. 2) The temperature distribution is averaged spanwise, and so is T_r, then equation (4-11) is applied and the result is the average η, as before. The result of both methods is shown in figure 4-17.

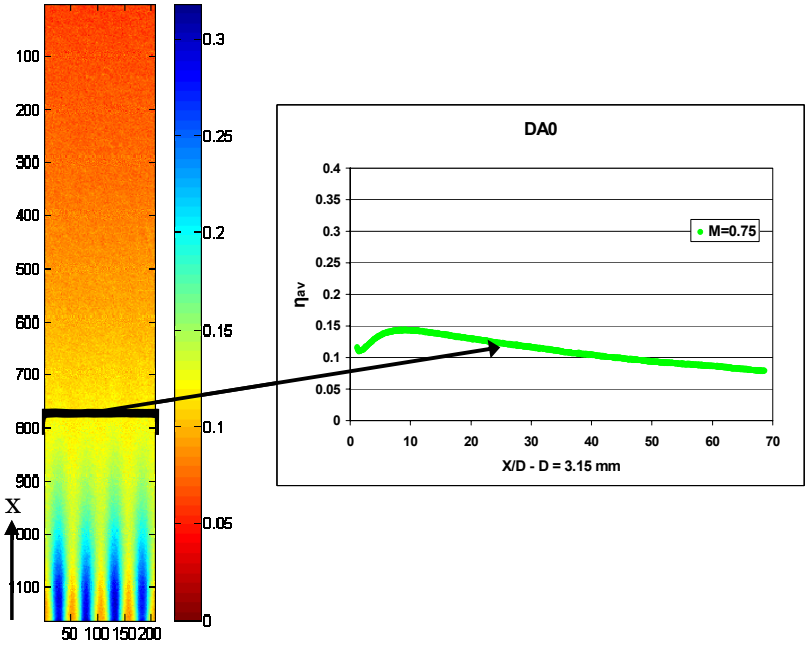

Figure 4-17 – Results of averaging η; arrow indicates collapse into one point

The MATLAB code then saves the information to a "results" file, which is used to continue the post-processing. The data file output by MATLAB is easily opened in a spreadsheet program, in this case EXCEL. Thus, film cooling effectiveness is obtained on a pixel-by-pixel basis downstream of the cooling holes. All effectiveness results for this thesis were obtained in this fashion and are reported in Chapter 5.

4.5 Measurement Uncertainty

The uncertainties reported were estimated following the procedure described by Kline and McClintock (1953). The effectiveness as defined in equation (4-11) is used to find the derivatives in the uncertainty equation:

$$U_\eta = \sqrt{\left(\frac{d}{dTc}\eta \cdot U_{Tc}\right)^2 + \left(\frac{d}{dTr}\eta \cdot U_{Tr}\right)^2 + \left(\frac{d}{dTaw}\eta \cdot U_{Taw}\right)^2} \qquad (4\text{-}13)$$

In this case U_{Tr} and $U_{Taw,}$ the uncertainties in the recovery and adiabatic wall temperatures are equal since both are obtained with TSP. Their value is 0.93ºC (Liu, 2006). U_{Tc} is 1.0ºC, which is the uncertainty in the coolant temperature, as measured with the plenum thermocouple set up. The values of U_η are evaluated at every point on the η_{la} curve, and give the uncertainty band shown in figure 4-18.

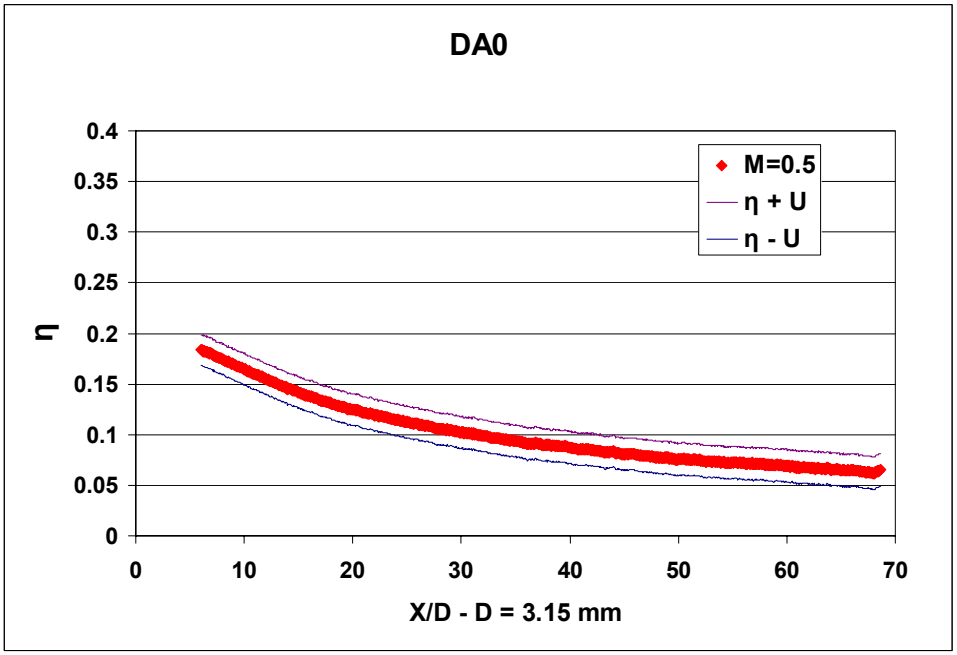

Figure 4-18 – Uncertainty distribution for film cooling effectiveness

The uncertainty in the discharge coefficient has been calculated similarly, with equation (4-14), but at fewer points:

$$U_{C_D} = \sqrt{\left(\frac{d}{dm}C_D U_m\right)^2 + \left(\frac{d}{dP_{stat}}C_D U_p\right)^2 + \left(\frac{d}{dP_c}C_D U_p\right)^2 + \left(\frac{d}{dTave}C_D U_t\right)^2 + \left(\frac{d}{dD_{ave}}C_D U_D\right)^2} \quad (4\text{-}14)$$

This equation yields results that suggest the uncertainty at the lower pressure ratios is on the order of ± 9%, compared to only ± 1% at the higher pressure ratios. The results at four pressure ratios are shown in figure 4-19.

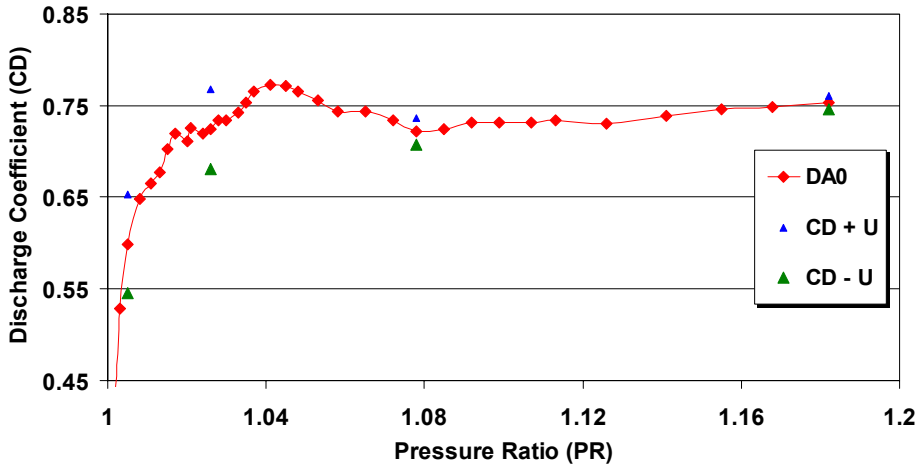

Figure 4-19 – Uncertainty in CD measurement for DA0

With these error bans in mind, we are now able to look at Chapter 5, which gives the full set of results for all tests.

CHAPTER 5

RESULTS AND DISCUSSION

5.1 Discharge Coefficient

A plot of the discharge coefficient, C_D, for all configurations is shown in figure 5-1.

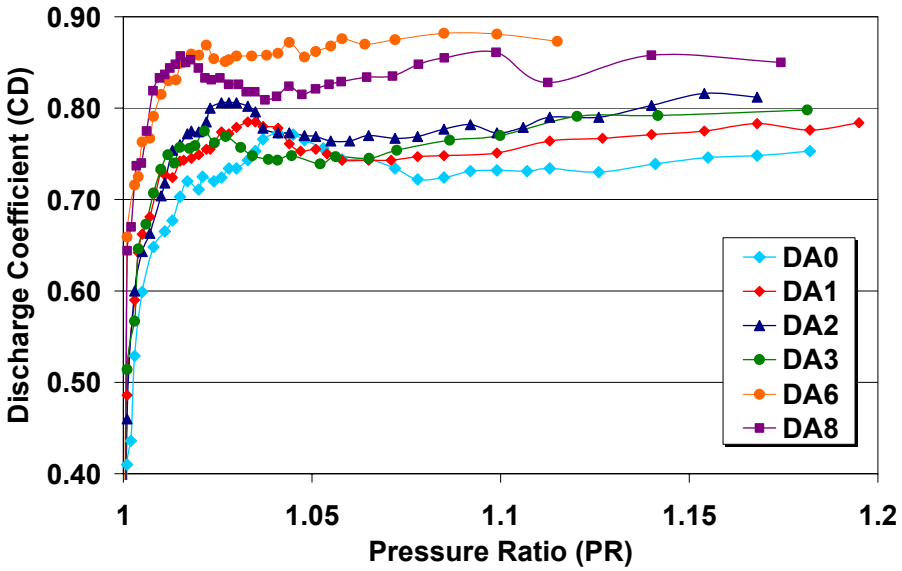

Figure 5-1 – Combined discharge coefficient for conical coupons

Observing figure 5-1, it is possible to see that, on the average, DA0 has the lowest values. As the angle of diffusion is increased to 1 and 2 degrees, the overall values of the C_D curves increase. The peak value of DA2 occurs at a lower PR than for DA1 and DA0. This trend in peak values continues also for DA3, however, the overall value of the curve is shifted down. Looking at DA6 and DA8, one can also notice that increasing angle means peak C_D value at lower PR for these coupons, too. However, DA6 seems to sustain higher C_D values overall.

Figure 5-1 is excellent for following trends in the overall behavior of all the coupons, but it does lack clarity when there is the need of singling one coupon out or comparing it with other configurations. For this purpose, figures 5-2 and 5-3 are included.

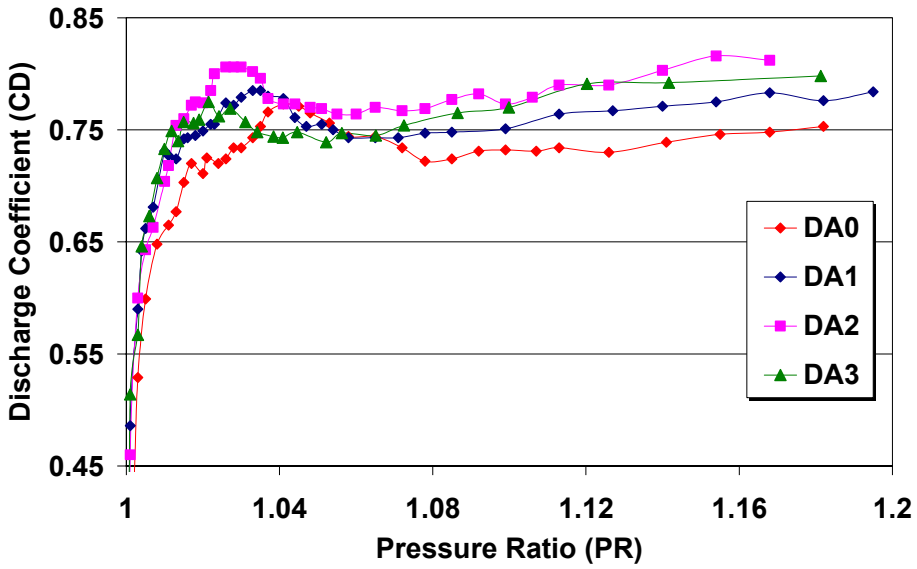

Figure 5-2 – C_D Chart for 0º to 3º Coupons

It is possible to notice the behavior of the 3º configuration, DA3, more clearly. One of the theories for this behavior, assuming there are no anomalies in the testing, is that DA3 has a larger diameter than DA2 and DA6, which may translate into a larger effective flow area. So, when comparing C_D values for these plates, the results, which should only illustrate the effect of the increasing diffusion angle, might be polluted by the variations in diameter as well. A suggested explanation is that the larger diameter may be affecting the behavior of the C_D, since C_D is also a function of L/D. DA8, with such large inlet diameter might be doing the same.

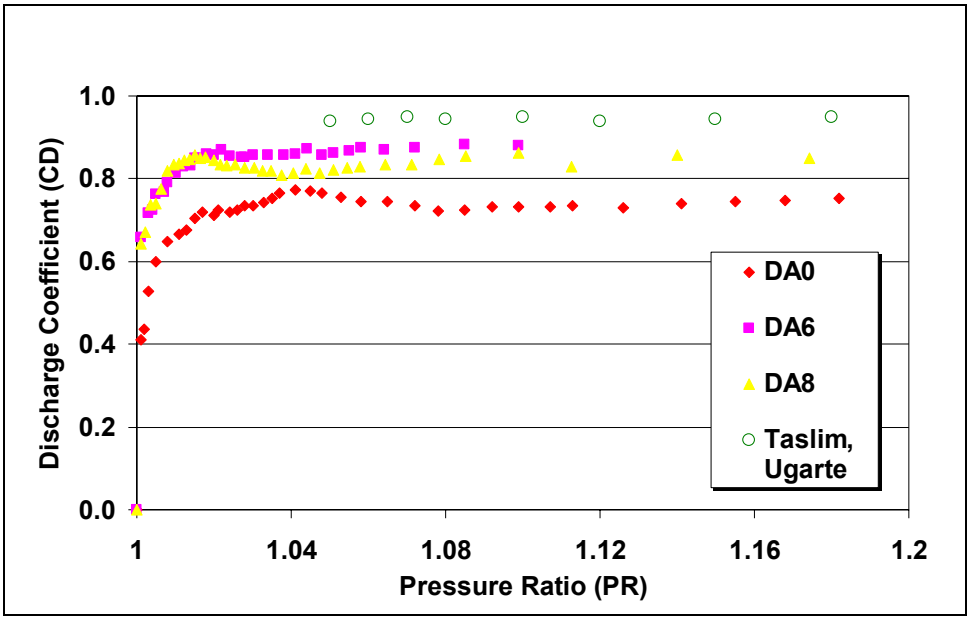

Figure 5-3 – C_D chart for DA6 and DA8 with comparison to the literature

In figure 5-3, configuration DA6 has a more consistently high value than that of DA8. DA0 is included for base reference. Results for the test by Taslim and Ugarte, 2004, are also included in this plot for comparison purposes. The main explanation for the deviation in results is that AR for the 2004 study was 4.0. Such high of AR values tend to raise the CD of holes, since their behavior is less cylindrical.

A comparison of the two DA0 configurations in figure 5-4 shows that both have very similar values for C_D, except that the development of the C_D curve for DA0(2mm) occurs more "slowly" in terms of the pressure ratio. So, here the effect of the increase in L/D or the decrease in diameter (since we can not say at this point whether the diameter dimension alone is responsible for this trend, given they both have the same length) is to spread the C_D, even though the values are very similar. Comparing both 2-mm holes, one can see that the addition of a 3º diffusing section increases discharge coefficient.

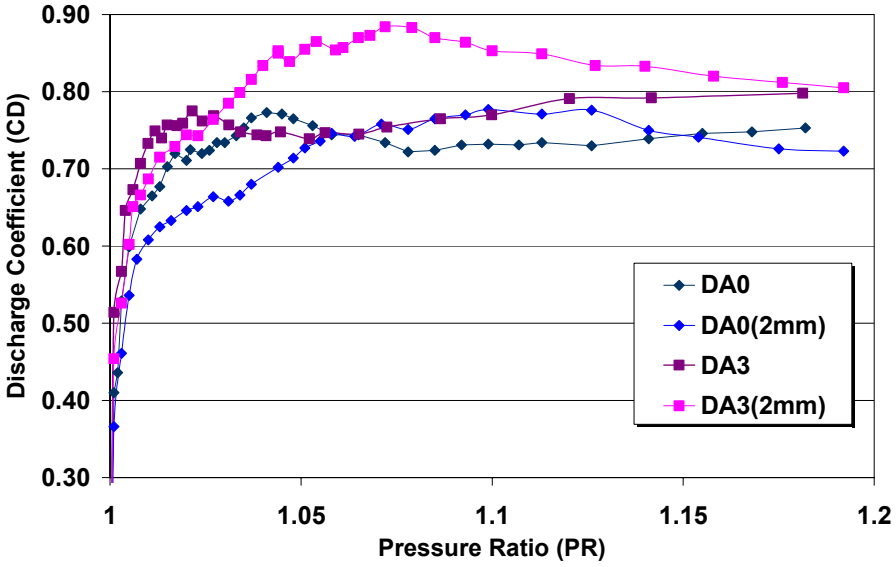

Figure 5-4 – Discharge coefficient for compound hole coupons

Shifting focus to the DA3 and DA3(2mm) plates, one can see that the same "spreading" of the curve occurs, however, the values of the C_D for the DA3(2mm) plate are significantly higher. So, it is possible to say that the added entry length may be responsible for the increase in CD, while the higher L/D leads to the spreading of the curve. The effects these results have on the film cooling effectiveness are explored in the next section.

5.2 Spanwise-Averaged Film Cooling Effectiveness

Results of the film cooling tests are presented in this section. However, before looking at them, the validity of the data must be assessed by comparing results obtained in sample tests against those found in the open literature. For this purpose, the studies chosen were: Sinha et al. (1991), Pedersen et al. (1977), and Baldauf et al. (2004). These studies were chosen because of the similarity in blowing ratios and their test configurations for simple cylindrical holes.

5.2.1 Validation of Results

According to Goldstein et al. (1968), it is appropriate to compare effectiveness data at very low blowing ratios, even if the geometry is slightly different. Their study showed this in a dramatic fashion since they presented data for holes at inclination angles (α) of 90º versus 35º with satisfactory results. Data from one important study conducted by Lutum and Johnson in 1999, and with which this study is most compatible geometrically, were not presented for M~0.25. Neither were data for the cylindrical 2-mm-diameter plate used in the present study. Data are available, however for other blowing ratios. Figure 5-5 shows η_{la} for DA0 and data from several studies, both recent and from several decades ago. Testing conditions for these tests are summarized in Table 5-1.

Table 5-1 – Summary of parameters of tests in Figure 5-5

Study	M	L/D	Diameter	α	Tu (%)
Pedersen	0.213	40	1.17 cm	35º	~0.35
Sinha	0.25	1.75	1.27 cm	35º	0.2
Baldauf	0.2	6	6 mm	30º	1.5
Present	0.3	3.5	3.15 mm	35º	0.6

Figure 5-5 shows the spanwise-averaged film cooling effectiveness (η_{la}) for DA0 at a blowing ratio of 0.3. It is possible to see that the data matches quite well, even the trend downstream at X/D > 20 holds very well.

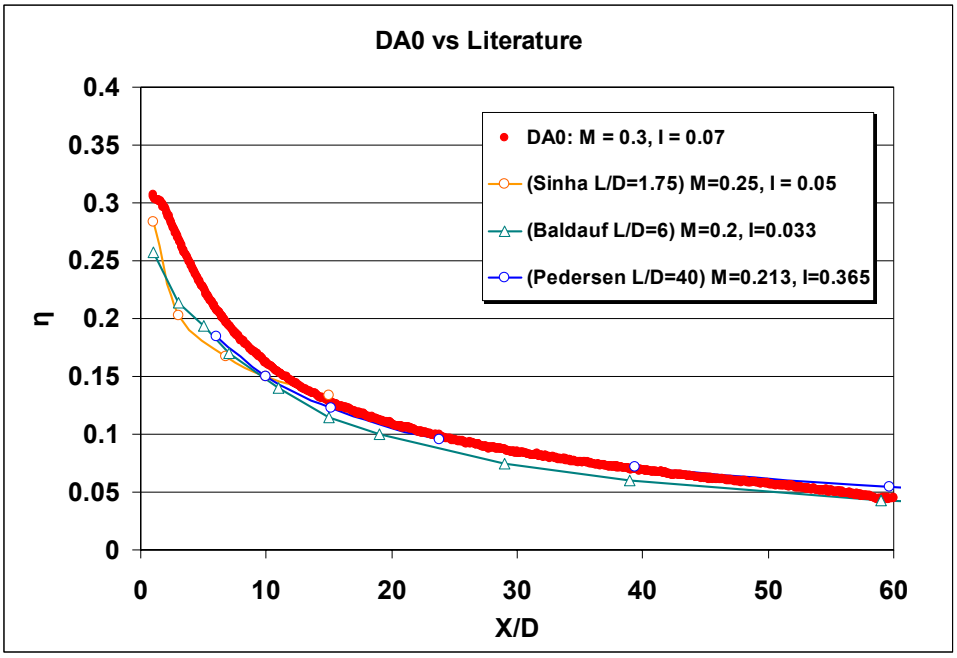

Figure 5-5 – Comparison of results against previous studies for low M

For this study, the blowing ratio (M) of 0.3 was performed on DA0 only for comparison purposes. It was not practical to obtain M=0.3 for other configurations, such as DA3 or DA8 due to the very low pressure ratios at which the coolant would have had to be kept. At such low pressures, it is very difficult to control the nitrogen supply, keep it steady, and to keep the coolant from picking up heat. For blowing ratios of 0.5 and higher this is not as great a problem. The problem arises at the highest blowing ratios, 1.5 and 2.0, at which there is so much coolant mass going through the supply plenum that its temperature could drop well below -40 ºC if not managed carefully. For the blowing ratio of 2.0, this was always the case. The amount of coolant needed for the larger conical holes was so much, that it was taxing on the nitrogen tank and its temperature would plummet to the point that it would start flooding the coolant circuitry with liquid, a very hazardous situation. For this reason, the blowing ratio of 2.0 was not tested, either.

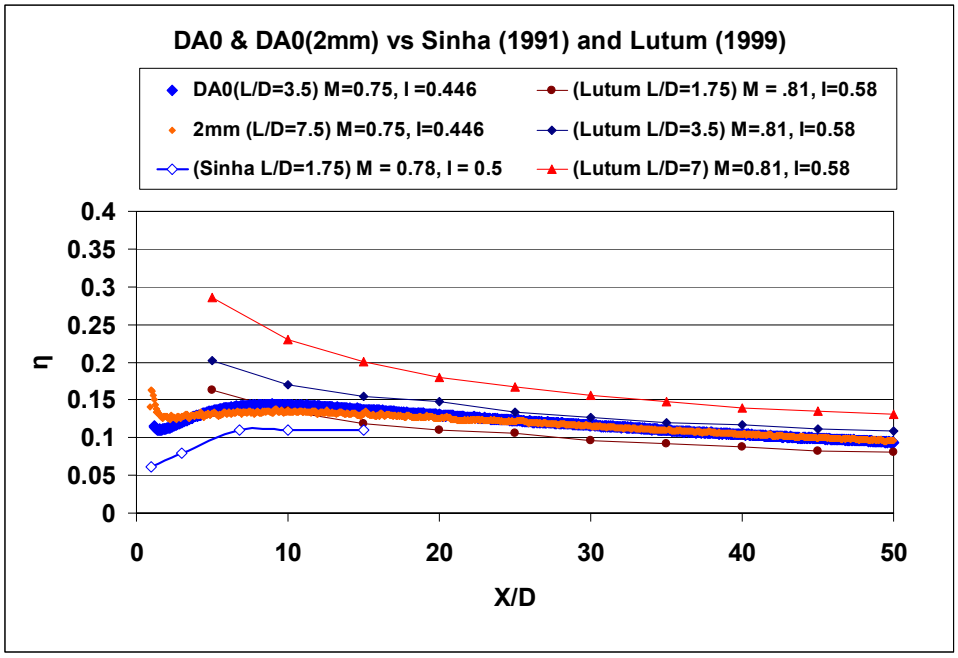

Figure 5-6 – Comparison of η_{la} versus literature at M = 0.75

Looking at figure 5-6, it is possible to notice that the results begin to diverge when compared to open literature. Since the blowing ratio is moderate at 0.75, it is safe to say that at this point the peculiarities of the rig, as well as operating conditions need to be addressed. For example, it is now well understood from the Lutum and Johnson (1999) study, that if you have coolant holes at L/D of 3.5 and 7.5, those with L/D = 7.5, will outperform those with the shorter L/D. However this is not the case for the present study, except at low values of X/D. In Lutum's case they used holes with a diameter of 4 mm, and as they varied the L/D, they increased the length only. So, they also kept the mass flow rate constant and in doing so, they were able to isolate the L/D effect. Given the conditions in their wind tunnel, as well as blowing ratio, and coolant hole diameter, it is possible to back-calculate the mass flow rate for all the blowing ratios in their study with the following formula, obtained after simple manipulation of the blowing ratio equation (5-1):

$$m_c = M \cdot \rho_m \cdot U_m \cdot \pi \cdot \frac{D^2}{4} \quad (5\text{-}1)$$

The resultant mass flow rate (per hole) for Lutum's coolant holes at a M=0.81 becomes 11.67E-04 kg/s. Using the same formula for both the DA0 and DA0(2mm) configurations yields 3.21E-04 and 1.22E-04 kg/s respectively. The large difference in coolant flow between the DA0 and the DA0(2mm) explains why those two plates exhibit the observed trends, when DA0(2mm) should have higher η_{la} than DA0 since it has a larger L/D. However, the fact that both have very similar η_{la} values, even though DA0(2mm) is using only 38% of the amount of coolant as DA0, is a testament to the influence that L/D has on the value of η_{la}. Lutum uses 3.63 and 9.57 times as much coolant as that used through the DA0 and DA0(2mm) holes, respectively, plus the geometry used by Lutum, as discussed in Chapter 2, has a PI/D of 2.86, meaning that the holes are relatively closer together than in the present study, naturally yielding higher η_{la} values. Therefore, it is difficult to obtain Lutum's exact η_{la} distribution, since the amount of coolant, and the spacing of the holes he is using will definitely have a large impact on the film cooling performance, even though other aspects of the geometry are very similar. At larger distances downstream of the holes (X/D >25) the curves begin to exhibit similar values; the exit geometry should not matter at this point.

The difference between Sinha et al.'s results (1991) and those of the present study show that a low L/D causes a decrease in η_{la}, and agree quite well in the trend they follow. It is important to point out that the present results fall in the middle of well established data, and that it seems prudent to believe that results obtained with the present test set up are reliable.

Since the present study is also conducted at values of M up to 1.5, it is necessary to compare sample results against those in literature. To that aim, figure 5-7 is presented.

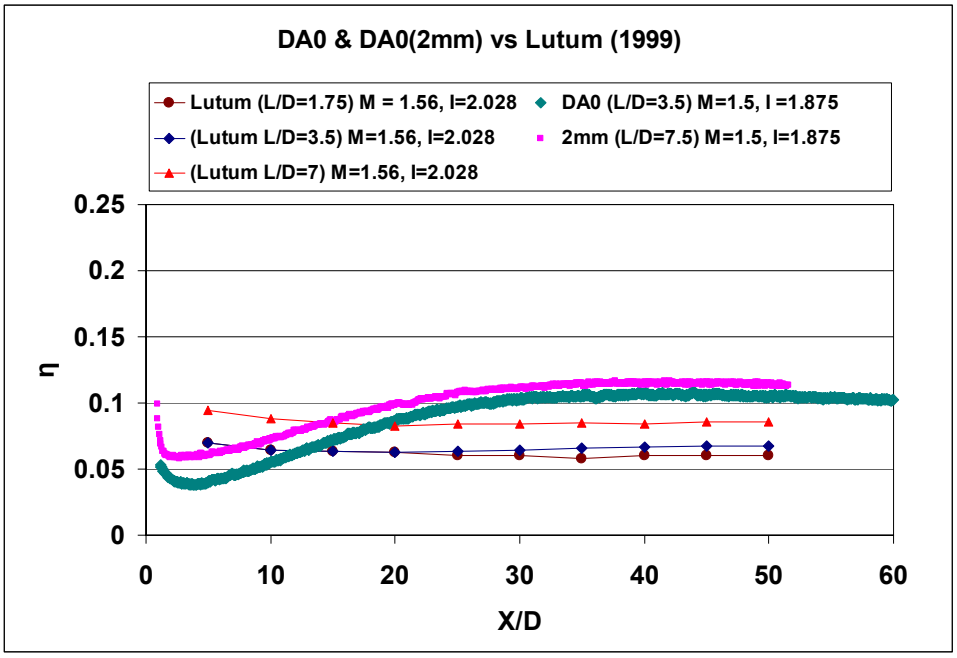

Figure 5-7 – Comparison of η_{la} at M = 1.5 vs. Lutum

The values of η_{la} observed in figure 5-7 for DA0 and DA0(2mm) are again satisfactory, and agree with the expected trend of the higher L/D yielding higher performance. For all results on chart, it is possible to see that the coupons with the higher L/D perform better, overall. What sets apart both sets of data is the difference in mainstream conditions. While in the present study, the turbulence intensity level is at 0.6%, with a boundary layer thickness of 4.85 cm [15.4 diameters for DA0, and 24.9D for DA0(2mm)], Lutum's tests were run at Tu = 3.5%, with a boundary layer thickness of 4mm (1 diameter). The resulting effect is that even though the jets lift off in the present study (the η values dip), the low turbulence level does not completely destroy or dissipate the structure of the jets, and allows them to reattach (at about X/D =20) and continue offering protection downstream. The increase in L/D allows the jets in the DA0(2mm) configuration to stay closer to the wall, and thus reattach, just as in DA0, while keeping relatively cooler temperatures (higher η_{la}) than the DA0 configuration. In Lutum's case,

the high turbulence, combined with the very thin boundary layer thickness, present a setup in which the jets are battered by the mainstream right from the hole exits, and do not have a chance to reattach. The resulting flow downstream has no structure; it is just the large mass flow what keeps the η_{la} at 0.08 and lower. For Lutum's study, the increased L/D effect is what allows the coolant for the holes with L/D = 7 to remain closer to the surface and thus provide slightly higher η_{la}. For this blowing ratio, the mass flow rates for DA0 and DA0(2mm) are 6.42E-04 and 2.45E-04 kg/s, respectively, while for Lutum's study m_c is 22.5E-04 kg/s.

Part of the reliability of data is the ability to reproduce it. The experiments for this study were conducted over a period of approximately 15 months. During that time, there were opportunities to repeat several tests, and choose the results for which the data yielded seemed to have better resolution, or to have a longer range. Such is the case presented in figure 5-8, below, in which the test labeled Test 1, showed results within acceptable uncertainty, but there had been questions about the cleanliness of the data, as well as the extent of the range over which it was presented. Thus, the test was repeated months later, over a longer stretch of TSP for the current study. Two weeks later, the test was repeated again and the data is shown for a blowing ratio of 0.75. For that case, a completely new layer of TSP was used, and the results were identical. For a given set of data, multiplying the maximum X/D by the diameter of the hole yields the maximum distance downstream of the exit; the shorter the value, the older the test. When observing the plots in the next section, the age of the tests does not seem to affect the trends, only the range.

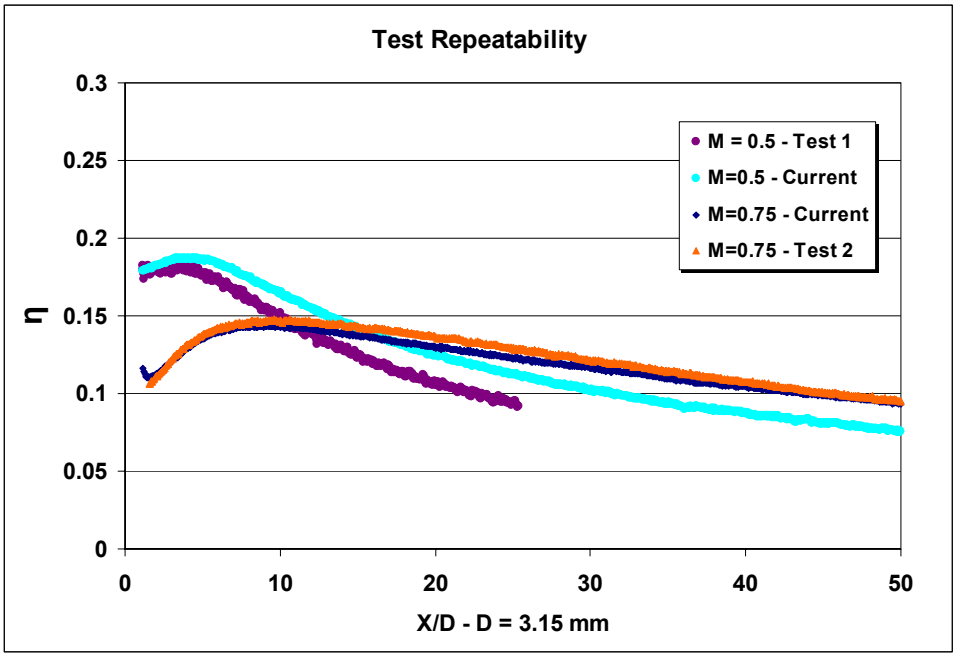

Figure 5-8 – Data from current study vs. repeats and older tests

It has been shown in this section that the results obtained for the configurations DA0 and DA0(2mm) compare satisfactorily against previous studies by showing acceptable η_{la} values and consistently follow expected trends, both from literature and between themselves. It is then, with this in mind that the results for the laterally averaged film cooling effectiveness for each configuration are presented next.

5.2.2 Results for All Configurations

Results for the laterally-averaged film cooling effectiveness are shown first grouped by blowing ratio, and then grouped by geometry.

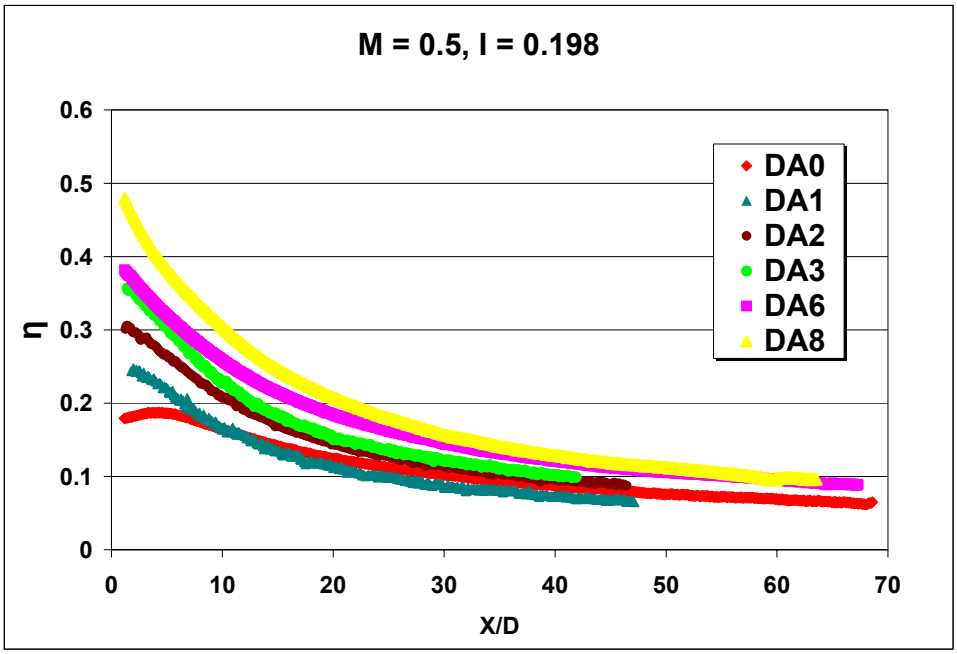

Figure 5-9 – Laterally averaged effectiveness for M = 0.5

Figure 5-9 shows that DA8 offers the highest η_{la} of all the configurations at M=0.5, with DA0 and DA1 offering the least protection. Even though DA1 does not apparently follow the trend is not reason for concern, since the difference between its η_{la} values and those for DA0 are within uncertainty. At distances downstream greater than 20 X/D, the observed higher effectiveness of some holes over others continue. This agrees with trends observed in studies showing long ranges of data such Lutum et al. (1999) and Baldauf et al. (2004). These studies suggest that effectiveness values persist well after values of X/D greater than 80. Figure 40 suggests that at such value of I for DA0, the film remains attached to the walls offering protection well downstream of the holes. It is important to keep in mind when looking at this data that the coverage values of all the holes are different. While coverage for DA0 is 33%, it is 65% for DA8. This means that the highest value of DA8 at the exit of the holes should be toward η_{la}=0.65, while only 0.33 for DA0. The implications of this will be discussed later in this

section. For now, only general trends will be discussed, in the context of the parameters M and I as defined in literature.

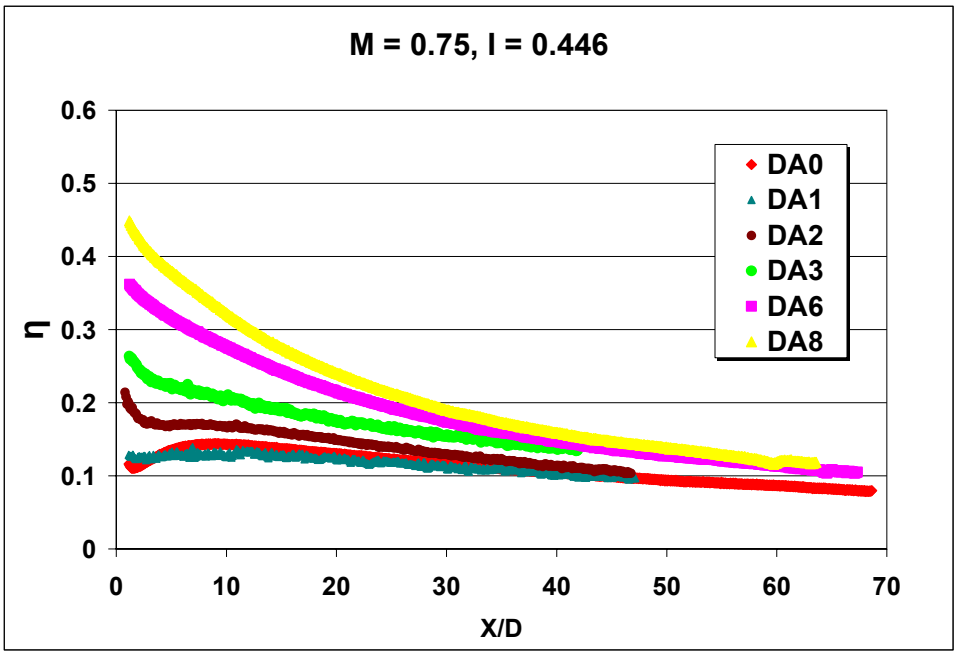

Figure 5-10 – M = 0.75

Increasing the blowing ratio to 0.75 brings changes in the performance of the coupons. The general shape of the curves in figure 5-10 is flatter, a trait more pronounced in the DA0 and DA1 configurations. Even though the higher diffusion angled plates show lower η_{la}, at low X/D, close inspection reveals that at X/D = 20 all plates have higher values than the previous case. At X/D = 40, the same observation applies. The trend continues for all remaining values of X/D.

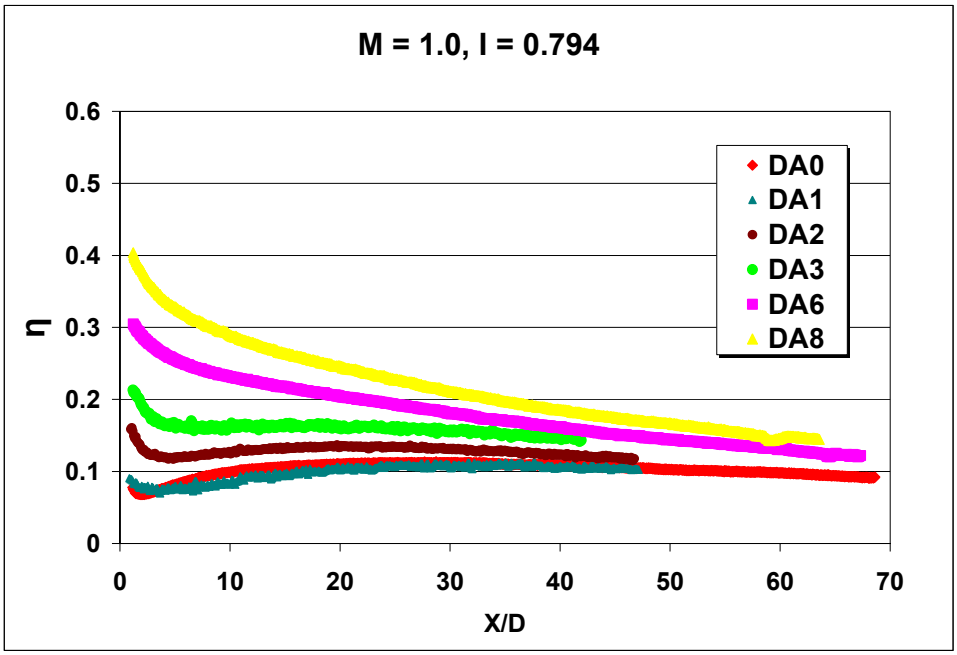

Figure 5-11 – M = 1.0

At blowing a ratio of 1.0, DA0, DA1 and DA2 start to lift off. This is evident in the "dip" of the curves at low X/D, and the subsequent rise and preservation of the η_{la} value of 0.1. DA3 also flattens out, while DA6 and DA8 show very similar values of η_{la} at X/D =20 as in M=0.75. However, the performance of these two plates, DA6 and DA8 improves for values of X/D > 30 when compared to M=0.75. As discussed extensively by Baldauf et al. in their 2004 study, it can be seen that while the laterally averaged effectiveness of these coupons is not higher than that for values of M of 0.5 and 0.75 close to the holes, if these jets (mainly for DA3, DA6 and DA8) are not detaching, then the increased flow must have another effect. The effect on the curves is a sort of shift toward the higher X/D values, compared to the previous M values. What this indicates is that the jets coming out of the holes have so much momentum that they travel downstream more quickly, and as they travel, they spread, eventually widening enough to the point that they start to interact with each other. Baldauf et al. say that the effect of this

interaction is the creation of a new massive "thickened closed film" whose thermal capacity prevents intense hot gas entrainment and early cooling film degradation. This concept will become more evident observing the individual effectiveness curves for each configuration.

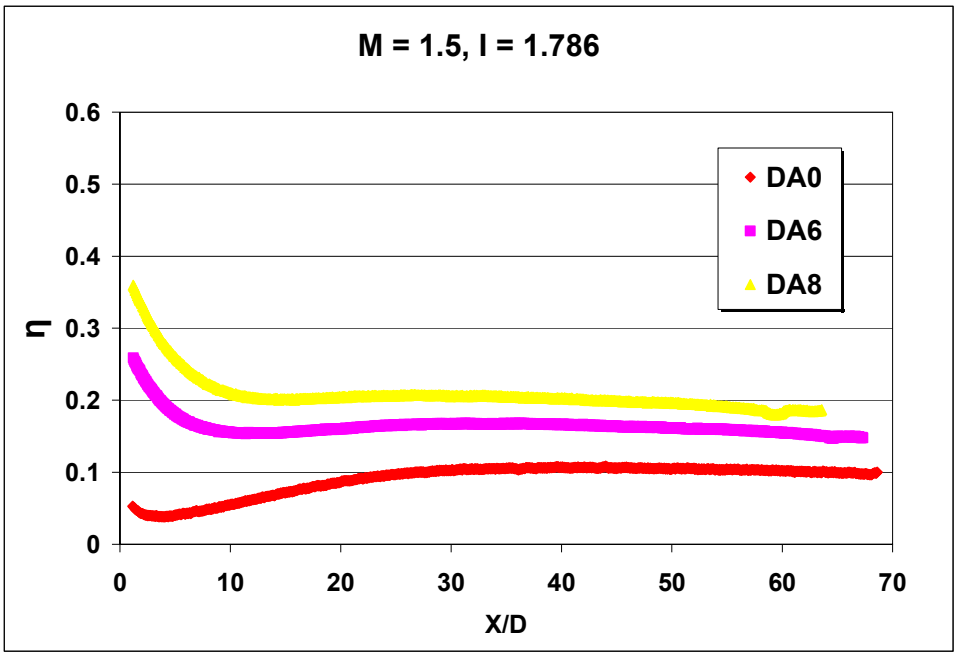

Figure 5-12 – M = 1.5

For plates DA1, DA2 and DA3 data is not presented. However, given the previous trends, it is easy to imagine the effectiveness curves to be packed together between the DA0 and DA6 curves. Figure 5-12 shows the DA6 curve hinting at detachment, while DA0 is detached. DA8 is still attached, but barely. DA0 seems to reattach after an X/D of 30. At X/D of 10, the value of η_{la} for DA8 falls by 25%, while after X/D of 32, the trend is reversed, and the values of η_{la} actually increase, and are preserved, further suggesting that jet interaction does help keep effectiveness values at an impressive 0.2 after sixty diameters downstream. For DA6, the same happens, but since the amount of mass flow for this coupon is less, 27% less, increase in effectiveness as a result of reattachment occurs and starts to fade over a shorter scale than that

for DA8. A closer look at the second "peaks" of the curves, which happen close to X/D =36, η_{la} = 0.1683, for DA6, and at X/D = 27, with η_{la} = 0.2074 for DA8, shows that there is less than 20% difference in effectiveness between them.

Now that all conical coupons have been compared against each other, in order to gain a different perspective into the behavior of each configuration, it is appropriate to look at them individually. For this purpose, laterally averaged film cooling effectiveness curves are presented for each coupon. Data for the compound holes DA0(2mm) and DA3(2mm) are also shown. However, to gain more of an insight into the coolant flow, the mass flow rates are shown in table 5-2. The discrepancy between the values of m_c for DA3 and DA6 can be explained by pointing out that the inlet diameter of DA3 is greater than that of DA6, thus having a larger flow area at the inlet. Ideally, if all holes were the same diameter, the mass flow rates would be equal for all holes for a specific blowing ratio.

Table 5-2 – Mass flow rates (per hole) for coupons at each blowing ratio

	M =0.5	M = 0.75	M = 1.0	M = 1.5
Coupon	m (kg/s)	m (kg/s)	m (kg/s)	m (kg/s)
DA0	2.14E-04	3.21E-04	4.28E-04	6.42E-04
DA1	2.36E-04	3.54E-04	4.72E-04	
DA2	2.51E-04	3.76E-04	5.01E-04	
DA3	2.83E-04	4.24E-04	5.66E-04	
DA6	2.56E-04	3.83E-04	5.11E-04	7.67E-04
DA8	3.07E-04	4.60E-04	6.13E-04	9.20E-04
DA0(2mm)	8.16E-05	1.22E-04	1.63E-04	2.45E-04
DA3(2mm)	8.24E-05	1.27E-04	1.64E-04	2.47E-04

For the sake of brevity, instead of presenting them one at a time, the coupons are shown in three groups. First, DA0 through DA3 are shown together as the low diffusion angle plates in figure 5-13. DA6 and DA8 are shown as the large diffusion angle plates in figure 5-14, and DA0(2mm) and DA3(2mm) are shown together as the compound hole group, figure 5-15.

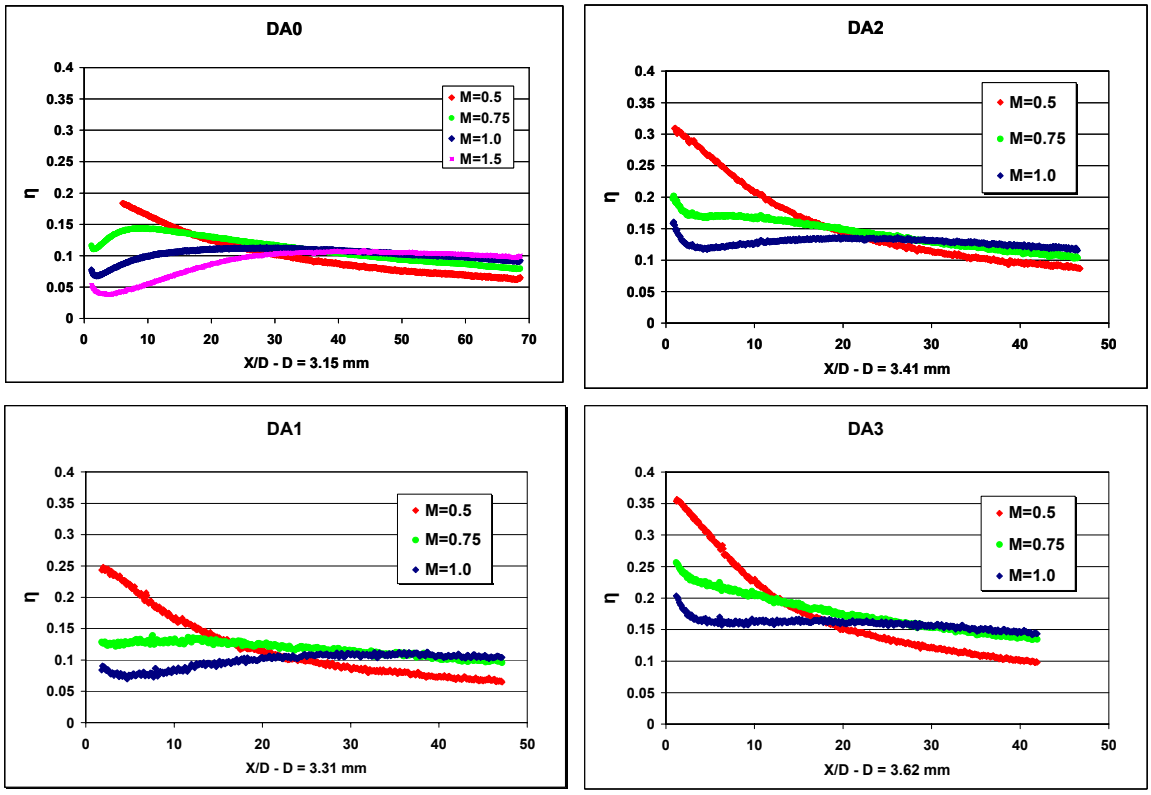

Figure 5-13 – Laterally averaged effectiveness for lower DA plates

As mentioned before, the blowing ratio of 0.3 was performed only for DA0 for literature comparison purposes. In general, DA0 and DA1 behave similarly, while DA2 and DA3 begin to show heightened values of laterally averaged effectiveness because of the aggregate effects of increased mass flow, lateral spreading of the jets, and reduced flow momentum at the exit. The last point will be explored in more detail in the next section.

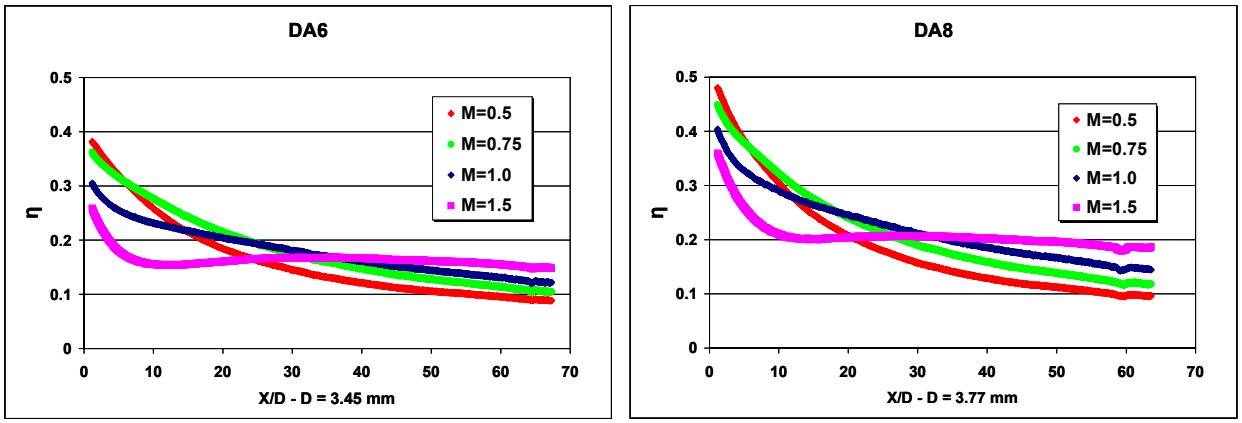

Figure 5-14 – Laterally averaged effectiveness for higher DA coupons

The trend of higher overall effectiveness at increasing blowing ratios continues for the two coupons in figure 5-14. For both plates, when the jets liftoff, even though they do so weakly, the existence of a second peak in effectiveness can be seen. This is especially true when M = 1.5. There are no signs of detachment for blowing ratios of 1.0 or less.

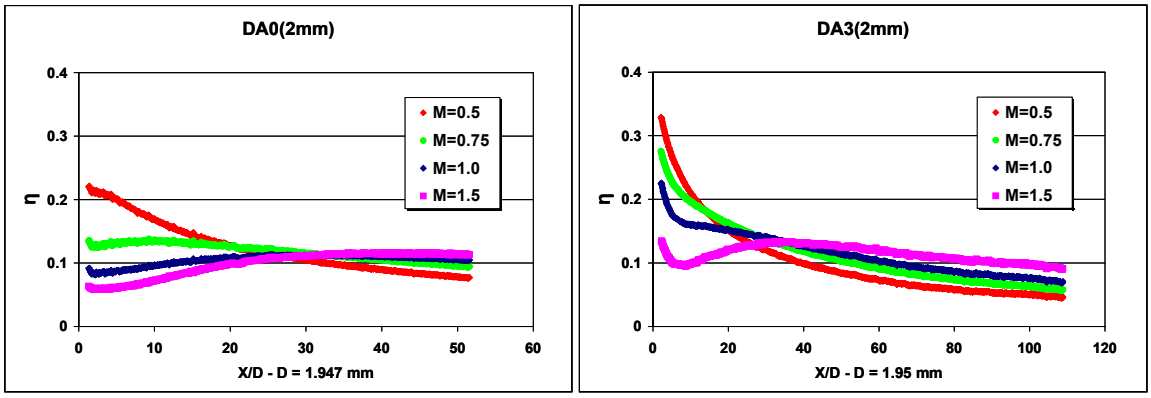

Figure 5-15 – Laterally averaged effectiveness of compound holes

For the two sets of data in figure 5-15, we see that η_{la} for the DA3(2mm) follows trends very similar to the other conical plates. Its effectiveness is higher at all blowing ratios compared to the nominal DA0(2mm), however the effect of the interaction of jets downstream is not as visible for DA3(2mm) as it is for the purely conical plates, i.e. DA3, for blowing a ratio of

1.0. For a closer look at this comparison, refer to figure 5-16. Figure 5-16 shows that the only difference in film cooling effectiveness between DA3 and DA3(2mm) is a slightly higher effectiveness in the near field region (X/D < 17). Up to this point the jets remember the exit geometry, and behave accordingly, suggesting that the jets from DA3(2mm) have a more well formed structure and are more prone to remain attached. Hence they have a higher effectiveness over this range. DA3 has a shorter L/D, so the effectiveness is not as high, but it is not significantly lower. Thus it is obvious that adding an entry length to a conical geometry does not have a negative influence on the values of effectiveness, au contraire, it enhances it.

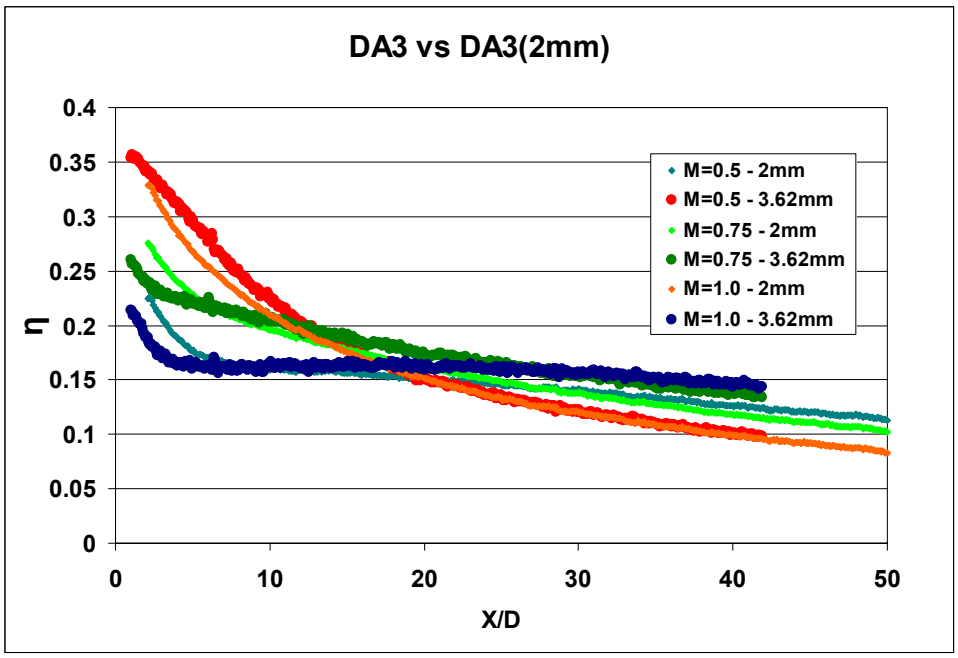

Figure 5-16 – Comparison of η_{la} for DA3 and DA3(2mm)

Figure 5-17 is included for completeness. It shows the performance of DA0 against that of DA0(2mm). In this case, there are two competing effects: on one hand is the increased L/D of DA0(2mm), which should lead to higher η_{la}, and on the other hand, the low mass flow rate through DA0(2mm), which is about 3.4 times less than that for DA0, bringing the

effectiveness down. The resulting effect helps DA0(2mm) to keep a relatively higher η_{la} at the hole exit region, and a higher overall effectiveness at M=1.5.

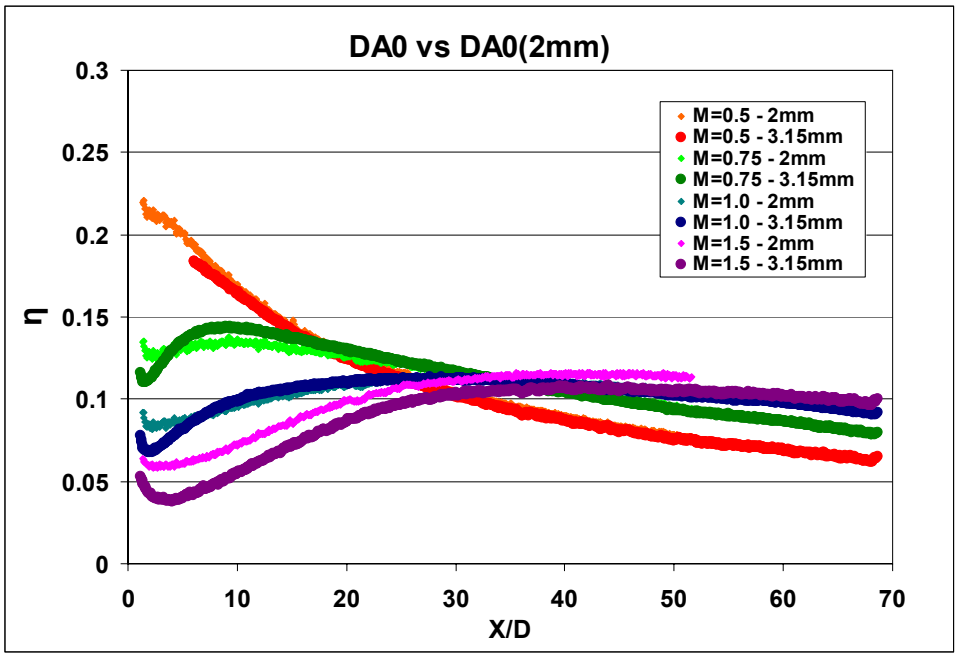

Figure 5-17 – Effectiveness comparison for DA0 and DA0(2mm)

The higher effectiveness values for DA0(2mm) also suggest a more compact jet structure with less momentum than that of the DA0 jets, which helps it retain its cooling ability more efficiently.

5.2.3 Comparison of Data Based on Hole Exit Conditions

As it was pointed out in the previous section, there is a certain amount of inadequacy when using the blowing ratio and the momentum flux ratio, as classically defined based on the hole inlet diameter, when comparing η_{la} for cylindrical holes against values for conical holes. The definition of the blowing ratio is based on the momentum of the coolant at the inlet area because, for cylindrical holes, the exit area is also the same. However, for diffusing holes such

as conical or fan shaped holes, the effect of the increasing exit area lowers the velocity of the coolant, thus lowering the momentum, resulting in a lower blowing ratio at the exit. Assuming perfect diffusion at the exits of the conical holes, a simple manipulation of terms in the definition of the blowing ratio, M, yields the blowing ratio at the exit, M_e.

$$M_e = \frac{M}{AR} \tag{5-2}$$

This subsequently leads to the new definition of the exit momentum flux ratio.

$$I_e = \frac{\left(\frac{M}{AR}\right)^2}{DR} \tag{5-3}$$

Having calculated those figures for each configuration, gives a more complete picture of what is happening at the exit of each individual hole type.

Table 5-3 summarizes the value of the exit blowing ratios and exit momentum flux ratios for each plate, corresponding to each inlet blowing ratio (shown as Mi) reported previously. The gray bands in the table highlight the values of the nominal plates, DA0 and DA0(2mm), which are unaffected by the new definition. The light gray values show values that would have resulted from tests that were not reported for the present study. Included in this table are also the values of the Reynold's number for each coupon, at all blowing ratios, based on the inlet diameter.

Table 5-3 – Coolant ratios at the exit of diffusion holes

	Mi=0.3					
Coupon	Re_D	Me	Ie			
DA0	3269	0.300	0.071			
	Mi=0.5			Mi=0.75		
Coupon	Re_D	Me	Ie	Re_D	Me	Ie
DA0	5449	0.500	0.198	8173	0.750	0.446
DA1	5726	0.436	0.151	8588	0.653	0.339
DA2	5897	0.375	0.112	8845	0.563	0.252
DA3	6265	0.351	0.098	9397	0.527	0.220
DA6	5955	0.197	0.031	8933	0.295	0.069
DA8	6524	0.181	0.026	9786	0.271	0.058
DA0(2mm)	3366	0.500	0.198	5049	0.750	0.446
DA3(2mm)	3371	0.255	0.051	5057	0.382	0.116
	Mi=1.0			Mi=1.5		
Coupon	Re_D	Me	Ie	Re_D	Me	Ie
DA0	10898	1.000	0.794	16347	1.500	1.786
DA1	11451	0.871	0.602	17177	1.307	1.355
DA2	11793	0.751	0.447	17690	1.126	1.006
DA3	12530	0.703	0.392	18795	1.054	0.882
DA6	11911	0.394	0.123	17866	0.590	0.277
DA8	13048	0.362	0.104	19573	0.543	0.234
DA0(2mm)	6732	1.000	0.794	10097	1.500	1.786
DA3(2mm)	6742	0.509	0.206	10113	0.764	0.463

Looking at the new exit blowing ratio figures yields three clusters of plates that can be classified according to the new exit measurements, they are: very low blowing ratio, low blowing ratio, and moderate low blowing ratios. However, showing results of the laterally averaged effectiveness for the new blowing ratios is not totally fair either, since the lateral diffusion of caused by the conical holes will always yield higher laterally averaged values of film cooling effectiveness due to the increased coverage area. Thus, a way to scale the lateral values to a per-span basis, is to divide the effectiveness by the coverage. If all effectiveness values were available starting from the hole exits, all curves would start at 1. For example, we can expect the laterally averaged effectiveness of the DA8 configuration to be higher than that of DA0 at the

exit of the holes, as well as say 20 diameters downstream from the holes, however, for a blowing ratio of 1, it is hard to tell how the coolant is behaving for each set of holes, since both have very different starting points. Thus, looking at the effectiveness normalized with the coverage, as well as the exit blowing ratios for each configuration will yield somewhat qualitative data that will reveal more about the physics of the coolant's travel downstream of the exit holes, regardless of what coverage or PI/D the holes have.

For comparison, data from the study by Gritsch et al. (2005) are included. Table 5-4 below shows important information about the geometry of the fan holes used in their studies. These specific fans were chosen, not because of their similarity to the present study, but because of the exit blowing ratios, as well as the fact that some had geometry, mainly the lateral expansion, that has a certain similarity to those tested for this thesis. Also, there is a certain element of real world applicability to the fan plates in those studies, as well as certain engine like operating conditions that are used.

Table 5-4 – Operational details of Gritsch study

	M(in)	M(ex)	I(ex)	Diameter	Diff angle	α	AR	Coverage	Total L/D	Entry L	Pitch	DR	Tu (%)
Gritsch M	1	0.286	0.048	4mm	4 lat, 4 laidback	30	3.5	0.43	11.5	2D	6D	1.7	4
Gritsch N1	1.5	0.319	0.06	4mm	8 lat, 3 laidback	30°	4.7	0.63	11.5	2D	6D	1.7	4
Gritsch L1	2	0.476	0.133	4mm	9 lat, 0 laidback	30°	4.2	0.63	11.5	2D	6D	1.7	4
Gritsch N2	2.5	0.531	0.166	4mm	8 lat, 3 laidback	30°	4.7	0.63	11.5	2D	6D	1.7	4
Gritsch L2	2.5	0.595	0.208	4mm	9 lat, 0 laidback	30°	4.2	0.63	11.5	2D	6D	1.7	4
Gritsch H	1.5	0.6	0.212	4mm	4 lat, 2 laidback	30°	2.5	0.37	11.5	2D	6D	1.7	4

Figure 5-18 shows the data for the coupons under the new exit condition of very low blowing ratio and normalized laterally averaged effectiveness.

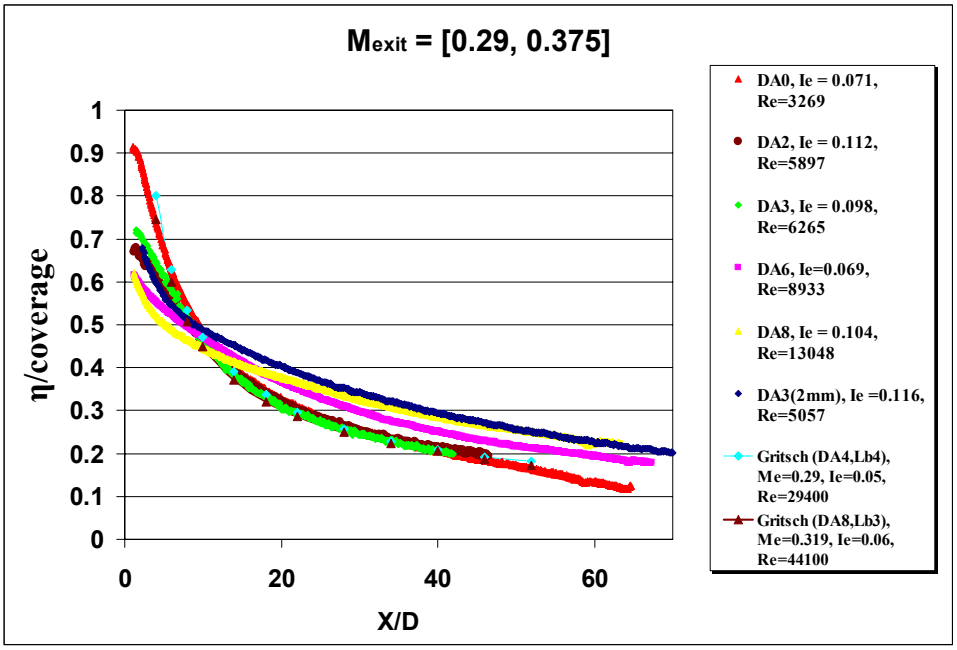

Figure 5-18 – Performance comparison at very low exit blowing ratio

In this figure, it is obvious that the performance of all coupons is essentially the same after a distance of about 8 diameters. This indicates that all coupons are behaving very similarly, and that differences in η_{la} are caused mainly by the coverage of the holes, which, when normalized, becomes very apparent. The reader is also invited to observe that the Reynolds numbers for Gritsch's study are consistently much higher than those in the present study, even though the differences in inlet diameter are on average only 25%.

Looking at DA8 and Gritsch's DA8,Lb3 holes, the laidback hole starts out with a higher effectiveness, but after 8 diameters both are at the same value. After that, the conical configuration remains higher than the fan. While the fan decreases to an effectiveness of 0.2 at X/D = 40, the conical holes reach that at about 55 X/D. For that matter, even the DA6 configuration performs very well after X/D = 8, even though the Reynolds number inside those holes is about 1/5 of that inside the fan holes. One can imagine that the story these holes are

telling is that the conical holes, at their respective inlet blowing ratios are not as evenly spread over the cooled wall as are the fan holes. This works in the favor of the fan holes closer to the exits. However, this also means that the film gains more heat from the wall, warming up more quickly, and losing performance over a lower X/D, explaining the steeper drop in η_{la}. For the fan plates, it was pointed out by Saumweber et al. (2003) that the jets come out and begin to interact immediately, thus yielding higher η_{la} values in the near field region. Other configurations (cylindrical, and conical) may be actually reattached by the jet interactions downstream, helping them regain and preserve some of their film cooling capabilities, a finding definitely worth further inquiry.

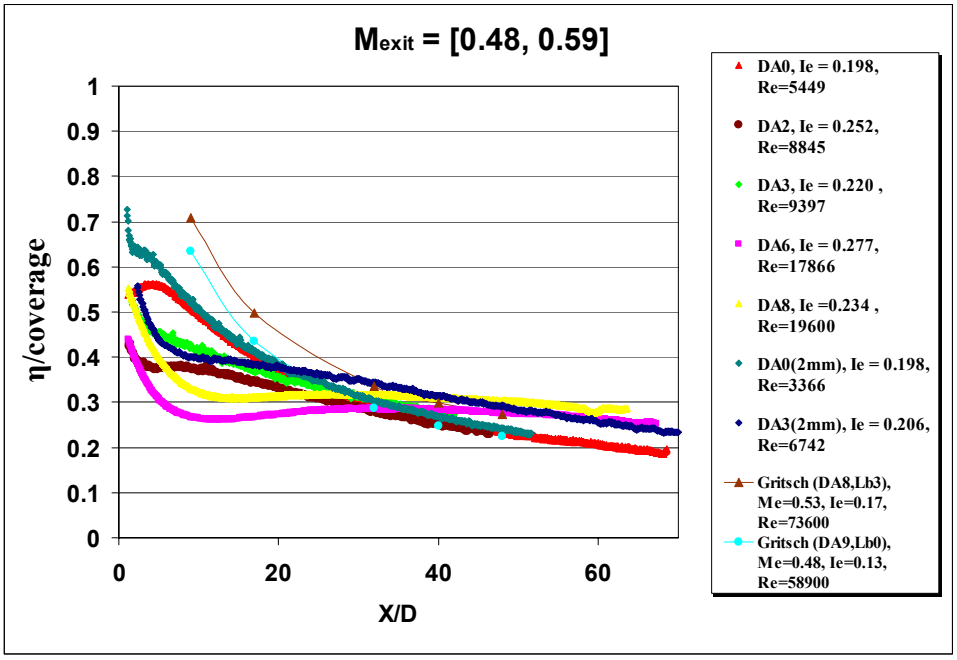

Figure 5-19 – Comparisons at low exit blowing ratios

Figure 50 shows the normalized laterally averaged effectiveness for most configurations compared to a pair from Gritsch's study. Their configurations were chosen because of the 8 and 9 degree lateral diffusions, which are similar to those in the present study.

One can clearly see that at their high (inlet) blowing ratios, DA8,Lb3 and DA9,Lb0 perform very well compared to the conical holes up to X/D = 20. All of the conical and cylindrical holes (with the exception of DA8) remain attached. DA0, DA0(2mm) and DA3(2mm) behave very similarly, with higher effectiveness per coverage close to the hole exit, compared to the conical holes. DA8 is detached for the lower values of X/D. It is important to point out that even though DA8 becomes detached, the jet reattaches and begins a period of protracted even protection. Three scenarios for this difference are possible: 1) the natural layback of DA8 (since it is conical, it has an 8 degree sort of layback) may be helping the flow reattach downstream, or 2) the expansion of the coolant at the exit progresses downstream and at X/D = 20 begins to form a layer, mentioned by Baldauf et al (2002), which helps the coolant preserve its thermal integrity further. This second theory is helped by the emergence of the second peak in effectiveness which helps maintain the curve relatively flat over a length of about 40 diameters, starting at L/D of 11. Thus, even though DA8 is detached at this point, in its reattached form it creates a film layer that allows it to eventually outperform all the configurations over a long stretch. This is an especially noteworthy observation since in industrial applications one would like to have extra extended performance (meaning more space between rows of holes) and use of less coolant per unit span (DA8 Re_D is much lower than that of DA9,Lb0); not to mention the smooth temperature gradients that having such even film cooling effectiveness can provide, whose impact in the lifespan of parts can be critical. The third theory is that the levels of turbulence, in the tunnel are so low that the film is allowed to continue virtually undisturbed, as opposed to the film in the Gritsch study, in which the 4% turbulence intensity does affect the integrity of the coolant jets, which have nothing to gain from the levels of turbulence, except at the near-exit

region. This is a subject worth investigating further, and will be mentioned again in the recommendations.

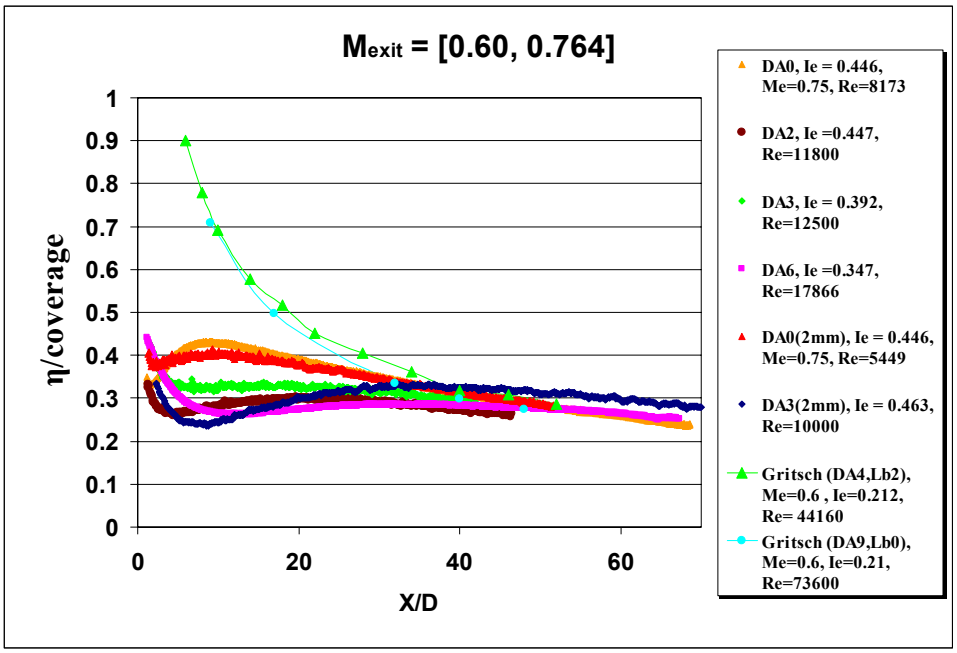

Figure 5-20 – Comparisons at moderately low exit blowing ratios

Figure 5-20 shows that at this range of exit blowing ratios, that the chosen fan shaped holes are outperforming the conical plates since these are detaching or hinting at detachment. Possible explanations for this behavior are that the fan holes are helped in staying attached because of the entry length of the holes. The fans, as seen in table 5-4, have and entry length of 2D, while the cones have none. The fans also have a total L/D of 11.5, compared to the 3.5 of the cones. This larger L/D in the fans provides ample space with favorable conditions for the jets to expand and attach to the walls of the diffuser-like geometry. This is on top of the entry length, which has been shown to be of utmost influence in jet attachment. However, the most striking difference between the fan geometry and the conical is the momentum flux ratio. While the conical holes have values of I somewhere between .35 and .45, the fan plates are still at 0.21.

This means that the jets are going to remain attached, and perform very well, even at such high jet Reynolds numbers. It is safe to say that one the influential parameters bringing about such dramatic results are the large area ratios. Therefore, it would be more appropriate to test the conical at the same exit momentum flux ratios as the fans, as well as the same blowing ratios. An even better way to establish the differences between conical and fan-shaped holes would be by building fan-shaped holes that mimic the area ratios and angles of diffusion of the conical geometry. When tested in the same rig, and at the same exit conditions, such a study would yield far more conclusive data.

Aside from the realization that more evenly matched fan and conical geometry comparisons are needed, the more striking result in this section is that the performances of the DA3 and DA3(2mm) geometries are very similar. Showing this accomplishes the goal of finding an easier way to implement the use of conical geometry for industrial applications. In the past, the use of conical holes has been hampered by the need to have a reliable metering diameter. Analogous to entry-length used on fan-shaped holes, adding a cylindrical entry length accomplishes the same results for conical holes. While the setbacks of having an entry length may not have surfaced in this study, if there are any, it is easy to say that cooling effectiveness is not negatively affected, thus, opening the door for wider use of conical cooling holes.

CHAPTER 6

CONCLUSION

From the observed behavior of the conical holes and the coupons with cylindrical entry length, a set of conclusions can be drawn:

Conical holes, in general, have higher discharge coefficients than the cylindrical holes tested in this study. Increasing the angle of diffusion shifts the peak in the C_D curve toward a lower pressure ratio. The general trend after this peak is for the C_D to increase slowly with higher PR, suggesting there is less resistance to flow with the increasing diffusion angle. Results vary slightly for the DA6 configuration, which stays at higher C_D values than the DA8, perhaps showing that DA6 has the optimal diffusion angle.

For the DA3(2mm) configuration, the CD curve behaves similarly to that of the conical holes, but over a larger range of pressure ratios. The higher L/D appears to "spread" the CD over a higher range of PR, while the diffusion angle allows higher C_D values. The combined effect of these geometric modifications appears to be a much higher C_D curve than that of the DA3 configuration.

It is recommendable that further studies be carried out to extend the trends that the added cylindrical entry length has on the conical holes. Higher discharge coefficients can lead to more effective cooling schemes, while economizing in the use of coolant, thus it would be easier to achieve the desired blowing ratios at a lower PR than those of cylindrical holes.

When comparing laterally averaged film cooling effectiveness results at low inlet blowing ratios, DA0 and DA1 have the lowest η_{la} for all X/D. As the angle of diffusion is

increased, the values of η_{la} also increase. This trend continues as the inlet blowing ratio increases to 1.0. At that point, the configurations DA0, DA1, DA2 and DA3 detach and reattach, with this feature more pronounced for the lower DA coupons. This trend is easily explained by the exit momentum flux ratio values having reached at least 0.3 for all plates, which in literature has been found to be a number that determines the tendency for detachment. The only contribution of the conical hole geometry is that it maintains the values of effectiveness relatively higher, even when detached, due to the increased lateral coverage.

At the highest tested inlet blowing ratio, M=1.5, the exit jets of all the tested plates detached. The conical holes still yielded higher η_{la} compared to the nominal configuration. Again, the conclusion is that this is a manifestation of the effect of the increased lateral coverage.

DA0 and DA0(2mm) behave very similarly, with DA0(2mm) yielding slightly higher values of η_{la} at the higher blowing ratios. This is explained by the higher L/D of DA0(2mm) and also to the low turbulence levels in the test section, which may help the less developed jets of DA0 to preserve their structure as a result of this. At higher turbulence levels, the values of the η_{la} curve should shift down with respect to DA0(2mm) as in the study by Lutum et al. (1999).

DA3(2mm) follows the same trends in effectiveness as the other coupons. Compared to DA3, the added cylindrical length improves effectiveness slightly at the near field region, but its effects dissipate farther downstream. This means that it is possible to manufacture cooling holes that will provide the benefits of the conical geometry, but that will have a metering diameter, similar to fan-shaped holes..

Normalizing the effectiveness by the coverage and comparing the data exit conditions of blowing ratio and momentum flux ratio is a useful tool in gauging behavior of the film cooling

effectiveness for holes of different expanded exits with similar inlet geometry, since it also highlights the relative trends in downstream jet interaction and its effect on η_{la}.

Examining the normalized effectiveness data and comparing it to fan shaped cooling holes of relatively higher diffusion angles, it can be said that while the effectiveness values of the conical configurations is not as high as that of the fans at the low X/D (< 20), the conical holes eventually provide more even and extended film protection. This is in part due to the lateral widening of the conical jets as X/D increases, which eventually allows them to join, interact, and form a "super-layer" that lets the coolant retain its thermal properties over extended distances. This is a very attractive feature since industry is always trying to get the most out of fewer holes and less coolant. The evenness of this layer also fosters lower temperature gradients, which are desirable features in the design of parts with long operational life. On the subject of coolant, in order to attain the same blowing ratios as those of the fans (inlet and exit), the conical holes were found to spend considerably less coolant than the fans. Recommendations for further study of conical holes include the manufacturing and testing of plates with fan shaped holes of similar angles of diffusion, L/D, and area ratios, under the same conditions. This will provide a fairer comparison, since different test setups naturally tend to influence the data they produce.

Testing more conical holes at higher diffusion angles and blowing ratios will further the understanding of the observed trends, and help pinpoint at which point performance suffers due to diffusion or other unforeseen geometric effects. Again C_D and η_{la} values should be compared against fans of similar configurations.

The emergence of the entry length as an influential parameter in the behavior of conical holes needs to be further explored. Trends in increasing the entry-length L/D from zero to other values beyond 10 should help point out the benefits or hindrances caused by this parameter.

Changes in the conical-section L/D should also be explored and compared to trends in variations of it, such as in Lutum and Johnson's study.

And, lastly, flow visualization studies need to be conducted to characterize the behavior of the jets as they exit, detach, reattach, join, interact, and carry coolant. Why they are able to form a cohesive long-lived cooling blanket even after detachment and reattachment should be a very interesting, and potentially beneficial answer. The effects of mainstream turbulence definitely play a role in this, and should be accounted for in such study. Thus, a better understanding of the intricacies of the behavior and interaction of conical holes has the potential to change the way industry applies coolant holes to its designs.

APPENDIX A: POST-PROCESSING MATLAB CODE

This is the code that was used to process all TSP images. The code yields a results matrix, which can be accessed with a spreadsheet program such as EXCEL.

```
%Finding the amount of shifts for each picture
r=imread('lon.tif');
imagesc(r);imagemenu;
%repeat above two lines for one of the pictures of all the runs
%i.e br0,run1...etc. Basically change "r1" in line 1 to "br01", "11"
%etc.

%Input Image limits. jmin is the y coord value of the centerline of the
%first hole of interest (or) beginning of the paint, jmax is the y coord value
%of the centerline of the last hole of interest (or) end of the paint. imax is
%the x coord value of the starting of the paint and imin is 500 pixels less
%than imax.

imin=1;
imax=1162;
jmin=317;
jmax=795;

%Set Reference Temperature
tr=25.5;

%Read in the running "hot" image
i1=imread('11.tif');
i2=imread('12.tif');
i3=imread('13.tif');
i4=imread('14.tif');
%The above 4 images has to be changed for every run i.e "11.tif" is to be
%replaced by "21.tif" etc.

%Convert to double for imagesc sake
i1=double(i1);
i2=double(i2);
i3=double(i3);
i4=double(i4);
I=(i1+i2+i3+i4)./4;

%Truncate & Shift particular image if necessary
I=I(imin-1:imax-1,jmin-3:jmax-3);
%The limits have to be changed for every run.

%Read in the reference "cold" image
r1=imread('r1.tif');
r2=imread('r2.tif');
r3=imread('r3.tif');
r4=imread('r4.tif');

%Convert to double for imagesc sake
r1=double(r1);
r2=double(r2);
```

```
r3=double(r3);
r4=double(r4);
R=(r1+r2+r3+r4)./4;

%Truncate & Shift Reference Image if necessary

R=R(imin:imax,jmin:jmax);

%calc Tr first using the 3rd order polynomial calib relation of 12/18
ta=(tr-22)/100;
f=0.5875*ta^2-1.4844*ta+1.0086;
Rc=f.*I ./R;

t1=-0.9013*Rc.^3;
t1=t1+2.2206*Rc.^2;
t1=t1-2.5598*Rc;
t1=t1+1.2422;
t1=100*t1+22;

dat1=t1;%change this for every run   <<<<<   <<<<<<    <<<<<

imagesc(t1);imagemenu;

%Repeat above lines of code for all runs and obtain matrices
%dat0,dat1,...etc

%After completing the above lines of code for all the runs, delete all
%files other than dat0, dat1.v.etc from the workspace using the CLEAR
%command. EXAMPLE: clear I , this clears the variable I from the workspace.
%Once the files are cleared, use the SAVE command to save workspace for
%future reference

save 'data_071706';

%This will save the matrices dat0, dat1...etc into the disk in the file
%data_031306.mat. It can be retrieved in the future using the LOAD command.
%Use the date of run as the filename.

load 'data_062906';

%Define pixel per mm, calculated from a known physical distance.
pmm=5.44432;

%Define x in mm

for i=1:imax-imin+1
    k=imax-imin+2-i;
    x(i)=(k/pmm)+1.2; %Here 1.2 is the distance between the edge of the hole
and the beginning of the paint
end

%Obtain the mean temperature value as a column vector of all the runs

%T5=mean(dat5,2);
T4=mean(run4,2);
```

```
T2=mean(run3,2);
T3=mean(run2,2);
T1=mean(run1,2);
Tr=mean(run0,2);

x=x'; %Convert row vector to a column vector

%Create a variable T which has all the temperatures and the x-values

T(:,1)=x;
T(:,2)=Tr;
T(:,3)=T1;
T(:,4)=T2;
T(:,5)=T3;
T(:,6)=T4;
%T(:,7)=T5;

dlmwrite('Results.csv',T,',');

%Obtaining ETA colour plot from TSP image: Run this for as many runs as
%needed. Make sure to use the corresponding coolant temperature

%now take the Lon image and cut same area that is being used for the
%temperature files and make a new matrix out of it. From this new image
%find the J locations of the strips of paint that need to be processed
%in other words, if the effectiveness is to be calculated between two
%centerlines, then find the y location of those two holes and name them
%accordingly

j1=137;
j2=344;

a0=dat0(1:1162,j1:j2);
a1=dat1(1:1162,j1:j2);
a2=dat2(1:1162,j1:j2);
a3=dat3(1:1162,j1:j2);
a4=dat4(1:1162,j1-2:j2-2);
a5=dat5(1:1162,j1-2:j2-2);

%This next segment averages the temperatures on those strips of paint.

Tr1=mean(a0,2);
Taw11=mean(a1,2);
Taw21=mean(a2,2);
Taw31=mean(a3,2);
Taw41=mean(a4,2);
Taw51=mean(a5,2);


% This next segment writes all the average temperatures into a matrix

T(:,1)=x;
T(:,2)=Tr1;
%T(:,3)=Tr2;
%T(:,4)=Tr3;
```

```
T(:,3)=Taw11;
%T(:,6)=Taw12;
%T(:,7)=Taw13;
T(:,4)=Taw21;
%T(:,9)=Taw22;
%T(:,10)=Taw23;
T(:,5)=Taw31;
%T(:,12)=Taw32;
%T(:,13)=Taw33;
T(:,6)=Taw41;
%T(:,15)=Taw42;
%T(:,16)=Taw43;
T(:,7)=Taw51;
T(:,8)=Taw61;


%The matrix can now be written into a CSV file

dlmwrite('Results.csv',T,',');

%The following lines can be used to calculate effectiveness on the spot
only input the coolant temperature

eta6=(a6-a0)./(-13.2-a0);
eta5=(a5-a0)./(-14-a0);
eta4=(a4-a0)./(-16.4-a0);
eta3=(a3-a0)./(-16.7-a0);
eta2=(a2-a0)./(-15-a0);
eta1=(a1-a0)./(-16-a0);
```

APPENDIX B: C_D PROCESSING MATHCAD CODE

This is the Mathcad code used to calculate the Discharge Coefficient:

Discharge Coefficient (C_D) Calculation

ORIGIN:= 1

Input Variables

D = diameter of cooling hole

m_a = mass flow rate thru cooling holes

P_{stat} = hole exit pressure (main flow static pressure)

P_c = plenum pressure

T_c = plenum temperature

N_h = number of holes

Air Properties

κ = specific heat ratio

R = gas constant

ρ = density

Units / Conversions

$SCFH := 9.439 \times 10^{-6} \frac{kg}{s}$ $\quad in\_H2O := \frac{in\_Hg}{13.55}$ $\quad P_{atm} := 101325 Pa$

Constants

$\kappa := 1.40$ $\quad R := 287 \cdot \frac{J}{kg \cdot K}$ $\quad N_h := 8$ $\quad T_o := 273 K$

Measured Values

$D := 0.1343 in$ $\quad P_{stat} := -.04 \cdot psi$

$P_{bias} := 0.0818 psi$

$$P_c := \begin{pmatrix} -.04 \\ -.02 \\ 0 \\ .03 \\ .065 \\ .1 \\ .124 \\ .148 \\ .167 \\ .192 \\ .229 \end{pmatrix} \cdot psi$$

Flow values are input from measurements

$i := 1..11$

$$Q_{meter} := \begin{pmatrix} 0 \\ 63.874 \\ 117.722 \\ 166.87 \\ 210.818 \\ 258.44 \\ 285.314 \\ 320.562 \\ 342.936 \\ 372.184 \\ 411.032 \end{pmatrix} \cdot SCFH$$

$m_a := Q_{meter}$

$m_a =$

	1
1	0
2	$6.029 \cdot 10^{-4}$
3	$1.111 \cdot 10^{-3}$
4	$1.575 \cdot 10^{-3}$
5	$1.99 \cdot 10^{-3}$
6	$2.439 \cdot 10^{-3}$
7	$2.693 \cdot 10^{-3}$
8	$3.026 \cdot 10^{-3}$
9	$3.237 \cdot 10^{-3}$
10	$3.513 \cdot 10^{-3}$
11	$3.88 \cdot 10^{-3}$

$\frac{kg}{s}$

Temperatures

$D_{ave} := D$

$$T_1 := \begin{pmatrix} 28.7 \\ 27.7 \\ 27.4 \end{pmatrix}$$

$$T_{main} := \begin{pmatrix} 62.9 \\ 63.2 \\ 63.3 \end{pmatrix}$$

$T_{main} := mean(T_{main}) \cdot K + 273K$

$T_{main} = 336.133K$

Correct Measured Values

$P_{stat} = -0.04psi$

$P_{stat} := P_{stat} + P_{atm} - P_{bias}$

$P_c := P_c + P_{atm} - P_{bias}$

$T_1 := T_1 \cdot K + T_o$

$Tave := mean(T_1)$

Pressure Ratio

$$Pr := \frac{P_c}{P_{stat}}$$

$Pr =$

	1
1	1
2	1.001
3	1.003
4	1.005
5	1.007
6	1.01
7	1.011
8	1.013
9	1.014
10	1.016
11	1.018

$$\rho := \frac{P_{stat}}{R \cdot T_{main}}$$

$P_c =$ psi

	1
1	14.574
2	14.594
3	14.614
4	14.644
5	14.679
6	14.714
7	14.738
8	14.762
9	14.781
10	14.806
11	14.843

C_D Calculation

$$C_{D_i} := \frac{\frac{m_{a_i}}{N_h}}{\frac{\pi}{4} \cdot D^2 \cdot P_{c_i} \cdot \left(\frac{P_{stat}}{P_{c_i}} \right)^{\frac{\kappa+1}{2 \cdot \kappa}} \cdot \sqrt{\frac{2 \cdot \kappa}{\kappa - 1} \cdot \frac{1}{R \cdot Tave} \cdot \left[\left(\frac{P_{c_i}}{P_{stat}} \right)^{\frac{\kappa-1}{\kappa}} - 1 \right]}}$$

$C_{D_i} =$

	1
1	0
2	0.46
3	0.6
4	0.643
5	0.663
6	0.704
7	0.718
8	0.754
9	0.769
10	0.788
11	0.808

Final Discharge Coefficient

$C_D =$

	1
1	0
2	0.46
3	0.6
4	0.643
5	0.663
6	0.704
7	0.718
8	0.754
9	0.769
10	0.788
11	0.808

$$P_{total} := 0.1675\,psi + P_{atm} - P_{bias}$$

$$\rho := \frac{P_{stat}}{R \cdot T_{main}} \qquad \rho = 1.042 \frac{kg}{m^3}$$

$$V_{main} := \sqrt{\left(P_{total} - P_{stat}\right) \cdot \frac{2}{\rho}}$$

$$V_{main} = 52.412 \frac{m}{s}$$

$$BlowRatio := \frac{\frac{m_a}{N_h}}{\left[\frac{\pi \cdot (D)^2}{4}\right] \cdot \rho \cdot V_{main}}$$

$Pr =$

	1
1	1
2	1.001
3	1.003
4	1.005
5	1.007
6	1.01
7	1.011
8	1.013
9	1.014
10	1.016
11	1.018

REFERENCES

1. Ames, F. E., 1997, "The Influence of Large-Scale High-Intensity Turbulence on Vane Heat Transfer," ASME J. Turbomach., 119, pp. 23–30.
2. _____, 1998, “Aspects of Vane Film Cooling with High Turbulence: Part II - Adiabatic Effectiveness,” ASME Journal of Turbomachinery, Vol. 120, pg. 777.
3. Baldauf, S., Scheurlen, M., Schulz, A., and Wittig, S., 2002, “Correlation of Film-Cooling Effectiveness from Thermographic Measurements at Enginelike Conditions,” ASME Journal of Turbomachinery, 124, pp. 686–698.
4. Bons, J. P., MacArthur, C. S., and Rivir, R. B., 1996, "The Effect of High Free-Stream Turbulence on Film Cooling Effectiveness," ASME J. Turbomach., 118, pp. 814–825.
5. Bunker, R. S., 2005, “A Review of Shaped Holes Turbine Film Cooling Technology”, ASME J. Heat Transfer, 127, pp. 441–453.
6. Burd, S. W., Kaszeta, R. W., and Simon, T. W., 1996, "Measurements in Film Cooling Flows: Hole L/D and Turbulence Intensity Effects," ASME Paper No. 96–WA/HT–7.
7. Cho, H. H., Rhee, D. H. and Kim, B. G., 1999, "Film Cooling Effectiveness and Heat/Mass Transfer Coefficient Measurement around a Conical-Shaped Hole with a Compound Angle Injection," the 44th ASME Gas Turbine and Aeroengine Technical Congress, Exposition and Users Symposium, June, Indianapolis, USA, 99-GT-038.
8. Dittmar, J., Schulz, A., Wittig, S., 2003, “Assessment of Various Film-Cooling Configurations Including Shaped and Compund Angle Holes Based on Large-Scale Experiments”, ASME J. Turbomachinery., 125, pp. 57–64.

9. Eriksen, V. L., and Goldstein, R. J., 1974, “Heat Transfer and Film Cooling Following Injection Through Inclined Circular Tubes”, ASME J. Heat Transfer, 96, pp. 239–245.
10. Fric, T. F, and A. Roshko, "Vortical structure in the wake of a transverse jet," J. Fluid Mech. 279, 1 (1994).
11. Foster, N. W., and Lampard, D., 1980, “The Flow and Film Cooling Effectiveness Following Injection Through a Row of Holes”, ASME J. Eng. Power, 102, pp. 584–588.
12. Goldstein, R. J., Eckert, E. R. G. and Ramsey, J. W., 1968. “Film Cooling with Injection Through Holes: Adiabatic Wall Temperatures Downstream of a Circular Hole,” ASME Paper 68–GT–19.
13. Goldstein, R.J., 1971. “Film Cooling,” in Advances in Heat Transfer (edited by T.F. Irvine, Jr. and J.P. Hartnett), Vol. 7, 321-379, Academic Press, New York.
14. Goldstein, R. J., and Taylor, J. R., 1982, "Mass Transfer in the Neighborhood of Jets Entering Crossflow," ASME J. Heat Transfer, 104, pp. 715–721.
15. Gritsch, M., Schulz, A. and Wittig, S., 1998, “Adiabatic wall Effectiveness Measurements of Film-Cooling Holes with expanded Exits”, ASME J. Turbomachinery., 120, pp. 549–556.
16. _____, 1998, “Discharge Coefficient Measurements of Film-Cooling Holes with Expanded Exits,” ASME Journal of Turbomachinery, 120, pp. 557–563.
17. Gritsch, M., Colban, W., Schär, H. and Döbbeling, K., 2005. “Effect of Hole Geometry on the Thermal Performance of Fan-Shaped Film Cooling Holes,” Transactions of the ASME, 127, pp. 718–725.
18. Han, J. C., S. Dutta., and S. Ekkad. Gas Turbine Heat Transfer and Cooling Technology. Great Britain: Taylor & Francis, 2001.

19. Haven, B. A., Kurosaka, M., 1997, “Kidney and anti-kidney vortices in crossflow jets”, J. Fluid Mechanics, 352, pp. 27–64.
20. Haven, B. A., Yamagata, D. K., Kurosaka, M., Yamawaki, S., and Maya, T., 1997, “Anti-Kidney Pair of Vortices in Shaped Holes and Their Influence on Film Cooling Effectiveness”, IGTI Turbo Expo, Orlando, Paper 97–GT–45.
21. Hay, N., and Lampard, D., 1995. “Discharge Coefficient of Flared Film Cooling Holes.” ASME Paper 96-GT-492.
22. Jackson, D. J., Lee, K. L., Ligrani, P. M., Johnson, P. D., and Soechting, F. O., 1999, “Transonic Aerodynamic Losses Due to Turbine Airfoil Suction Surface Film Cooling”, IGTI Turbo Expo, Indianapolis, Indiana, Paper 99–GT–260.
23. Jovanović, M., de Lange, A. and van Steenhoven, A., 2005, “Influence of LASER Drilling imperfection on Film Cooling Performances,” IGTI Turbo Expo, Reno-Tahoe, Nevada, Paper GT–2005–68251.
24. Kadotani, K., and Goldstein, R. J., 1979. “On the Nature of Jets Entering a Turbulent Flow Part A—Jet-Mainstream Interaction,” ASME Journal of Engineering for Power, 101, pp. 459–465.
25. _____, and Goldstein, R. J., 1979. “On the Nature of Jets Entering a Turbulent Flow Part B—Film Cooling Performance,” ASME Journal of Engineering for Power, 101, pp. 466–470.
26. Kline, S., and McClintok, F., 1953, “Describing Uncertainties in Single-Sample Experiments,” Mechanical Engineering, 75, pp. 3–8.
27. Kohli, A., and Bogard, D. G., 1998, "Effects of Very High Free-Stream Turbulence on the Jet-Mainstream Interaction in a Film Cooling Flow," ASME Journal of Turbomachinery, 120, pp. 785–790.

28. Liu, Quan. Study of Heat Transfer of Impinging Air Jet Using Pressure and Temperature Sensitive Luminescent Paint, Ph.D. Dissertation, University of Central Florida, 2005.
29. Liu, Q., Kapat, J. S., Douglass, C. J., and Qiu, J., 2003, "Applicability of Temperature Sensitive Paints for Measurement of Surface Temperature Distribution," IGTI Turbo Expo, Atlanta, Georgia, Paper 2003-GT-38591.
30. Lutum, E., Johnson, B. V., 1999, "Influence of the Hole Length-to-Diameter Ratio on Film Cooling With Cylindrical Holes", ASME J. Turbomachinery, 121, pp. 209–216.
31. Moustapha, H., M. Zelesky, N. Baines, and D. Japikse. Axial and Radial Turbines. United States: Concepts NREC, 2003.
32. Pedersen, D. R., Eckert, E. R. G., and Goldstein, R. J., 1977. "Film Cooling with Large Density Difference between the Mainstream and the Secondary Fluid Measured by the Heat-Mass Transfer Analogy, "ASME J. Heat Transfer, 99, pp. 620–627.
33. Saumweber, C., Schulz, A., and Wittig, S., 2003, "Free-Stream Turbulence Effects on Film Cooling With Shaped Holes," ASME Journal of Turbomachinery, 125, pp. 65–73.
34. Sinha, A. K., Bogard, D. G., and Crawford, M. E., 1991, "Film Cooling Effectiveness Downstream of a Single Row of Holes with Variable Density Ratio", ASME J. Turbomachinery, 113, pp. 442–449.
35. Sinha, A.K., Bogard, D.G. and Crawford, M.E. 1991 Gas Turbine Film Cooling: Flowfield Due to a Second Row of Holes, J. Turbomach. 113, 450–456.
36. Taslim, M. E. and Ugarte, S., 2004. "Discharge Coefficient Measurements for Flow Through Compound-Angle Conical Holes with Cross-Flow," International Journal of Rotating Turbomachinery, 10, pp. 145–153.

37. Thole, K, Gritsch, M., Schulz, A. and Wittig, S, 1998, “Flowfield Measurements for Film-Cooling Holes with Expanded Exits”, ASME J. Turbomachinery., 120, pp. 327–336.

38. York, W. D., Leylek, J. H., 2003. “Leading-Edge Film-Cooling Physics—Part III: Diffused Hole Effectiveness,” ASME Jorunal fo Turbomachinery, 125, pp. 252–259.

39. Yu, Y., Yen, C.-H., Shih, T. and Chyu, M. K., 2002. “Film Cooling Effectiveness and Heat Transfer Coefficient Distributions Around Diffusion Shaped Holes,” ASME Journal of Heat Transfer, 124, pp. 820–827.

40. Zuniga, H., Vaidyanathan Krishnan, Sleiti, A., Kapat, J. S. and Sanjeev Bharani, 2005. “Discharge Coefficient and Effectiveness Measurement for Conical Shaped Film Cooling Holes” ASME Proceedings of IMECE 2005, Orlando, Florida, Paper IMECE–81713.